Seafloor Geodetic Approaches to Subduction Thrust Earthquakes

Hiromi Fujimoto

International Research Institute of Disaster Science, Tohoku University, Sendai 980-8579, Japan
e-mail: fujimoto@aob.gp.tohoku.ac.jp

Received March 3, 2013; **Revised** January 15, 2014; **Accepted** January 16, 2014; **Online published** March 31, 2014.

Citation: Fujimoto, H. (2014), Seafloor geodetic approaches to subduction thrust earthquakes, *Monogr. Environ. Earth Planets*, *2*, 23–63, doi:10.5047/meep.2014.00202.0023.

Abstract Observation systems and some observed results of seafloor geodesy are reviewed with a focus on the research activities of Japanese groups, especially those of Tohoku University. Seafloor acoustic ranging has been adopted as the simplest way to continuously monitor local crustal activities. The GPS-Acoustic (GPSA) method has been the most important for seafloor positioning. It seems that commercial technologies can be used to lessen the considerable differences in repeatability and spatio-temporal resolution of GPSA and land based GPS. Ocean bottom pressure sensors have been used to continuously monitor vertical crustal movements. Improvements in the resolution and long-term stability of pressure sensors will lead to monitoring slow slip events and interplate locking. Ocean bottom and underwater gravimeters have been developed for precise gravity mapping and monitoring mass change beneath the seafloor. The 2011 Tohoku-oki earthquake is an historical event demonstrating that seafloor geodetic observations are crucial to understanding the mechanism of giant earthquakes. Coseismic displacements detected through geodetic observations on the seafloor have indicated huge slips on the shallow part of the plate boundary. A slow slip event near the zone of the coseismic slip preceding the main event has been detected from slight pressure variations. This illustrates the importance of real-time monitoring with a cabled seafloor observatory, which is also a key to establishing a reliable early tsunami warning system.

Keywords: Seafloor geodesy, Seafloor crustal movement, 2011 Tohoku-oki earthquake, Interplate coupling, GPS-Acoustic, Ocean bottom pressure.

1. Introduction

1.1 Subduction thrust earthquakes near the Japan Trench

Most large earthquakes occur on a boundary between a subducting oceanic plate and an overlying plate. The locking of the two plates caused by friction deforms the upper plate, which is mechanically much weaker than the oceanic plate. The tectonically accumulated strain is then released by a destructive slip on the plate boundary. Progress in the precise positioning of the GPS (Global Positioning System) and its observation networks, such as the GEONET extending over the Japanese Islands (Hatanaka *et al*., 2003), have made it possible to geodetically observe the crustal movements associated with the locking and unlocking of the plate boundary. Now we can roughly estimate an interseismic increase in, and a sudden release of, strain through inversion analyses of geodetic data (e.g., Matsu'ura *et al*., 1986).

The distribution of the slip deficit along the Japan Trench had been thus estimated from GPS observations (e.g., Nishimura *et al*., 2000, 2004; Suwa *et al*., 2006; Hashimoto *et al*., 2009) before the occurrence of the magnitude (M) 9.0 2011 off the Pacific coast of Tohoku earthquake (hereafter referred to as the Tohoku-oki earthquake). The result estimated by Suwa *et al*. (2006) is shown in Fig. 1(a). We realized, after the Tohoku-oki earthquake, that the broad distribution of slip deficit was not an artifact due to the limited resolution of the GPS observations in seafloor geodesy. The resolution in the strike-parallel direction is good owing to the distribution of the GPS array along the NE Japan arc. But the resolution in the strike-normal direction is a problem. Suwa *et al*. (2006) estimated that the inversion analysis has certain resolution in the off-shore area about 150 km from the Pacific coast, but cannot estimate any slip deficit near the Japan Trench. Figure 2 (T. Matsuzawa, personal communication) indicates the source regions of large earthquakes that have occurred off Miyagi. The source region of the Tohoku-oki earthquake covers the area from the coast to the trench axis. Measured along the ESE-WNW line, the width of northeastern Japan is about 150 km, and the Japan Trench is about 220 km off-shore. Seafloor geodesy is required to estimate the locking in the shallow part of the plate boundary.

The shaded areas in Fig. 1(a) show source regions of recent interplate earthquakes (Yamanaka and Kikuchi, 2003, 2004). Earthquakes of M 7.4–7.5 repeatedly occurred off Miyagi, on average every 37 years, as shown in Fig. 1(b). The last event occurred in 1978, and the Headquarters for

doi:10.5047/meep.2014.00202.0023 ISSN: 2186-4853

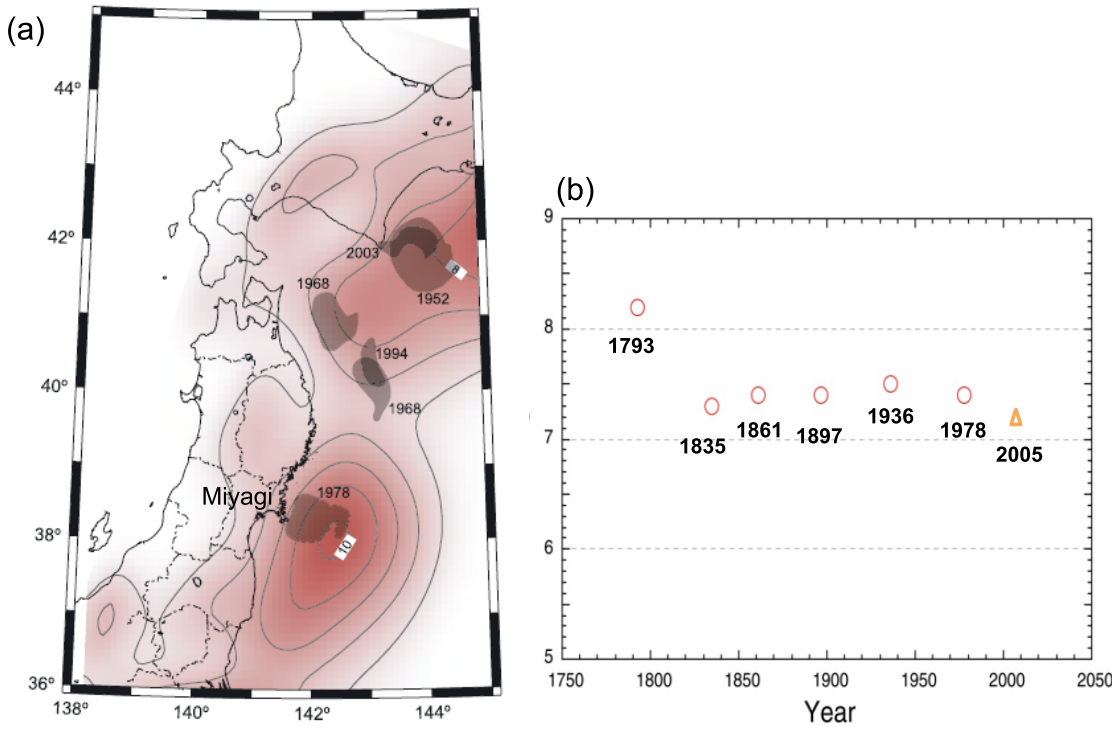

Fig. 1. (a) The distribution of slip deficit off northeastern Japan estimated by Suwa *et al.* (2006). Thin lines are slip deficit contours at intervals of 10 m. The shaded areas show the source regions of recent large earthquakes off NE Japan (Yamanaka and Kikuchi, 2003, 2004). (From Suwa *et al.*, 2006.) (b) The magnitude of large earthquakes estimated off Miyagi before 2011. Earthquakes of M 7.4–7.5 have repeatedly occurred off Miyagi, on average every 37 years. The 2005 M 7.2 event is interpreted to have ruptured about one third of the source region (Yaginuma *et al.*, 2006). It is estimated that two source regions off Miyagi, shown in Fig. 2, ruptured in 1793, resulting in an about M 8.1 earthquake.

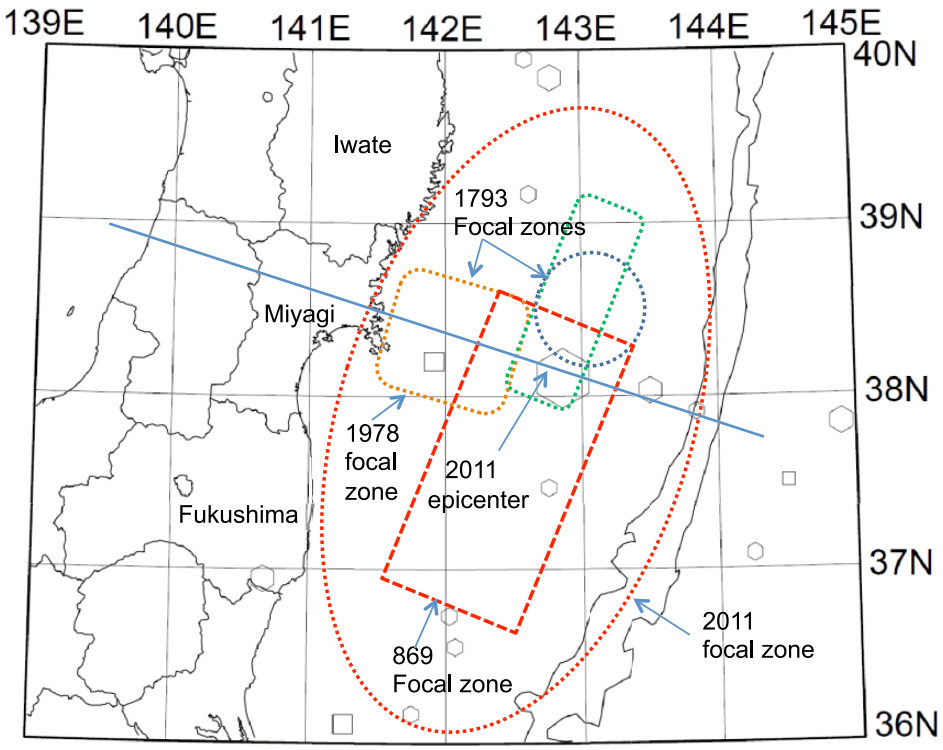

Fig. 2. A simplified map showing the relative location of the distribution of the slip deficit shown in Fig. 1(a) and the source regions of large earthquakes which occurred in this area (courtesy of Prof. T. Matsuzawa). Epicenters of earthquakes larger than M 6 are shown with hexagons (depth: 0–40 km) or with squares (depth: 40–80 km). The locations of Iwate, Miyagi, and Fukushima Prefectures are also shown.

doi:10.5047/meep.2014.00202.0023

Earthquake Research Promotion of Japan (2003) warned that the probability of $M \sim 7.5$ Miyagi-oki earthquakes occurring within the next 7 years was 50%. A larger earthquake around M 8.1 occurred in 1793 over the two source regions off Miyagi shown in Fig. 2. The source region of the big Jogan earthquake in 869, shown in Fig. 2, was estimated based on a limited distribution of tsunami deposits and some written documents. The Headquarters were planning to announce the importance of the Jogan earthquake for tsunami hazard assessment in April 2011. The unexpected giant earthquake, however, occurred before the announcement.

Based on the warning of the Headquarters for Earthquake Research Promotion, the Tohoku University group (hereafter referred to as the Tohoku group) deployed instruments for seafloor geodesy near the two source regions off Miyagi, and is continuing observations to detect crustal movements. The number of instruments was limited in the area near the trench, where the largest coseismic slip occurred on the plate boundary (e.g., Iinuma *et al*., 2012a). Observation of small repeating earthquakes on the plate boundary is another way to estimate the slip on the plate boundary (Igarashi *et al*., 2003; Uchida *et al*., 2003). It is also difficult to estimate slip deficit in the shallow part (0–30 km depth range) of the plate boundary by using this method, because the area is basically aseismic.

It is regrettable that our seafloor geodetic observations could not contribute to foreseeing the occurrence of such a huge earthquake. The Tohoku-oki earthquake, the first M-9 class earthquake that was monitored by seafloor geodetic instruments, as well as dense GPS and seismological networks close to the source region, has shown that the observation of seafloor crustal movement is crucial to solving the mechanism of a giant earthquake.

1.2 Geodetic observation on the seafloor

Because GPS positioning is unavailable on the seafloor, underwater crustal movements require new observation methods different from those on land. There are many barriers against geodetic observations on the ocean bottom. The deep-sea floor is far away from the coast and from the sea surface. The first, and difficult, task for marine geodesists is to acquire ship time for repeated observations. It is especially difficult to carry out diving experiments using a remotely operated vehicle (ROV), or a manned submersible, in the deep ocean. Therefore, most of the instruments for seafloor geodesy are deployed on the bottom through free fall. It is completely dark on the deep-sea floor and solar batteries are useless; even sunlight can only travel 200 m or so in seawater. Furthrmore, pressure increases by about 1,000 kg m^{-2} with every 1 m of water depth.

The most critical problem are the difficulties resulting from the unavailability of electromagnetic waves in sea water. The topography of the Earth's deep ocean has been measured with much less resolution than that of the surface of Mars or Venus, because direct remote sensing from artificial satellites is not available for mapping seafloor topography. The use of acoustic waves is actually a unique alternative. From the viewpoint of scientific measurement, there are large differences between electromagnetic and acoustic waves. Acoustic waves in seawater are slower in propagation and lower in frequency by about 5 orders of magnitude than electromagnetic waves in air. The efficiency of geophysical surveys depends on the input data rate, which is related to the propagation speed of the adopted wave. Frequency-dependent attenuation of acoustic waves in seawater causes another limitation. Acoustic waves of about 10 kHz are used in geophysical measurements in deep water and the serviceable range is about 10 km. Variations in the sound speed and the bending of paths in seawater are also serious problems.

Although there is a large difference in the efficiency of geodetic measurements in the sea and in the air, it does not mean that precise geodetic measurements are impossible on the seafloor. As the sound speed in the ocean is about 1,500 m s^{-1}, an acoustic wave of 10 kHz has a wavelength of about 15 cm. This is much the same as that of an electromagnetic wave adopted by the GPS (1.2–1.5 GHz, wavelength 20–25 cm). Both GPS and underwater acoustic positioning are based on precise range measurement. Because wavelength is a measure of the resolution of range measurement and because 1% of a wavelength is a reasonable estimate of the resolution, we can expect millimeter-order resolution in the ranging by GPS and by underwater acoustics. The expected resolution has almost been attained by GPS, but there remain major problems for acoustic ranging due to the much larger variation of the sound speed in the ocean.

Geophysical observations on the ocean bottom were quite difficult in times gone by. Now they are carried out in various ways owing to recent developments of infrastructures for underwater observations. The first are pressure-tight vessels made of glass, aluminum, stainless steel, titanium alloy, or ceramics. The second are the systems for the deployment and recovery of instruments. The simplest, and the most laborious, system is a rope down to the bottom. The development of an acoustic release system for ocean bottom seismometers (Kanazawa *et al*., 2009) was an important breakthrough for seafloor observations. This system has made it possible to drop an instrument with a weight from the sea surface to be deployed on the sedimented seafloor and then to release the instrument from the weight for self-surfacing with an acoustic command from a survey ship. An instrument equipped with this system is a sort of simple robot for marine experiments. Various seafloor instruments are now deployed by using ROVs or manned submersibles. The third is the power source. Lithium batteries have made stand-alone observations possible for as long as 10 years. Also, ocean bottom cables have realized seafloor networks for long-term, continuous, and real-time observations.

Bearing these factors in mind, I have worked to develop systems for the observation of seafloor crustal movements, in collaboration with colleagues at Tohoku University.

2. Seafloor Acoustic Ranging

2.1 Overview

Direct horizontal acoustic ranging is a simple method of continuously monitoring local crustal movements on the seafloor like optical or laser ranging on land (Morton *et al*.,

doi:10.5047/meep.2014.00202.0023

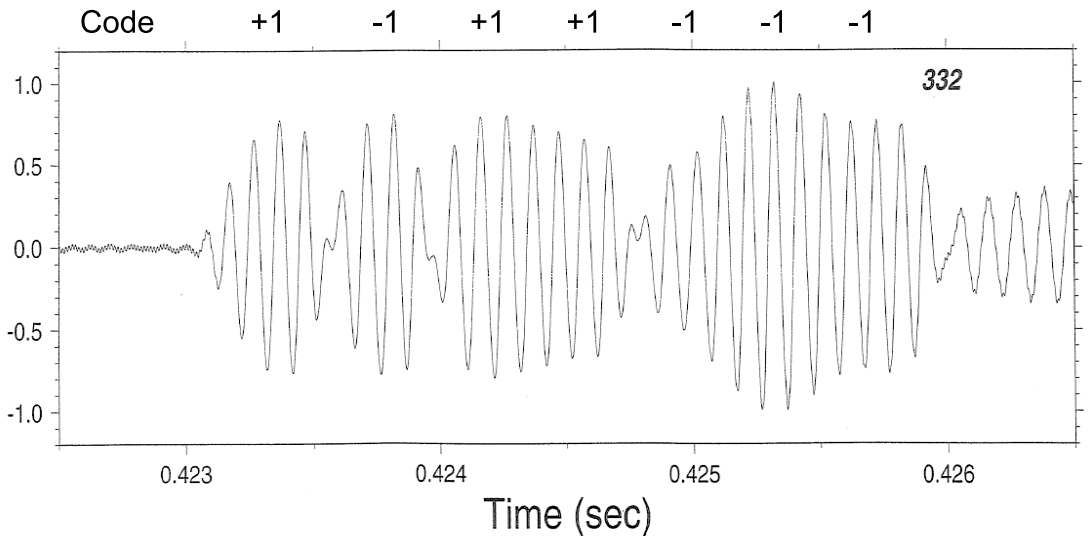

Fig. 3. A simple example of a phase-modulated acoustic signal with 10 kHz carrier waves. Four carrier waves are used for a bit of the code, and each bit is expressed by a phase change of zero degree for $+1$ or 180 degrees for -1. The acoustic wave shows certain delays to respond to the phase change.

1994; Chadwick *et al*., 1995). The measurement of two-way travel times can eliminate the effects of both ocean currents and a long-term drift of the clock. There are several merits of this method. It can be a stand-alone system and can be deployed anywhere on the seafloor. The measurement is simple and suitable for the continuous observation of strain on the seafloor. Combined with a cabled seafloor observatory, tectonic movements in a local area can be monitored in real time.

Acoustic ranging with a burst signal around 12 kHz is usually used for locating the position of an instrument on the seafloor. The sound speed in the ocean is about 1,500 m s^{-1}, and the resolution of the ranging is about 1 m. The effect of a variation in sound speed is nearly canceled out by measuring at three or more points around the instrument. The resolution of acoustic ranging can be improved to a sub-centimeter level by using the pulse compression technique developed for anti-aircraft radars. The signal for pulse compression is usually phase- or frequency-modulated (Gold, 1967; Golumb, 1967). Both GPS positioning and underwater acoustic ranging adopt precise ranging based on cross-correlation analysis between a received signal and a reference one, by using a phase-modulated maximum-sequence code. A simple example of a phase-modulated signal is shown in Fig. 3. The acoustic signal usually adopts a carrier wave of 10–20 kHz, and is digitized at 0.1–1 MHz for cross-correlation analysis. Although the amplitude of the beginning of each bit of the code is reduced due to the phase shift, the effect is removed by the cross-correlation analysis which uses all the waveforms of the signal. The signal-to-noise (SN) ratio of the signal reception is enhanced by the number of bits in the code, as shown in Fig. 4. The chirp signal adopted by the satellite altimetry system is a typical example of a signal with linear frequency modulation.

The average sound speed along the ray path is used to convert a two-way travel time to a distance. Major problems in underwater acoustic ranging are caused by highly variable sound speeds due to variations in temperature, salinity and pressure. For example, an increase in temperature of 0.003°C, or salinity of 0.009‰, or a depth change of 0.9 m, would cause an apparent shortening by about 1 cm in the horizontal ranging of 1,000 m at a water depth of 2,000 m (Chen and Millero, 1977). Of these three factors, temperature variation has the largest effect on acoustic ranging, as is the case in any precise geophysical measurement. Acoustic ranging on the deep-sea floor has the merit that the sound speed is stable owing to a stable temperature. Since underwater sound noises are generated mainly by winds and surface waves, another merit of the deep-sea floor is the low level of acoustic noises making it an optimal place for acoustic observations.

Figure 5(a) shows vertical profiles of temperature and sound speed observed in Sagami Bay, Central Japan. The sound speed in mid-latitude oceans decreases with depth due to a decreasing temperature showing a minimum value at a depth of around 1,000 m, and then increases with depth due to the increasing pressure. Because a propagating wave bends towards a lower speed, a horizontal ray path of an acoustic wave in the deep ocean tends to bend downwards as shown in Fig. 5(b). For example, acoustic transducers used in the acoustic ranging system should be raised by at least 3 m in the case of acoustic ranging of 1,000 m on a flat bottom. This is one reason why horizontal acoustic ranging on the seafloor is often carried out over a short distance of 1,000 m or less. The effect of temperature variation is another reason; the longer the distance, the more difficult the correction.

2.2 Acoustic ranging system

Precise acoustic ranging is carried out by measuring the two-way travel time of an acoustic signal to a distance between two instruments. The master instrument transmits a signal and receives a return signal. The slave instrument, called a precision transponder (PXP), receives the signal from the master instrument and returns it after a fixed delay time. The precise measurement of a round-trip travel time needs a cross-correlation analysis, which requires a microprocessor

doi:10.5047/meep.2014.00202.0023

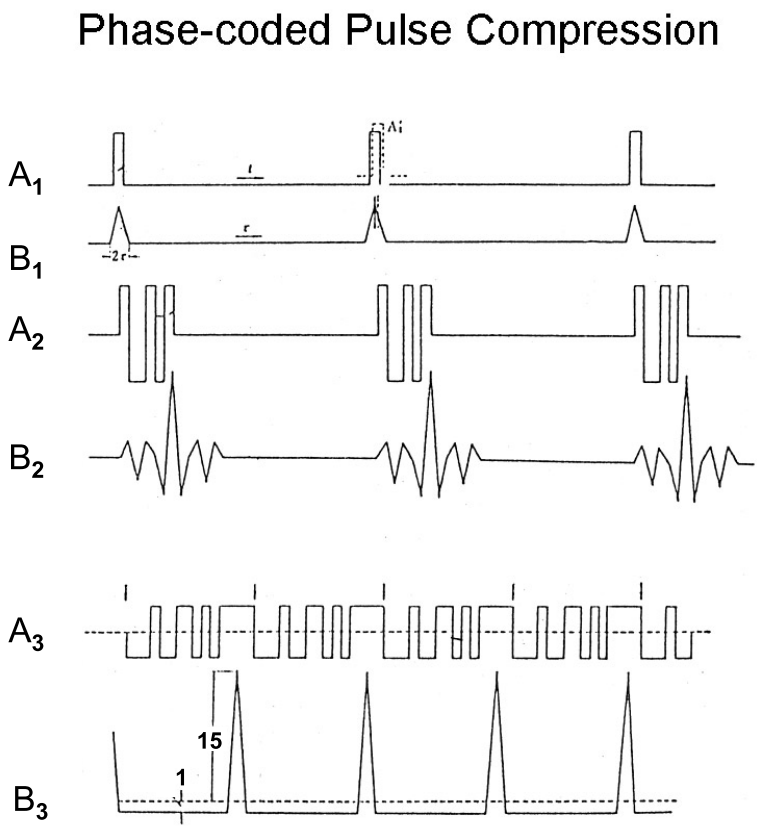

Fig. 4. Concept of pulse compression by cross-correlation analysis using a phase-coded maximum-sequence code. A_1 to A_3 are coded signals and B_1 to B_3 are outputs of cross-correlation of each coded signal. A_3 is a phase-modulated maximum-sequence code of 15 bits. B_3 shows that the output is enhanced by the number of the code's bits when the input coded signal is matched with the reference signal.

which requires much more power than a simple electronic circuit. The master instrument digitizes the received signal and logs the data in a memory to save the battery. Cross-correlation analysis is carried out after the master instrument has recovered. On the other hand, Spiess *et al*. (1980) found that cross-correlation analysis is not necessary for a PXP. A PXP adopting their idea, called a mirror transponder, simply returns a signal after a fixed delay time. This is one of the merits of measuring the round-trip travel time, especially in the case when PXPs are used for underwater acoustic positioning as discussed in Section 3.1.

Since the transmission loss of an acoustic wave is large in seawater, the source level of an acoustic signal should be high enough to overcome such a loss. We can roughly estimate the required source level by using the simplified sonar equation, in which all terms are expressed in logarithmic form, so that the decibel notation can be used (e.g., Medwin, 2005). The sound source level (SPL) in decibel notation is:

$$\mathrm{SPL\ (dB)} = 20\log_{10}(P/P_{\mathrm{ref}}), \tag{1}$$

where P is the root-mean-square (rms) sound pressure in the field, and P_{ref} is the reference pressure, which is usually 1 N $\mathrm{m}^{-2} = 1\ \mu$Pa. The SPL depends on the source level (SL) and the transmission loss (TL):

$$\mathrm{SPL\ (dB)} = \mathrm{SL\ (dB)} - \mathrm{TL\ (dB)}, \tag{2}$$

$$\mathrm{SL\ (dB)} = 20\log_{10}(P_0/P_{\mathrm{ref}}), \tag{3}$$

where P_0 is the sound pressure at the source reference distance. The transmission loss in the case of an acoustic wave spreading spherically from a point source is expressed as:

$$\mathrm{TL\ (dB)} = 20\log_{10}(R/R_0) + \alpha(R - R_0), \tag{4}$$

where R is the range from the source, R_0 is the reference distance of 1 m and α is the sound pressure attenuation rate. The attenuation rate in seawater for acoustic waves around 10 kHz is about 1 dB/km, about one order of magnitude higher than that in fresh water due to the effects of boric acid and magnesium sulfate (Francois and Garrison, 1982a, b).

The SN ratio is the sound source level minus the noise level as follows:

$$\mathrm{SN\ (dB)} = \mathrm{SL\ (dB)} - 20\log_{10}(R/R_0) - \alpha(R - R_0) - \mathrm{NL\ (dB)}, \tag{5}$$

$$\mathrm{NL\ (dB)} = \mathrm{N_{ss}} + 10\log_{10}(\mathrm{BW}) - \mathrm{DI\ (dB)}, \tag{6}$$

where NL is the noise level, $\mathrm{N_{ss}}$ is the sea state noise in the study area, BW is the system noise bandwidth (Hz), and DI is the directivity of the acoustic transducer. If the transducer is nondirectional, DI = 0. According to Urick (1983), a reasonable estimate of $\mathrm{N_{ss}}$ is about 52 dB. The output power from an acoustic transducer has a maximum value at its geometrical axis and decreases with the angle from the axis. The decrease is about 6 dB, or more, at 60 degrees from the axis.

doi:10.5047/meep.2014.00202.0023

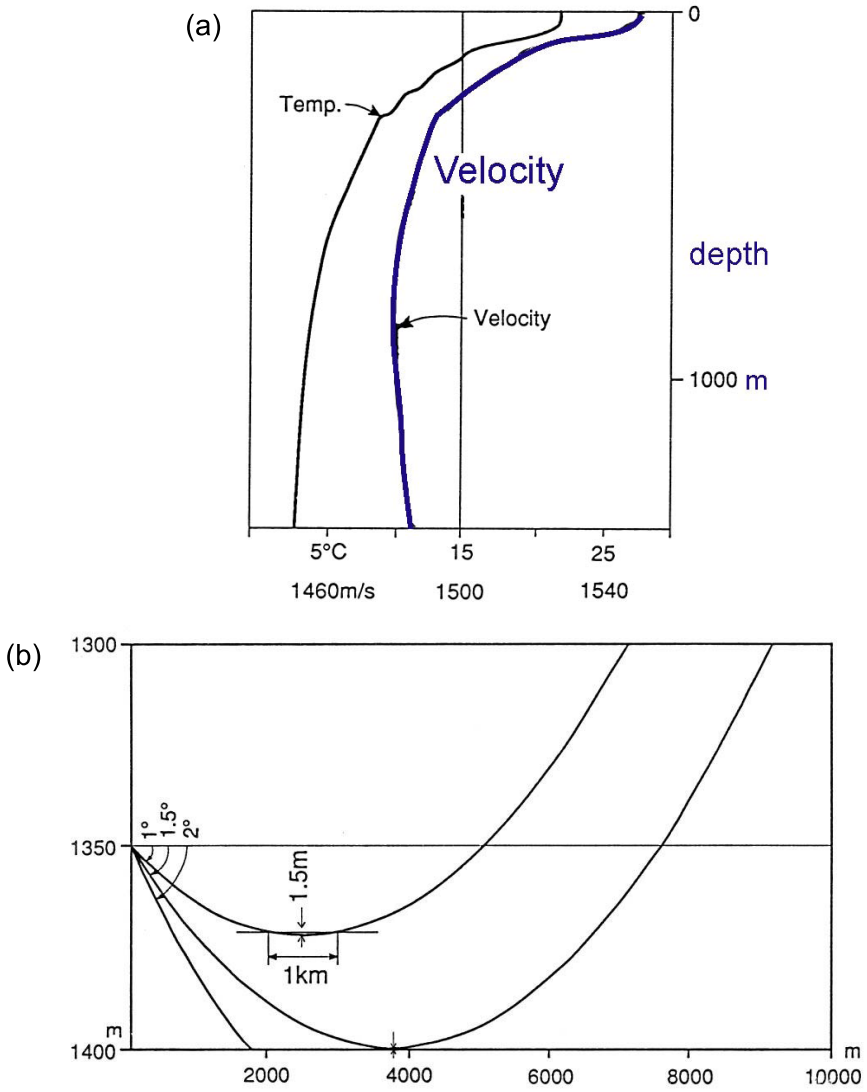

Fig. 5. (a) Vertical profiles of temperature and sound speed observed in Sagami Bay, Central Japan. (b) Ray paths calculated from the sound speed profile.

The Tohoku group developed PXPs in 2001 jointly with the geodetic group of the Scripps Institution of Oceanography, UCSD, (hereafter referred to as the SIO group) basically for the GPS-Acoustic seafloor positioning system discussed in Section 3.1 (Osada *et al*., 2003). We assumed the maximum range for the acoustic ranging to be 15 km, and adopted the value for the source level to be 197 dB (see Section 3.5 for the calculation). We confirmed precise acoustic ranging at ranges more than 15 km with the PXPs.

2.3 Some observed results

Various groups have successfully detected seafloor movements based on acoustic ranging. Long-term monitoring of seafloor crustal movements has revealed an intermittent ridge extension across the Juan de Fuca Ridge (Chadwick *et al*., 1995; Chadwell *et al*., 1999; Chadwick and Stapp, 2002). One interesting result which has not been reported well is related to acoustic ranging across the axis of the southern East Pacific Rise carried out in 1997–98 for 426 days by Nagaya *et al*. (1999). They deployed a pair of acoustic ranging instruments at a distance of 870 m across the spreading axis, where the full spreading rate was about 15 cm/yr (DeMets *et al*., 1994). A chirp signal with a frequency band of 30–50 kHz was used for the acoustic ranging. A vertical array of five thermistor sensors was deployed in the midst of the survey line to monitor the seawater temperature. Owing to temperature stability within 0.01°C, the acoustic ranging was quite stable; the rms residual from a linear trend was 0.38 cm. The linear trend indicated that a slight contraction, not extension, occurred just around the ridge axis during the observation period. It was generally believed, at that time, that the fast spreading Southern EPR might be spreading relatively steadily, unlike typical mid-ocean ridges spreading at a medium speed such as the Juan de Fuca Ridge. The result gave an important observational constraint to the physical model of seafloor spreading.

The Tohoku group has also engaged in seafloor acoustic ranging in the past several years (Osada *et al*., 2008a) using PXPs manufactured by Kaiyo Denshi, Ltd. Our purpose is to monitor the activity of splay faults that branch from the plate boundary along the Nankai Trough off Southwest Japan. Park

doi:10.5047/meep.2014.00202.0023

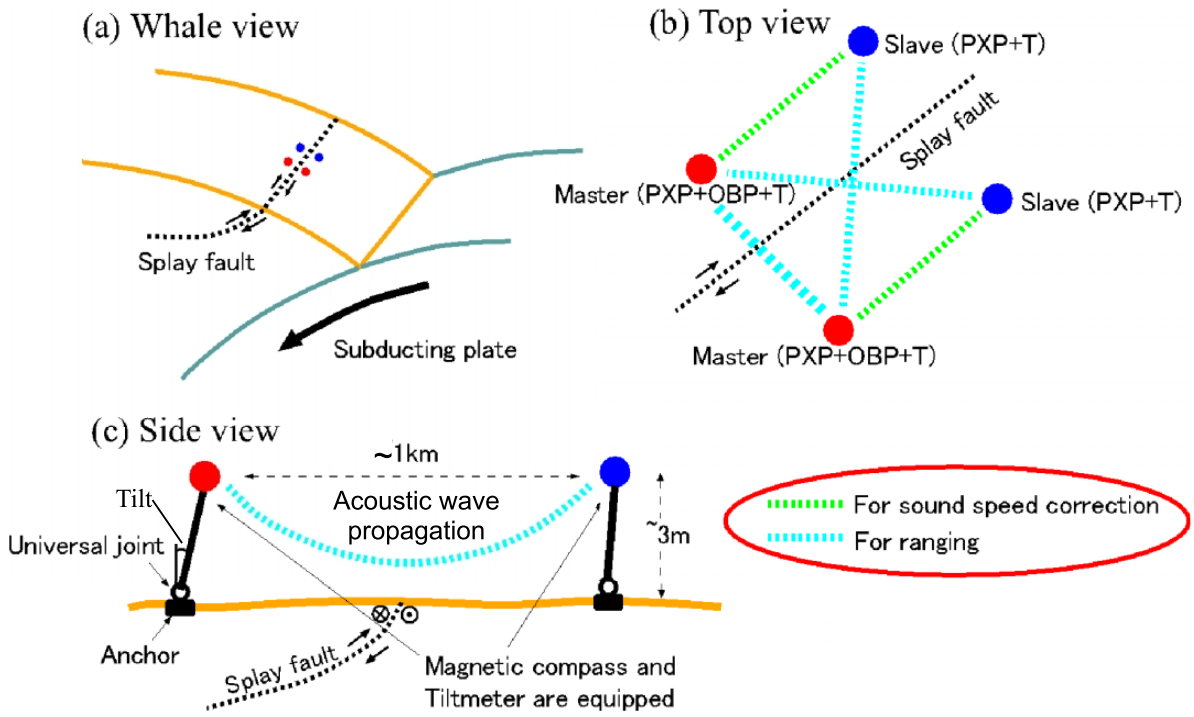

Fig. 6. Schematic illustration showing the concept of an observation system to monitor local crustal movements (courtesy of Prof. M. Kido). (a) Four acoustic units are installed across a splay fault, where localized strain is expected. (b) Master acoustic units (red) transmit acoustic signals to slave units (blue). The slaves act as precision transponders (PXPs) and return the signals. Then, each of the masters records the return signal to measure the round-trip travel time. A master also works as a slave for another master. The masters are equipped with ocean bottom pressure recorders (OBPRs) and temperature recorders (T) to monitor vertical crustal movements and temperature variations. Acoustic paths across the fault (light blue) are used to detect the horizontal strain, while the paths along the fault (green) are used to monitor the effect of sound speed variation on the acoustic ranging. (c) Acoustic transducers must be kept at least 3 m above the seafloor (for about a 1 km distance) to ensure that the downward bending path directly reaches from one to the other. The acoustic unit is sustained by a prop. Its bottom end is connected to an anchor through a universal joint, which reduces the torque acting on the anchor against bottom currents for long-term installation stability. The apparent change in the range due to the leaning of the prop can be corrected by a compass and a tiltmeter equipped in each instrument.

et al. (2002) estimated that a splay fault played a key role in the generation of big tsunamis associated with the Tonankai earthquakes that have occurred repeatedly off the Kii Peninsula. Ito and Obara (2006) showed that very-low-frequency earthquakes may have occurred near the splay faults and estimated the slip rate there to be 2–10 mm/yr. Our plan is to monitor the activities of these splay faults based on arrayed acoustic ranging by using the PXPs and differential pressure monitoring by using ocean bottom pressure recorders (OBPRs), as shown in Fig. 6. The key point is that the two along-fault lines measure sound speed variations in the study area because there should be little tectonic displacement each side of the fault, and that the effect of sound speed variation on the strike-normal measurements can be corrected by using the sound speed variations monitored in the two along-fault lines.

The Tohoku group carried out an experiment from August 2007 to June 2008 to examine the long-term stability of the acoustic ranging system. Four instruments were deployed on the flat bottom to form an array as shown in Fig. 6. Unfortunately one of the master units failed to record the data, and the observed record covered only four months due to a problem with the batteries. Each instrument measured the temperature and the tilt as well as the travel time every 30 minute. The observed round trip travel time between a master (M2) and each of two PXPs (S1 and S2) indicated a variation with a peak-to-peak amplitude of about 0.75 m. Most of the variation was caused by changes in sound speed due to temperature changes. The repeatability of the acoustic measurements is markedly improved with the correction for temperature and tilt, as shown in Fig. 7. The rms residuals of the results were about 1 cm (Osada *et al*., 2012a).

3. GPS-Acoustic Geodetic Observations on the Seafloor

3.1 Measurement system

Since the velocities of tectonic crustal movements are too slow to be directly measured, Spiess (1985) proposed a method for measuring seafloor crustal movements based on repeated precise positioning of an acoustic benchmark. He planned to measure the position combining sea surface GPS positioning and underwater acoustic positioning. Then, seafloor crustal movements are measured on the geodetic framework of GPS. This method is called GPS-Acoustic (GPSA) seafloor positioning. A schematic illustration of the observation is shown in Fig. 8. The PXPs for the acoustic positioning are basically the same as those for seafloor acoustic ranging. An array of PXPs acts as the acoustic benchmark on the seafloor. Three or four PXPs are used to remove the effect of sound speed variations in the ocean on the acoustic

doi:10.5047/meep.2014.00202.0023

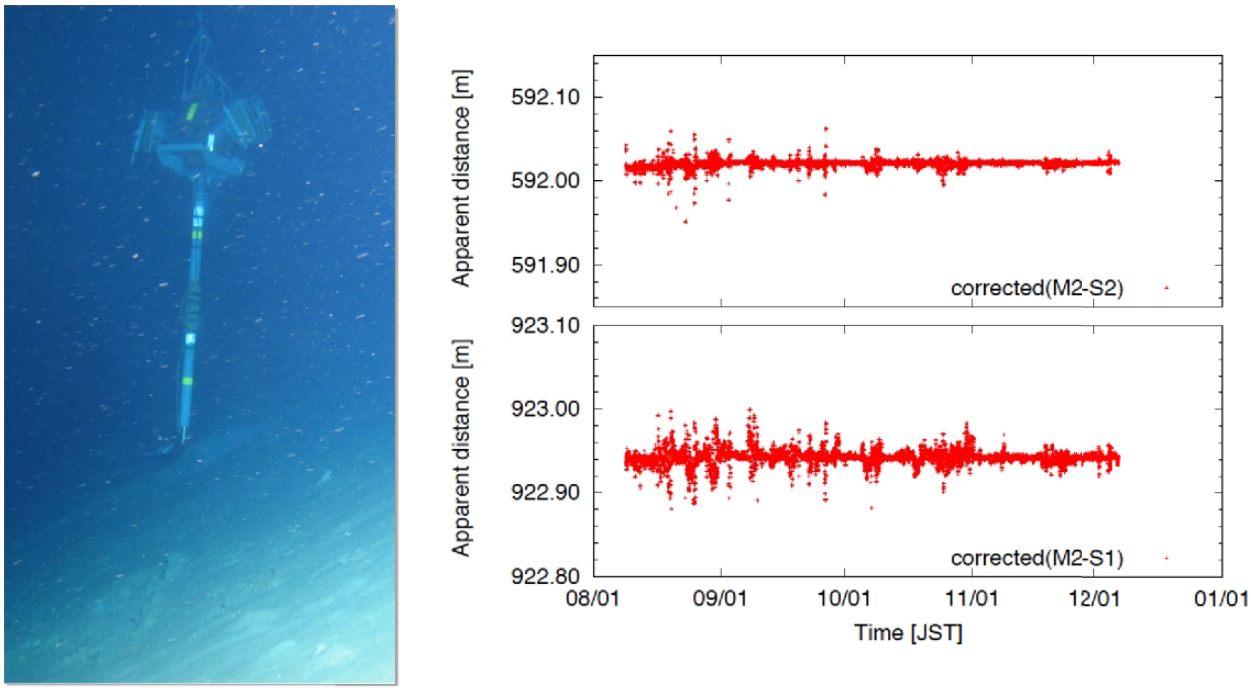

Fig. 7. Variation of acoustic ranging for about 4 months in ranges about 600 m and 920 m. Most of the apparent variations up to 0.75 m in the range were caused by changes in sound speed due to temperature changes, and the travel times after the corrections for temperature and tilt are stable within 1 cm rms (modified from *Ocean Eng.*, *51*, Osada, Y., M. Kido, and H. Fujimoto, A long-term seafloor experiment using an acoustic ranging system: precise horizontal distance measurements for detection of seafloor crustal deformation, Copyright 2012, with permission from Elsevier). The picture on the left shows one of the instruments observed by a remotely operated vehicle (courtesy of Dr. Y. Osada).

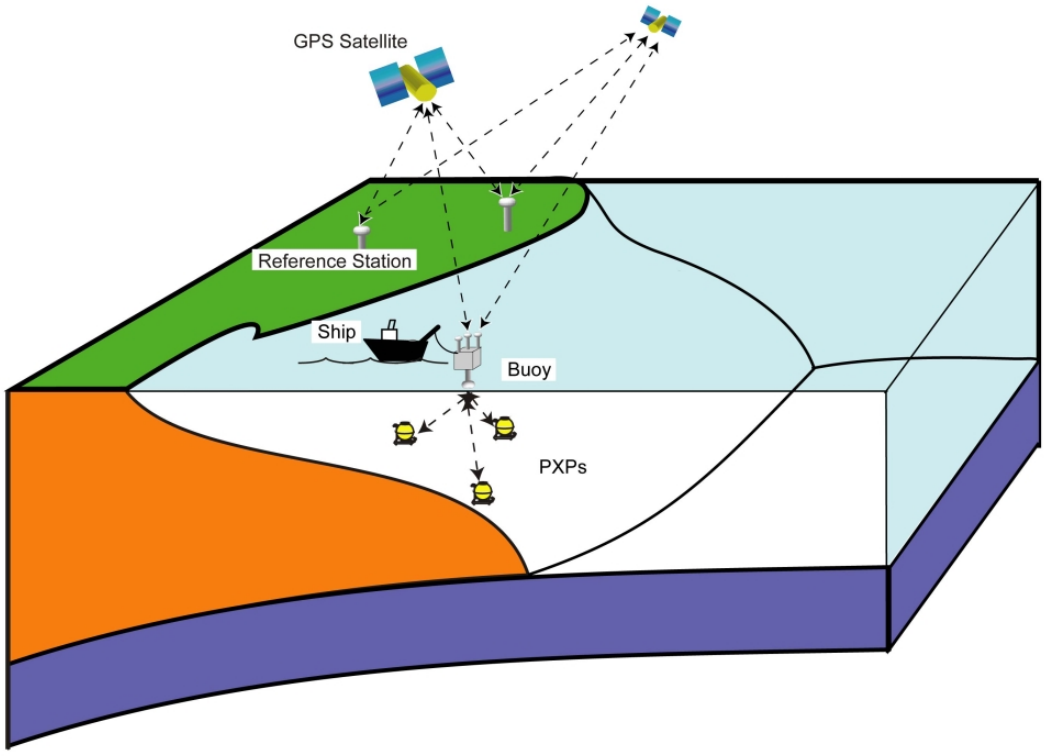

Fig. 8. Schematic illustration of GPSA seafloor positioning using a towed buoy. The array of PXPs acts as an acoustic benchmark on the seafloor. See the text for how the seafloor position is obtained.

doi:10.5047/meep.2014.00202.0023

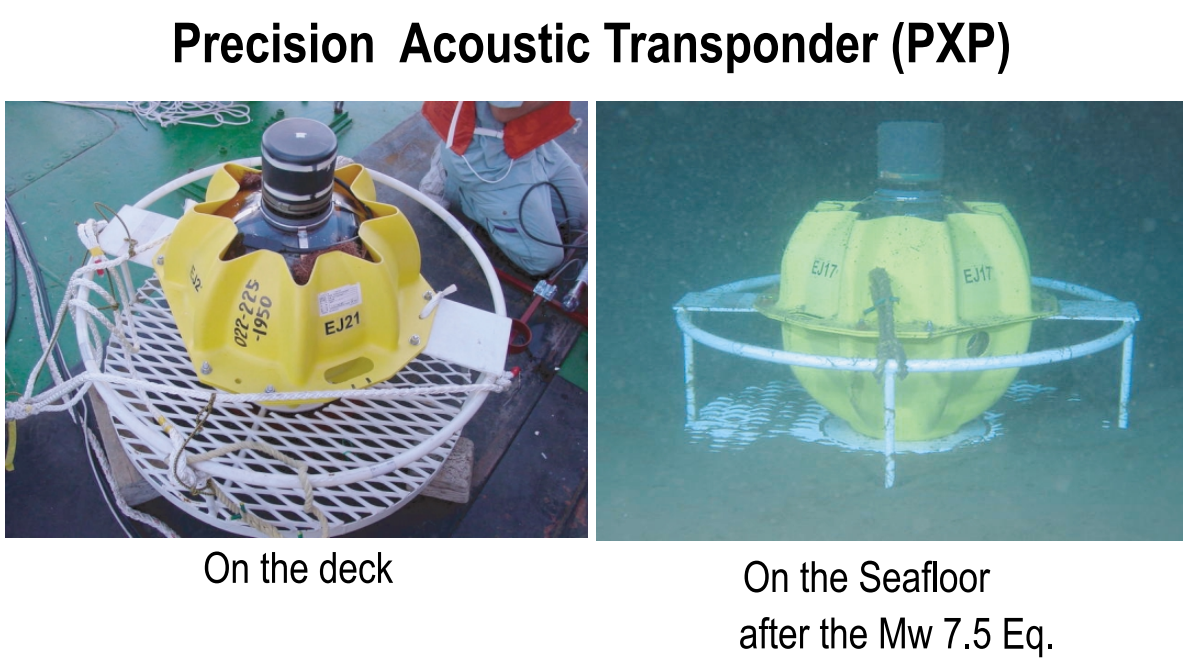

Fig. 9. Photographs of one of the PXPs taken on deck before deployment and on the seafloor after the 2004 *M* 7-class earthquakes off the Kii Peninsula. (Right, with kind permission from Springer Science+Business Media: *Modern Approaches in Solid Earth Sciences*, Long-term stability of acoustic benchmarks deployed on thick sediment for GPS/Acoustic seafloor positioning, *8*, 2011, 263–272, Fujimoto, H., M. Kido, Y. Osada, K. Tadokoro, T. Okuda, Y. Matsumoto, and K. Kurihara, figure 4(d).)

positioning. The Tohoku group used a buoy towed from a survey ship for the GPSA observation.

It is the progress in high speed digital signal processing that has enabled geodetic measurements on the seafloor. It is amazing, for example, that the position of a swaying GPS antenna at the top of a ship cruising a few hundreds of kilometers offshore can be determined every second, with a precision of 1 cm or better, by kinematic GPS (KGPS) positioning. KGPS is a method of GPS positioning for a mobile vehicle that needs post-cruise processing of the GPS data observed by the mobile unit and data observed at a stable reference station on land.

Usually, a sea surface KGPS unit comprises three GPS receivers and a motion sensor for measuring the position and attitude of the vessel. The position of the acoustic transducer installed on the bottom of the vessel relative to the GPS antennas is measured before a cruise, with a precision of a few millimeters, using a geodetic instrument. Then, the position of the transducer can be calculated from those of the three GPS antennas. The sampling interval of a GPS receiver has basically been 1 or 2 s. The signal for the acoustic ranging is transmitted in synchronization with a pulse-per-second signal from a GPS receiver. The position of the acoustic transducer at the signal transmission can then be accurately determined. Signals from the PXPs on the seafloor, however, arrive at various times. The motion sensor can interpolate the transducer's position in-between the GPS positioning owing to its short sampling interval. It is also useful to check the data of the three GPS receivers. A prevailing period of motions of a ship is several seconds, and a sampling interval of 1 s is permissible. The buoys we used for GPSA observations sway with a period of about 2 s, and the sampling interval of GPS receivers for the buoys was improved to be 0.1 s from the original 1 s (Osada *et al*., 2008b).

The acoustic positioning is obtained from the two-way travel time of a signal between the acoustic transducer attached on the bottom of a survey vessel and each of the PXPs on the seafloor. Since sound speed in the ocean is horizontally layered fairly well, acoustic ranging to three or more PXPs can cancel the effect of the temporal variation of the sound speed on the horizontal positioning of the PXP array. Another problem is the underwater acoustic noise generated by survey vessels used in the observations. At Tohoku University, to cope with this problem, we have used a buoy towed from a ship as shown in Fig. 8; this allows us to use various ships without having to make any modification to the ships.

The seafloor of subduction zones is inevitably covered with a thick sediment. One frequently asked question concerns the stability of the position of the acoustic transducers of PXPs deployed on the sedimented seafloor. The 2004 *M* 7-class earthquakes off the Kii Peninsula gave us a rare chance to evaluate the stability of seafloor benchmarks in the case of strong ground motions. Three research groups in Japan, including our group, had deployed PXPs near the source region, and coseismic horizontal seafloor displacements larger than 20 cm were detected (Kido *et al*., 2006; Tadokoro *et al*., 2006) as discussed in Section 3.3. It was suspected, however, that strong ground motions due to the earthquakes might have tilted the acoustic instruments deployed on thick sediment to cause an apparent crustal movement. We carried out diving surveys to settle this question. We visually inspected 10 PXPs deployed on the seafloor by the three research groups, and confirmed the stable attitude of the instruments. Figure 9 shows photographs of one of the PXPs taken on deck before

doi:10.5047/meep.2014.00202.0023

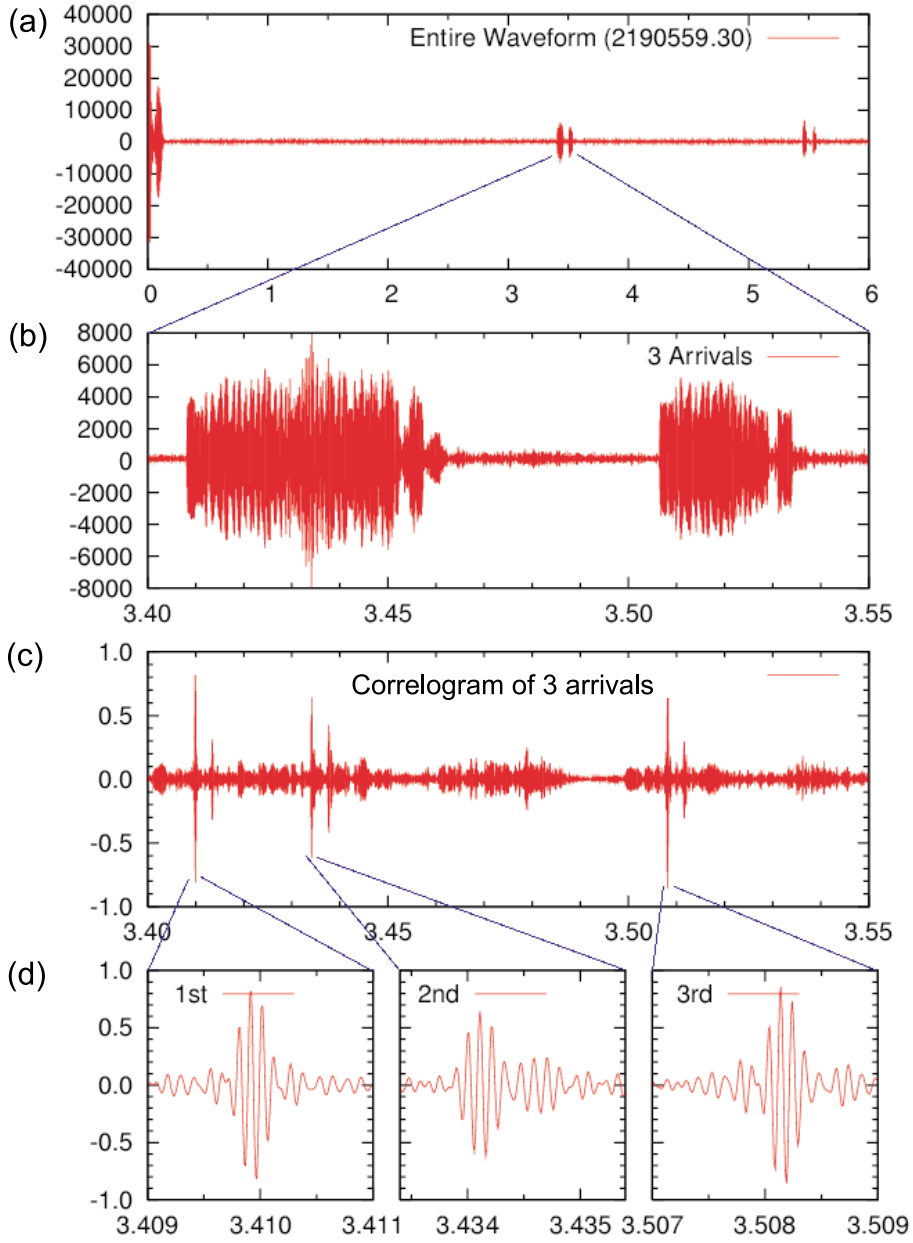

Fig. 10. Waveforms of observed acoustic signals in the panels (a)–(b) and the correlograms with a reference signal in the panels (c)–(d) (courtesy of Prof. M. Kido). The horizontal axis is in seconds. The small peaks some 0.004 s after the three main peaks in the panel (c) probably show the effect of the reflection of the acoustic wave at the sea surface.

deployment and on the seafloor after the earthquakes. Judging from the tilting angles of the PXPs, we confirmed that the position of the acoustic transducer of each PXP was stable within a few centimeters (Fujimoto *et al.*, 2011a).

3.2 Post-cruise data processing

The post-cruise data processing consists of two steps: KGPS positioning and underwater acoustic positioning. We employed the GIPSY OASIS II software (Lichten and Border, 1987) to simultaneously solve 1 to 10 Hz positions of the four antennas on the buoy relative to reference GPS stations on land, whose positions are calculated independently using Precise Point Positioning (PPP) analysis (Zumberge *et al.*, 1997). We also use the KGPS software called IT (Interferometric Translocation) which has been used by the group of the Japan Coast Guard and the University of Tokyo (hereafter referred to as the JCG group). It was developed for the precise determination of the trajectory of a mobile vehicle over very long baselines (Colombo *et al.*, 2000). The horizontal KGPS positioning is estimated to be accurate to 1–2 cm (e.g., Miura *et al.*, 2002). The position of the transducer at each acoustic transmission and reception is interpolated from the 1–10 Hz positions of the GPS antennas with the aid of data from a motion sensor (25–50 Hz).

KGPS processing has been carried out by using accurate information of the orbits and the clocks of the GPS satellites (ephemeris data) that are provided by the International GNSS Service (IGS) after data processing, which takes about two weeks. It has recently been confirmed that KGPS processing,

doi:10.5047/meep.2014.00202.0023

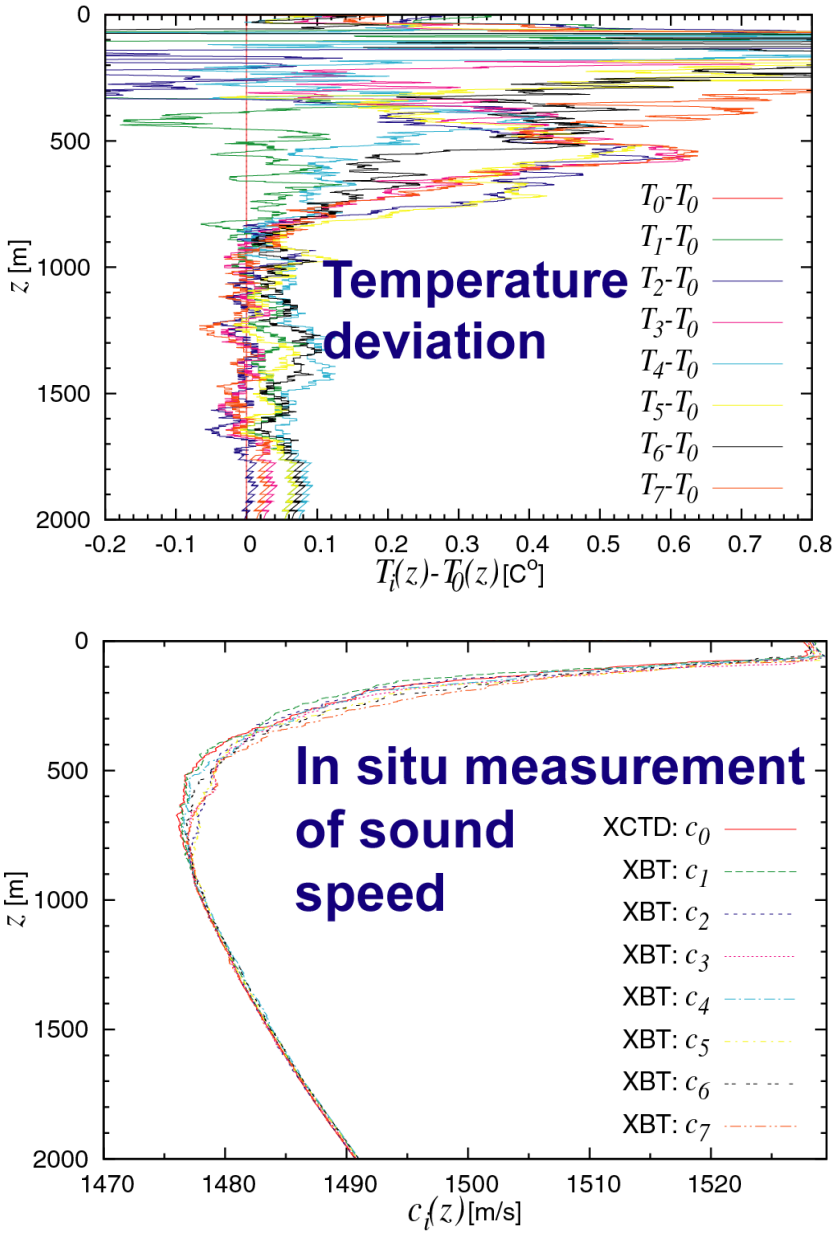

Fig. 11. An example of temperature and sound speed variations from XBT observations at times t_1, t_2, ... t_7, and from an XCTD observation at time t_0. C_0 to C_7 and T_0 to T_7 show the vertical profiles of sound speed and temperature observed at times t_0 to t_7. The effect of the sound speed variation is shown in Fig. 13 (modified from Kido *et al.*, 2008).

by using ultra-rapid ephemeris data provided by the IGS 3 hours after the KGPS data acquisition, is accurate enough for GPSA observation (Watanabe *et al.*, 2012).

The first step in underwater acoustic positioning is the determination of the two-way travel time of an acoustic signal by cross-correlation analysis between the transmitted and the received signals. The arrival time of the signal is identified as a maximum peak in the correlogram, as shown in Fig. 10. The sampling of the acoustic signal is about 1–10 μs corresponding to a range of 0.75–7.5 mm, and the resolution of the ranging by the correlogram is a few millimeters. While the Nagoya University group (hereafter referred to as the Nagoya group), as well as the Tohoku group, uses a relatively short acoustic signal of about 15 ms, the JCG group adopts a much longer signal of about 200 ms. The SN ratio of the correlogram becomes higher in proportion to the number of the code's bits. On the other hand, a longer signal requires more accurate processing to correct the Doppler effect of the vessel's motion on the acoustic signal. Suppose the relative motion of a transducer at the times of transmission and reception is 3 m s^{-1}, 1/500 of the sound speed. The Doppler effect causes about a 4 cycle shift in the carrier wave while receiving a signal composed of 2,000 (=10,000×0.2) cycles of the 10 kHz carrier.

The sound speed in the ocean can be estimated based on temperature profiles collected by a conductivity-temperature-depth profiler (CTD) before and/or after a GPSA observation at a site. We can also estimate the sound speed profile

doi:10.5047/meep.2014.00202.0023

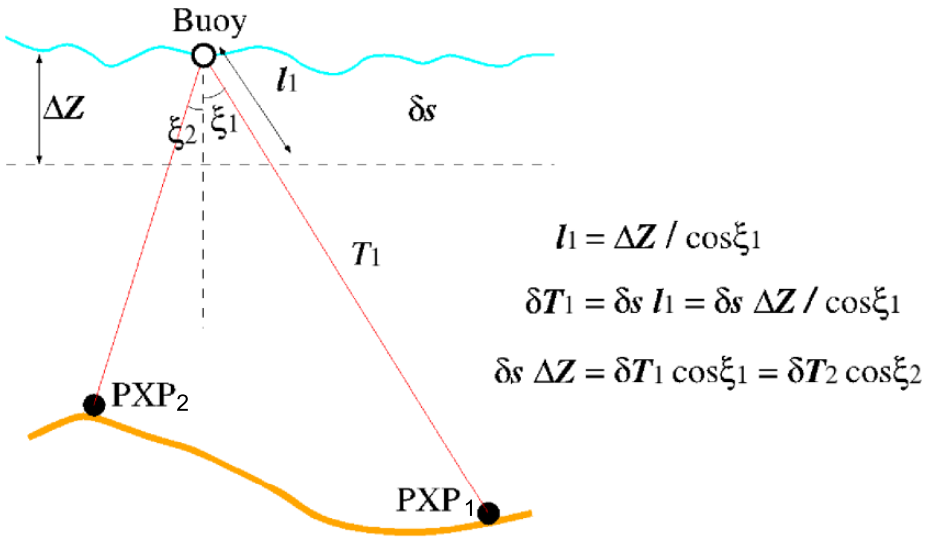

Fig. 12. The concept of the method to estimate the effect of a sound speed change in shallow water on GPSA acoustic positioning (courtesy of Prof. M. Kido). This method is useful when the buoy is away from the PXP array center. ΔZ: thickness of the surface layer of slowness anomaly δs, l_1: length of the ray path to PXP_1 in the surface layer, δT_1: slowness integrated along l_1, and ξ_1: slant angle to PXP_1.

of the upper layer of 1,850 m using an expendable CTD (XCTD) or expendable bathythermograph (XBT). However, the sound speed profiles obtained from these observations are not precise enough and neither is the resolution of temporal and spatial variations. Therefore, the observed sound speed profiles are used as the first approximation. The temporal variation of the sound speed is precisely estimated in the analysis of acoustic positioning. The observed sound speed profiles are also used as supplementary data to validate the analysis.

It is the surface layer of about 1,000 m that shows the most variation with time. An example of the sound speed profile observed in the Nankai Trough area is shown in Fig. 11. The variation of sound speed depends mainly on temperature as mentioned in Section 2.2. If the average temperature in the upper 1,000 m changes by 1°C, the effect corresponds to an apparent change of 4.7 m in acoustic ranging with a ray angle of 45 degrees.

The Tohoku group has used a towed buoy for GPSA observations and adopted the approach developed by the SIO group. Acoustic measurements are performed at a PXP array center simultaneously with all the PXPs under the assumption that the pre-determined array geometry is unchanged (Spiess *et al.*, 1998). An advantage of this method is that ray paths in shallow water are confined in a small area compared with the PXP array, and therefore the lateral variation in the sound speed is small. Thus, the sound speed in the ocean is well approximated by a time-dependent horizontally stratified structure. In this case, the effect of sound speed variations on travel times is common to the ray paths with all the transponders and can be easily removed (Chadwell and Spiess, 2008). The position of the PXP array is estimated to be the value that minimizes the residuals of the observed travel times from those estimated with the sound speed structure.

The SIO group positioned the survey vessel within about 10 m from the center of a PXP array during a GPSA observation (Chadwell and Spiess, 2008). On the other hand, it is quite difficult to maintain the position of a buoy towed from a survey vessel under ocean currents and winds. Consequently, the buoy's position can be kept within a few hundreds of meters from the center. Kido *et al.* (2008) modified the method of underwater acoustic positioning to be able to calculate travel time residuals with a large variability of the buoy's position. Suppose that the slowness anomaly δs in sound speed is confined in a surface layer of thickness ΔZ. The travel time residual to all PXPs normalized to their respective vertical components $\delta s \Delta Z$, will have the same value regardless of the buoy's position as indicated by the equations in Fig. 12. This method can be applied when there is a horizontal gradient in sound speed, but the gradient should be determined separately.

The temporal variation of the vertically averaged travel time residual ($\delta s \Delta Z$ in Fig. 12) can be precisely estimated through acoustic positioning near a PXP array center. Figure 13 shows an example of acoustic estimates in comparison with those estimated from *in situ* oceanographic measurements periodically carried out during the survey. The result shows that the estimated values are in a good agreement within 5% of the amplitude of the temporal variation in the acoustic estimates.

The JCG and Nagoya groups adopt another philosophy for the GPSA observations, which is to carry out a set of measurements uniformly over a PXP array within a short time (Fujita *et al.*, 2006; Sato *et al.*, 2011a; Tadokoro *et al.*, 2012). The observed travel-time data include information of the slant range and the average velocity along the ray path. Using the travel time residuals estimated with an *a priori* sound speed structure from CTD observations, Fujita *et al.* (2006) calculated coefficients for temporal variations in the sound speed for a given time window. This idea is similar to that of the atmospheric delay estimation for the precise GPS data analysis.

doi:10.5047/meep.2014.00202.0023

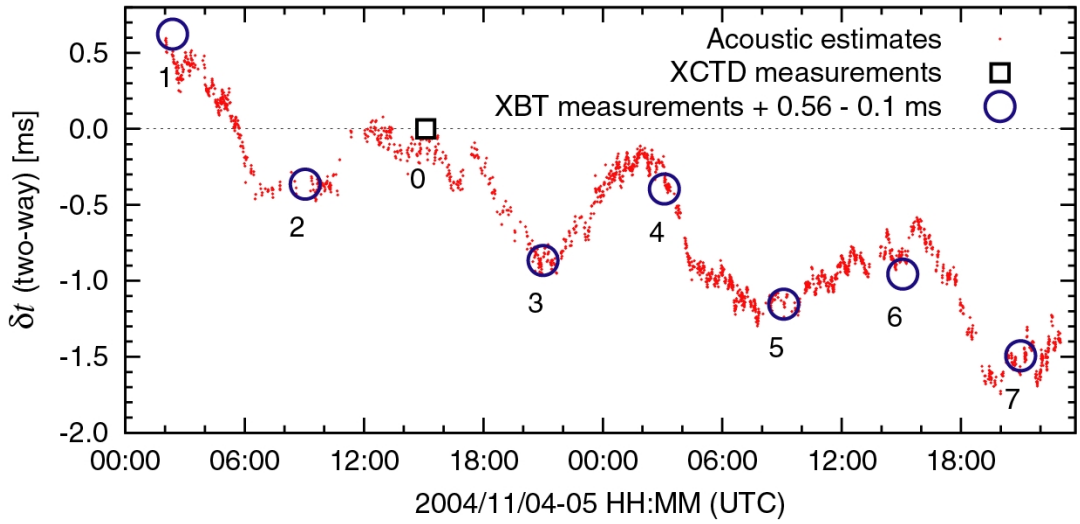

Fig. 13. A result of the temporal variation of the vertically averaged travel time residuals. Red dots: results estimated from the analysis of acoustic positioning. A dot corresponds to a shot of the acoustic ranging. Open circles (1–7): results obtained from XBT observations at times t_1 to t_7 shown in Fig. 11, square (0): a result from an XCTD observation at time t_0 shown in Fig. 11 (modified from Kido *et al.*, 2008).

3.3 Some important results of GPSA observations before 2011

Spiess *et al.* (1998) succeeded for the first time in observing plate motion on the seafloor off the Cascadia subduction zone from repeated GPSA observations. Chadwell and Spiess (2008) estimated the present-day plate velocity of the Juan de Fuca plate 25 km away from its spreading ridge axis based on GPSA observations over 4 years. The result suggests a continuous plate motion relative to the Pacific plate. It shows a clear contrast to the episodic motion across the 1-km-wide axial valley observed by acoustic ranging (Chadwell *et al.*, 1999; Chadwick and Stapp, 2002). Gagnon *et al.* (2005) presented important results of GPSA observations at the Peru-Chile Trench. They showed that the measured horizontal surface motion perpendicular to the trench is consistent with the model that has no slip along the thrust fault between 2 and 40 km depth and suggested interplate locking at shallow depths of the plate boundary.

GPSA observations have been carried out in the Kumano Basin in the Nankai Trough area by the JCG, Nagoya, and Tohoku groups. The area is located above the source region of the estimated Tonankai megathrust earthquake. A large earthquake of *M* 7.5 occurred in September 2004 off the Kumano Basin, as discussed in Section 3.1. The mainshock and two *M* 7-class earthquakes ruptured along two faults, and the rupture area of the shallower aftershock extended close (<10 km) to the seafloor stations, as shown in Fig. 14. The Tohoku and Nagoya groups observed large coseismic displacements at their stations for the first time in the history of seafloor geodesy (Kido *et al.*, 2006; Tadokoro *et al.*, 2006). Since the two stations were located close to the estimated rupture area, the observed results provided good constraints for the fault model.

The Nagoya group has monitored seafloor crustal movements using the GPSA seafloor geodetic observation technique at three sites in the Kumano Basin (Tadokoro *et al.*, 2012). The results show landward crustal movements of 40 mm/y in the N80W direction with respect to the Amurian Plate. The results show direct evidence for interplate locking during the interseismic period. Assuming a two-dimensional structure, the degree of interplate locking was roughly estimated at 0.6–0.8 on the plate interface, except the area of no observation within about 70 km from the trough axis, as shown in Fig. 15. Considering the large slip distribution of the Tohoku-oki earthquake, the most important area remains to be clarified by seafloor geodetic observation.

The JCG group repeated GPSA observations at six sites in the source region of the 2011 Tohoku-oki earthquake. Five of the six sites are shown in Fig. 16. At MYGI, GPSA measurements were made 7 times during the 3-year period of May 2002 to Apr. 2005, revealing a high degree of interplate locking offshore Miyagi (Fujita *et al.*, 2006). The result agreed well with the slip deficit estimated from land-based GPS observations, as shown in Fig. 1(a), and was interpreted at that time to show the strain accumulation in the seismogenic zone off Miyagi, where earthquakes of *M* 7.4–7.5 had repeatedly occurred. On the other hand, low interplate locking was suggested at FUKU off Fukushima from GPSA observations (Matsumoto *et al.*, 2008).

A *M* 7.2 earthquake occurred in August 2005 near MYGW, and a coseismic displacement of about 10 cm was detected from GPSA observations (Matsumoto *et al.*, 2006). Sato *et al.* (2011a) analyzed the time series of horizontal displacements obtained at MYGW and deduced a cycle of deformation: locking, seismic rupture, postseismic slip for about 2 years, and relocking of the rupture area around 2007.

3.4 GPSA observations related to the Tohoku-oki earthquake

It was a surprise for us that the *M* 9.0 Tohoku-oki earthquake occurred in a subduction zone with a very old incoming Pacific plate. Various coseismic slip models were reported based on seismological, geodetic, and tsunami observations

doi:10.5047/meep.2014.00202.0023

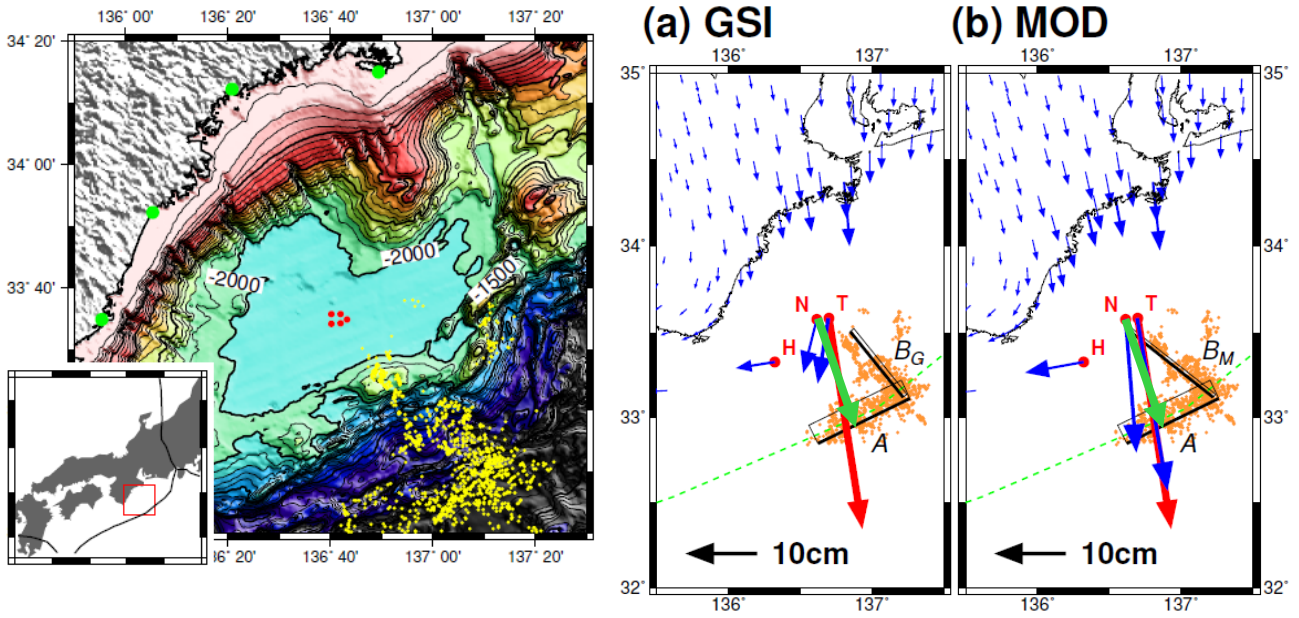

Fig. 14. The map on the left shows the GPSA observation site (five red points) of the Tohoku group in the Kumano Basin, and the aftershock distribution of the 2004 *M* 7-class earthquakes off the Kii Peninsula (yellow dots). Red and green arrows in the figures on the right show coseismic displacement vectors observed by the Tohoku (Kido *et al*., 2006) and the Nagoya (Tadokoro *et al*., 2006) groups, respectively. Blue arrows shows displacement vectors calculated by fault models constrained by (a) terrestrial GPS observation (GSI, 2004), (b) terrestrial GPS and offshore GPSA observations. T, N, H show seafloor stations of the Tohoku, Nagoya, and JCG groups, respectively (modified from Kido *et al*., 2006).

(e.g., Fujii *et al*., 2011; Ide *et al*., 2011; Ito *et al*., 2011a; Koketsu *et al*., 2011; Iinuma *et al*., 2012a). A strike-normal slip distribution became the focus of the discussion, and it was seafloor geodetic data that led to the final conclusion that quite a large slip had occurred in the shallow part of the plate boundary near the trench. This finding had a big impact on seafloor geodesy. In order to understand how the giant earthquake had occurred, and to estimate hazards that may be caused by future large earthquakes and tsunamis, key items are (1) the spatial distribution of coseismic slip, (2) strike-normal and strike-parallel variations in the locking state of the subduction interface, and (3) where and how postseismic deformation proceeds.

Although the seafloor geodetic observation array was limited, it played a key role in the estimation of the slip distribution of the 2011 earthquake. Sato *et al*. (2011b) provided definitive evidence of a large slip based on their prompt GPSA surveys at six sites after the earthquake. Their result showed that the exceptionally large slips were confined to a limited area off Miyagi as shown in Fig. 16. An eastward seafloor displacement of up to 24 m was observed at their easternmost survey site MYGI. Kido *et al*. (2011) reported a larger displacement amounting to 31 m at GJT3 about 50 km from the trench and a smaller displacement of 15 m at GJT4 100 km from the trench (Fig. 16). These observations, as well as vertical data observed with OBPRs discussed in Section 4.1, clearly show strong strike-normal and strike-parallel variations in the locking state of the subduction interface.

The strike-parallel variation was not well resolved by the onshore GPS observations. Iinuma *et al*. (2011) estimated the slip distribution by using GPS data at 345 GEONET stations and 38 Tohoku University stations (Ohzono *et al*., 2012). The results estimated a widely distributed slip with a maximum value of about 35 m along a line about 100 km from the trench. This result was basically the same as that of Ito *et al*. (2011a) from the GEONET data. From seafloor geodesy data, Iinuma *et al*. (2012a) revised the coseismic slip distribution combining the onshore GPS data with the GPSA data at 7 sites and OBPR data at 4 sites. Their result (Fig. 17) shows that a huge (>50 m) slip occurred in a small area (about 40 km in width and 120 km in length) near the Japan Trench and generated the huge tsunami. A significant slip larger than 10 m was estimated in the southern region off Fukushima. No significant slip was estimated for the very shallow (>15 km in depth) or deep (<40 km in depth) portions of the plate interface in this area. The result also shows a detailed distribution of the slip: little slip near the source region of the foreshock two days before the mainshock. In the source region of the earthquake off Miyagi, a large slip of about 10 m was estimated in the northern part, but little slip was estimated in the southern part where a *M* 7.2 earthquake occurred in 2005.

Strike-normal variations in the fault slip and surface displacements calculated by Iinuma *et al*. (2012a) are shown in Fig. 18. Along the WNW-ESE line, shown in Fig. 2, the displacement was 5 m at the Pacific coast and 1 m at the Japan Sea coast. We recognize the importance of seafloor geodetic observations; the displacement on the seafloor is larger than that on land by about one order of magnitude. The horizontal and vertical seafloor displacements along the profile show that GPSA observations are effective for mapping slip, and slip deficit, distributions on the plate boundary. The effect of the slip deficit is observed over a wider area on the horizontal component than on the vertical one due to the low angle of

doi:10.5047/meep.2014.00202.0023

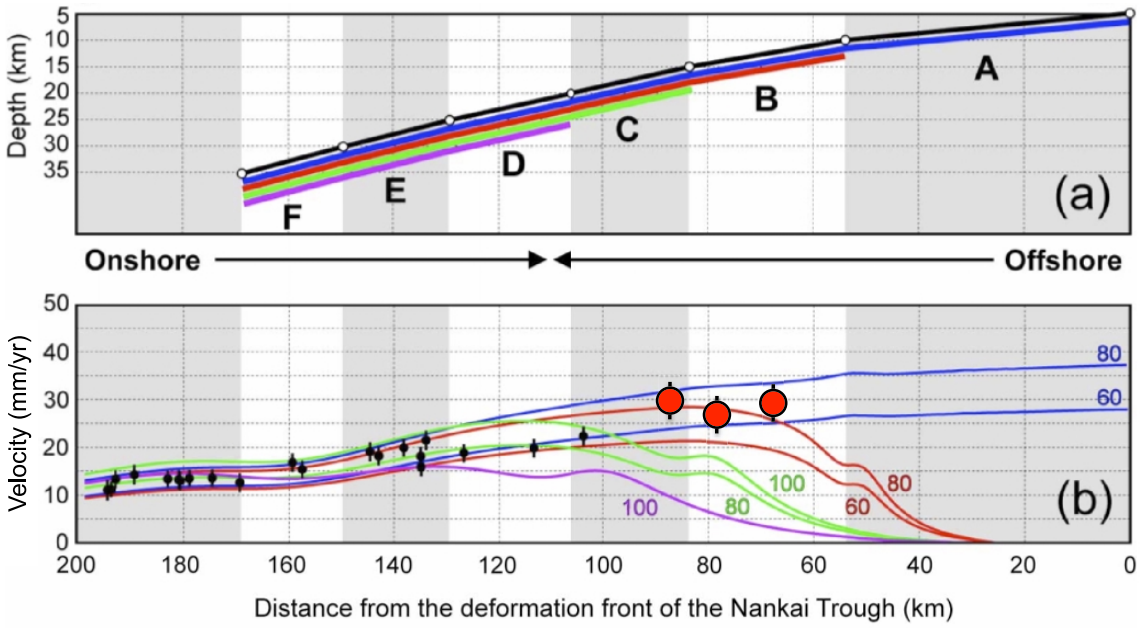

Fig. 15. Degree of interplate locking on the plate boundary of the Nankai Trough estimated from a two-dimensional analysis (modified from Tadokoro *et al*., 2012). (a) Fault geometry (black curve) for calculating theoretical surface crustal deformation. The areas A to F show the plate boundary divided by a depth increase of 10 km. The assumed extent of the locked portion in different models are shown in different colors; blue: from the trough to 35 km depth, red: 10 to 35 km depth, green: 15 to 35 km depth, violet: 20 to 35 km depth. (b) Theoretical surface crustal deformations in the strike-normal direction caused by the interplate locking distributions shown in (a) and coupling ratios (%) denoted by numerical values with different font colors. Solid black and red circles show strike-normal velocities measured on land (GEONET) and the seafloor (GPSA), respectively. Interplate locking in area A about 50 km from the trough is not constrained due to no observation on the seafloor.

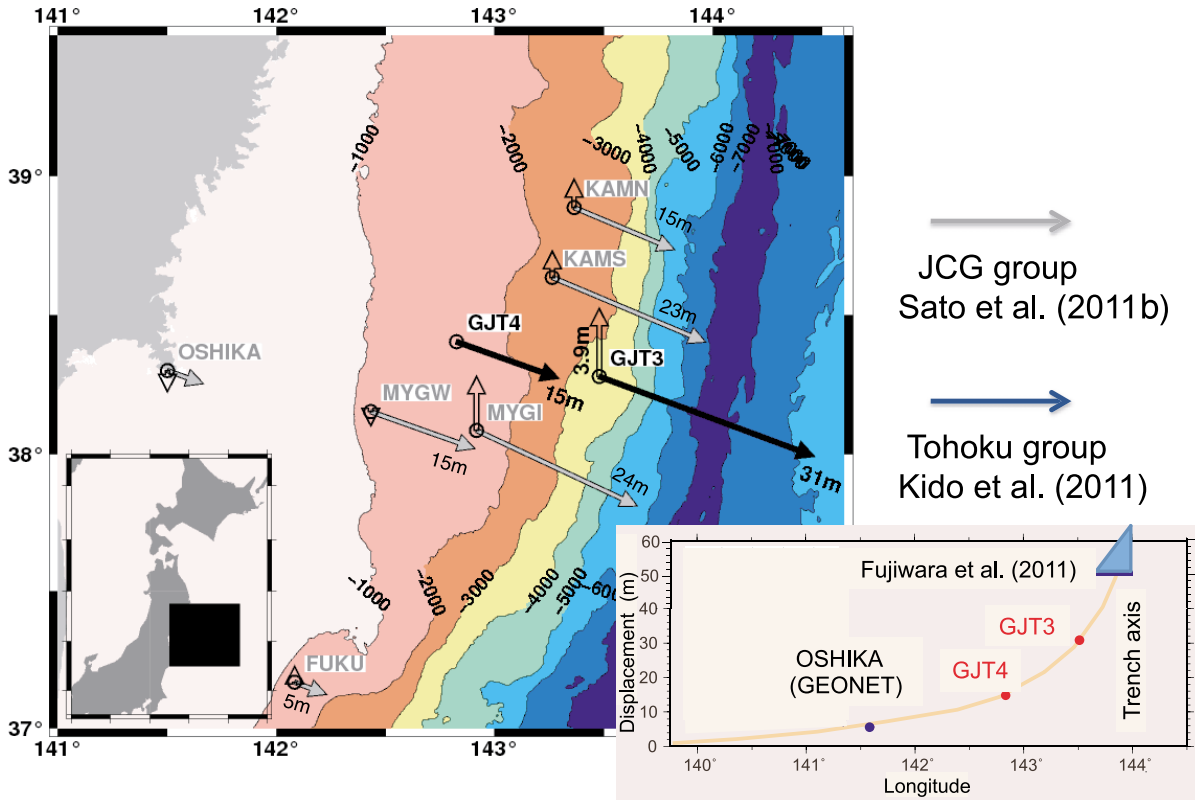

Fig. 16. GPSA observation sites off northeastern Japan and observed coseismic displacements associated with the 2011 Tohoku-oki earthquake (from Kido *et al*., 2011). Five PXPs were installed at the GJT4 site (see Fig. 28), but three of them were not available after the earthquake. The right-hand inset shows the distribution of horizontal coseismic displacements along an E-W line at about 38.3 degrees N estimated from various observations: Oshika from GPS, GJT4 and GJT3 from GPSA, and the value near the trench from bathymetry (Fujiwara *et al*., 2011).

doi:10.5047/meep.2014.00202.0023

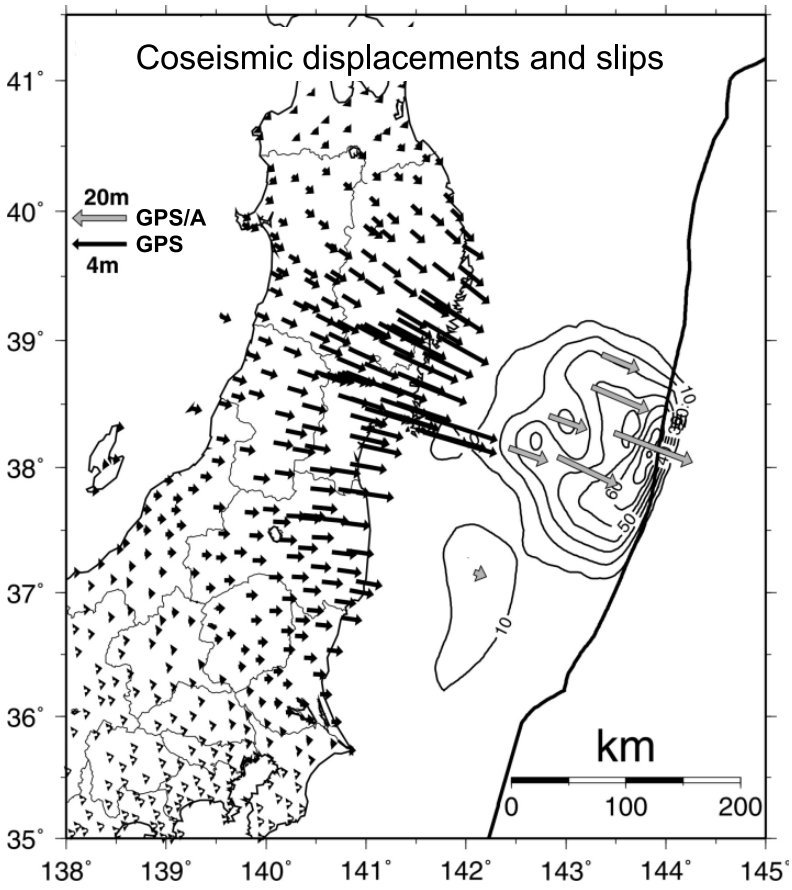

Fig. 17. Coseismic displacements observed by GPS (black arrows) and GPSA (grey arrows), and distribution of coseismic slip (m) on the plate boundary estimated from these observations (courtesy of Dr. T. Iinuma). The contour interval is 10 m.

the plate boundary in the shallow part. On the other hand, vertical observations show relatively local crustal movement and are sensitive to the location of a fault near the seafloor.

Because the onshore and offshore geodetic data suggest a large coseismic slip off Miyagi, the slip distribution obtained by Iinuma *et al*. (2012a) seems fairly good. However, quite high tsunami run-up heights are observed along the northern Sanriku coast. Mostly from tsunami waveform data, Satake *et al*. (2013) estimated that a huge slip occurred near the trench axis 3 min after rupture initiation and extended over a 400-km distance with more than a 10-m slip, at a location similar to the 1896 Sanriku tsunami earthquake, which occurred 100 km north of the largest slip area of the 2011 earthquake. Y. Hamano (personal communication) suggests another pattern of a huge tsunami from the data of seafloor electromagnetic observations on the outer rise of the Japan Trench. Further studies are needed to estimate a coseismic slip distribution that can explain not only seismic and geodetic observations but also tsunami observations.

The distribution of slip deficit on a plate boundary due to interplate locking provides basic information to cope with a probable large thrust earthquake. Onshore GPS observations gave us a rough image of the slip deficit, as shown in Fig. 1, before the Tohoku-oki earthquake. GPSA observations are, for the moment, the most effective to estimate the detailed distribution of interplate locking offshore. One of the critical reasons why the giant earthquake had not been suspected is the lack of information on the locking in the shallow part of the plate boundary. While GPSA observations by Gagnon *et al*. (2005) in the Peru-Chile subduction zone suggested that the shallow part of the plate boundary is locked, few repeating earthquakes had been observed on the shallow plate boundary off Miyagi (Uchida and Matsuzawa, 2011). A low degree of locking was estimated there, and GPSA observations in the area had been delayed.

An alternative interpretation of the result of Gagnon *et al*. (2005) is that the shallow part is not locked, but looks apparently locked due to the interplate locking in a deeper part of the plate boundary. Whether this difference can be observed by geodetic observations on the seafloor, or not, is an important problem. The answer for NE Japan is shown in Fig. 19 (T. Iinuma, personal communication). When the width of the locked zone is 40 km, the predicted horizontal displacement is about 3 cm/yr on the seafloor and 1 mm/yr on land. The locking can probably be detected by GPSA and not by GPS; GPSA observations can identify a difference of 1 cm/yr after repeated observations over a few years.

The tsunami height estimate for the next giant Nankai Trough earthquake has been doubled by the Japanese government since the Tohoku-oki earthquake, chiefly because the previous estimation did not consider the possibility of large slips near the trough. In order to cope with the serious threat

doi:10.5047/meep.2014.00202.0023

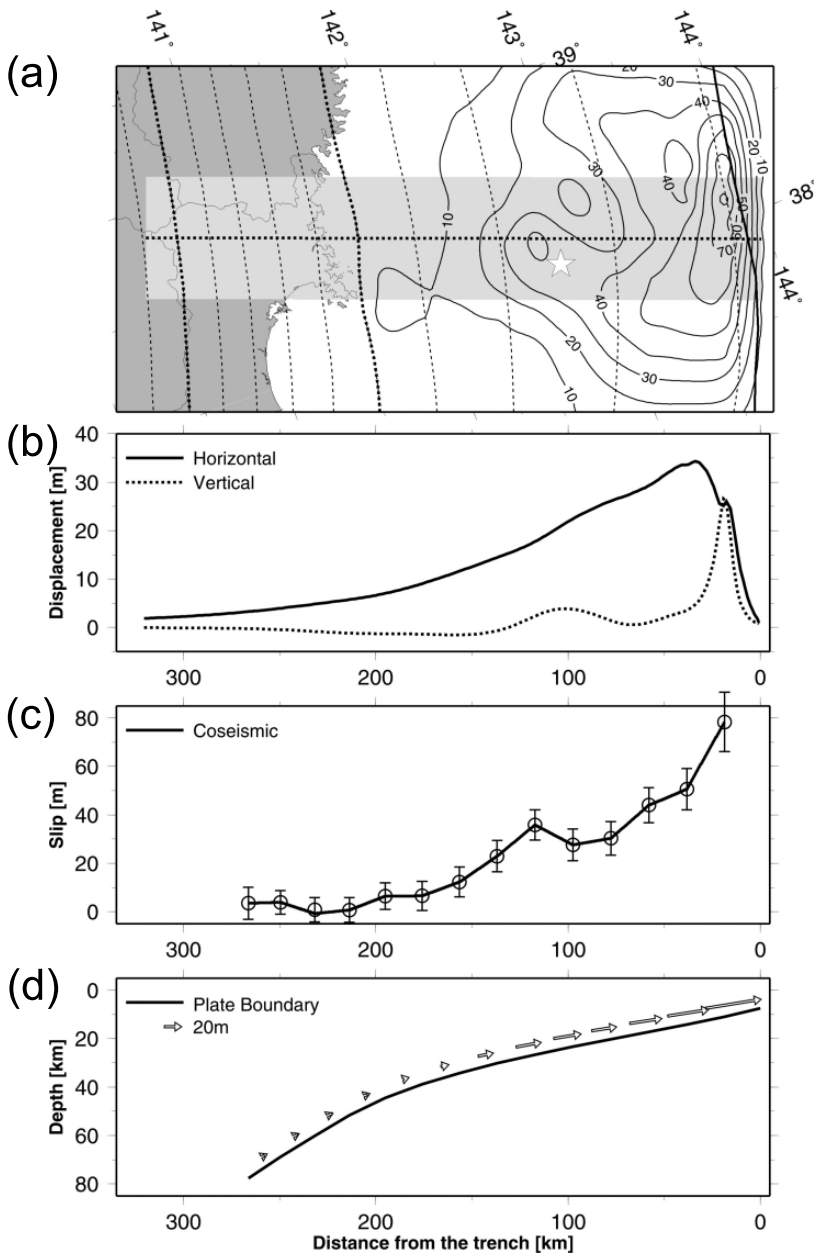

Fig. 18. Strike-normal profiles of estimated horizontal and vertical displacements on the seafloor, as well as the slip distribution on the plate boundary, calculated in the analysis by Iinuma *et al.* (2012a) (courtesy of Dr. T. Iinuma). (a) Coseismic distribution (m) and the line for the profiles, (b) estimated horizontal and vertical displacements on the seafloor, (c) estimated slip distribution on the plate boundary and estimation errors shown by error bars, (d) visual illustration of the slip distribution shown in (c).

of a giant tsunami, expansion of GPSA observations along the Japan Trench and the Nankai Trough should be initiated.

Analyzing the GPS data in the period from 1997 to 2000, and from 2007 to 2010, Suito (2010) reported that the degree of interplate locking off Miyagi and Fukushima in the period after 2007 was significantly smaller than that in the late 1990s. Sato (2012) found that the GPSA data off Miyagi also indicated that interplate locking after 2007 was weak compared with that before the 2005 M 7.2 earthquake. Based on continuous GPS data, Suito *et al.* (2011) estimated that postseismic displacements of the five M 7-class interplate earthquakes that occurred along the Japan Trench before the Tohoku-oki earthquake were much larger than the coseismic offsets. These reports, as well as the two transient slow slip events observed by OBPRs (see Section 4.1), may suggest the gradual weakening of interplate locking. Further studies are needed to understand the geophysical processes that occurred before the giant earthquake.

Observation of postseismic crustal movements is an urgent and important task. Several geophysical models have been proposed to explain the mechanism of the M 9 Tohoku-oki earthquake, e.g., overshooting of the slip by Ide *et al.* (2011), thermal pressurization by Mitsui and Iio (2011), and hierarchy in the interplate locking by Hori and Miyazaki (2011). Unfortunately, it seems that geodetic, seismological, and tsunami observations of the coseismic slip cannot give

doi:10.5047/meep.2014.00202.0023

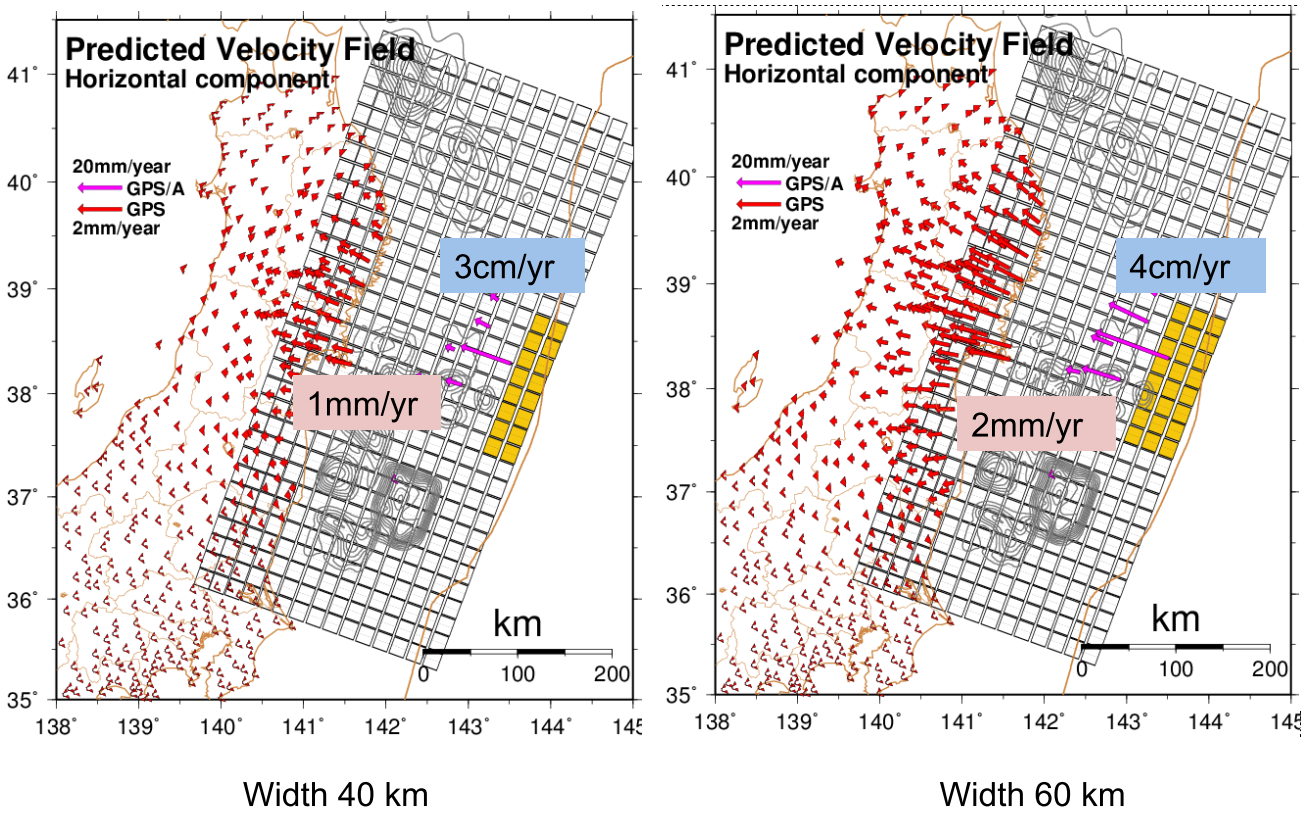

Fig. 19. Result of numerical experiments showing the effect of interplate locking on velocity fields (courtesy of Dr. T. Iinuma). The yellow area indicates the assumed interplate locking zone in the model. The assumed locked zone is (a) 40 km wide, and (b) 60 km wide.

a critical constraint to the models. It is expected that spatial and temporal variations in the postseismic deformation will be the key to solve this problem.

A large afterslip is estimated on the plate boundary near the Pacific coast from terrestrial GPS observations (Ozawa *et al*., 2011). However, GPSA observations in the main focal zone show a complicated distribution. For example, the displacements during a 10-month period were ESE 52 cm at FUKU, and WNW 23 cm at MYGI, as shown in Fig. 20 (Japan Coast Guard, 2012). Osada *et al*. (2012b) reported an ENE displacement of about 1 m at GJT3 in Fig. 16 for one and a half years. It has been found recently that this strange result was due to an insufficient estimate of the change in the relative location of the PXPs after the Tohoku-oki earthquake. The observed OBPR data indicated postseismic gradual depression in the focal zone, but the displacements are rather heterogeneous (see Section 4.1).

Iinuma *et al*. (2012b) estimated postseismic slips near the trench in the north and south of the main thrust zone by using the results of GPSA and OBPR observations. They pointed out that the calculated crustal movements vary significantly depending on the estimated viscosity in the deformation model. It is difficult to obtain a conclusive result for the moment, because most of seafloor geodetic data are confined to the offshore of Miyagi. We need GPSA observations along the Japan Trench, especially near the trench axis, to constrain the overall postseismic crustal movements. As pointed out by Wang *et al*. (2012), monitoring of the viscoelastic process is very important to understanding how mantle rheology affects subduction earthquakes.

3.5 Ongoing and future research activities

(1) Extended GPSA array along the Japan Trench

Considering the need for seafloor geodetic observations, the Tohoku and Nagoya groups have installed 20 new GPSA sites along the Japan Trench in 2012 with funds from the Ministry of Education, Culture, Sports, Science & Technology in Japan (MEXT). These GPSA observation sites cover the deep-sea floor near the trench (Fig. 21). One site is on the Pacific plate and will be used to measure the velocity of the incoming Pacific plate in comparison to the estimated plate velocity (e.g., DeMets *et al*., 1994). The JCG group added 9 GPSA sites along the Nankai Trough as is mentioned below.

PXPs have recently been developed, as shown in Fig. 22, to cope with the following three requirements: (1) observation on the deep-sea floor close to 6,000 m, (2) compatibility among the three institutions in Japan engaged in GPSA observations, and (3) repeated observations for ten years. These requirements were satisfied in collaboration with the manufacturer Kaiyo Denshi Ltd.

Before 2011, the GPSA sites offshore NE Japan were only on seafloor shallower than 2,500 m except the GJT3 site and a site on the outer rise. As mentioned in Section 2.2, the Tohoku group developed PXPs for GPSA observations on the seafloor at 6,000 m water depth on the outer rise jointly with the SIO group. We adopted glass-sphere pressure housings rated to 6,000 m water depth, which are cost effective. It is regrettable

doi:10.5047/meep.2014.00202.0023

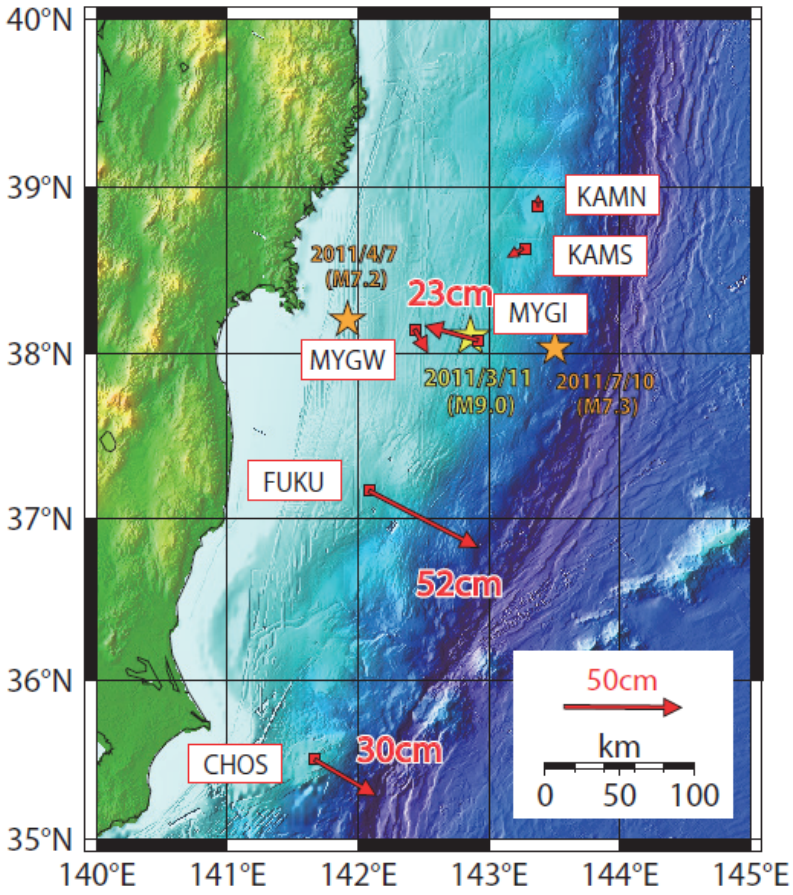

Fig. 20. Distribution of the postseismic displacements obtained from GPSA observations during a 10-month period (from Japan Coast Guard, 2012). While the result at FUKU is similar to that estimated from GPS observation (Ozawa *et al.*, 2011), crustal movements in the main focal zone are heterogeneous.

that we had a problem in the deployment of the PXPs on the outer rise. In 2010, we deployed another set of a PXP array on the outer rise during a cruise. Unfortunately, we could not carry out GPSA observations due to a sudden change in the sea conditions. If the observations had been carried out, we would have had a chance to observe the displacement of the incoming Pacific plate associated with the 2011 Tohoku-oki earthquake.

In 2012, we started GPSA observations at a water depth up to 6,000 m with the newly-developed PXPs. The PXPs are deployed on a relatively flat ocean bottom to minimize the risk of displacement due to earthquakes' ground motion. They are usually arranged on a circle with a radius much the same as the water depth. The slope of the seafloor west of the Japan Trench is, however, generally steep at depths deeper than 3,000 m, and we found that the maximum radius of the circle for the PXP deployment should be about 4 km. GPSA observations are often carried out up to 2 km outside the circle. Then the maximum slant range for the acoustic ranging at a 6,000 m water depth is approximately $((4+4+2)^2+6^2)^{1/2} = 11.7$ km. So we set the maximum range of the acoustic ranging to be 12 km.

An optimal source level was estimated for GPSA observations at slant ranges of 12 km by using Eqs. (5)–(6) (see Section 2.2). We assume that $\alpha = 1.0$ dB/km, $N_{ss} = 52.0$ dB, 5–15 kHz for BW, and 0 dB for DI. Zero dB of SN is the minimum requirement for accurate acoustic ranging. Then, NL = 92.0 dB, and the required value of the source level is estimated to be 185.6 dB relative to 1 μPa at 1 m. Considering the decrease of the output power from the acoustic transducer of 6 dB at 60 degrees from the geometrical axis, we adopted a value of 192 dB for the source level.

A transducer with a cylindrical acoustic element has a problem of a phase change at 45–60 degrees from the geometrical axis. The effect amounts to 1–2 cm in the acoustic ranging (D. Chadwell, personal communication). So we adopted a hemispherical transducer shown as the black unit at the top part of the PXP in Fig. 22. The acoustic element of the transducer has an output power that is about four times larger than the older PXPs.

We carried out a sea trial to examine its performance in the Japan Trench in July 2012 during the R/V Tansei-maru cruise KT-12-16. We deployed four PXPs and examined how far the signal could be transmitted with the required S/N ratio, as shown in Fig. 23. We confirmed that precise acoustic ranging with the four PXPs was performed with little trouble up to a range of 13 km. The first requirement for the PXPs was thus satisfied.

The new PXPs needed to be adaptable for GPSA observations by all the GPSA groups in Japan to increase the

doi:10.5047/meep.2014.00202.0023

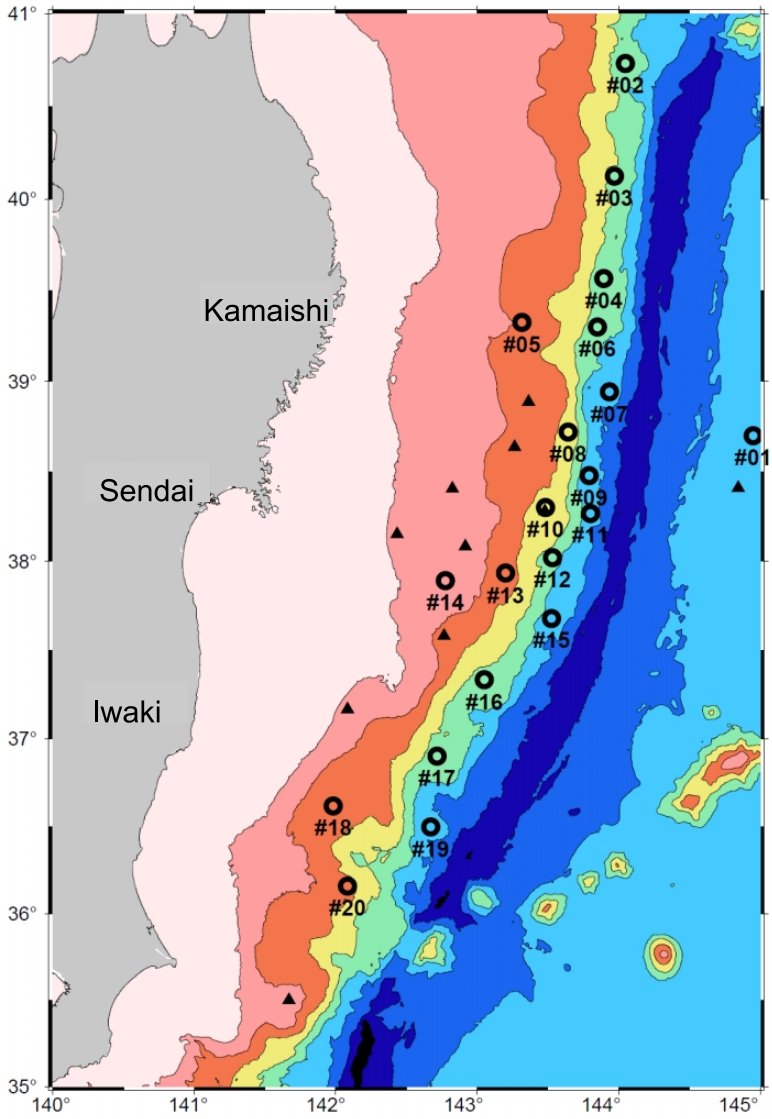

Fig. 21. GPSA observation sites now available along the Japan Trench (courtesy of Prof. M. Kido). Open circles show newly deployed sites and closed triangles show the sites deployed previously. The interval of the depth contours is 1,000 m. The dark blue zone shows the area of water depth deeper than 7,000 m along the Japan Trench axis.

chance of observations and to allow a mutual comparison of the observed results. The acoustic systems of the Tohoku and Nagoya groups were quite different from that of the JCG group, and the development of versatile PXPs was the most difficult task. The JCG group kindly carried out sea trials twice. From the results of the first unsuccessful trial, we deduced that the Doppler effect must be much larger than we estimated. We improved the signal processing of the PXPs through simulating the variable Doppler effect in a water tank of the manufacturer and successfully resolved the problem during the second sea trial.

The third requirement was the capability to carry out repeated observations for ten years. We estimated that one observation requires the transmission of 2,000 signals by each PXP, and that we would make observations three times a year on an average. We transmitted 70,000 relatively long acoustic signals used by the JCG group in an indoor water tank, confirming the capacity of the battery to last for more than 10 years. The electric currents for signal processing during active and inactive periods were measured, and another battery package of required capacity for the signal processing was added to the system.

(2) Improvement of repeatability and efficiency of seafloor positioning

Although GPSA seafloor positioning has become an indispensable geodetic observation, there are big differences between the onshore GPS and offshore GPSA observations such as: (1) the repeatability of the positioning: a few millimeters for GPS versus a few centimeters for GPSA; (2) the number of observation sites in and around Japan: approximately 1,300 versus 60; and (3) real-time continuous observations versus campaign style observations that are conducted 1–3 times a year.

There were 28 GPSA observation sites around Japan when

doi:10.5047/meep.2014.00202.0023

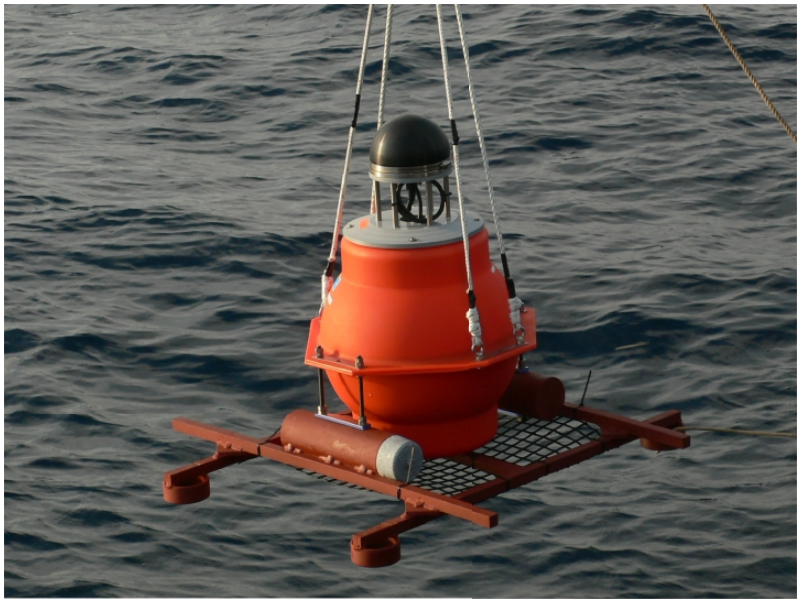

Fig. 22. A precision transponder (PXP) newly developed to expand the GPSA array along the Japan Trench. The hemisphere on the top is an acoustic transducer.

the Tohoku-oki earthquake occurred in 2011, and then the Tohoku and Nagoya groups added 22 sites mostly in the Japan Trench area and the JCG group added 9 sites in the Nankai Trough area, as shown in Fig. 24. GPSA observations at a site have been carried out by using a survey vessel for approximately one day to achieve a repeatability of seafloor positioning within a few centimeters. Therefore, the increased number of observation sites have resulted in a serious problem insofar as getting ship time is concerned for GPSA observations. We have to solve this problem to extend the GPSA array in other areas, such as the Ryukyu Trench.

We estimate that the main problem in GPSA positioning is the lateral variation in the sound speed structure in the ocean, because it directly affects the horizontal position. A simplified explanation of underwater acoustic positioning in GPSA geodetic observations is shown in Fig. 25, assuming four PXPs deployed at a water depth of about 3,000 m and that the sound speed in the ocean is laterally uniform in the layer deeper than 1,000 m. In this example, it is also assumed that the sound speed in the surface layer slightly increases eastward. Sound speeds averaged over the paths from E to A, B, C and D, i.e. V_{EA} to V_{ED}, include the effect of lateral variations in the sound speed in the upper 1,000 m along the ray paths to the PXPs. Suppose that acoustic ranging to each of the PXPs was carried out at E on the sea surface. We first assume that the positions of the PXPs are the same as those determined by the previous GPSA campaign. Assuming a laterally uniform sound speed estimated from a CTD cast, the position of E_1 is obtained from the acoustic ranges to the PXPs. Then, we adjust the average sound speed to obtain the position of E_2 on the sea surface. The position of E determined by KGPS observations is, however, slightly different from E_2 due to two reasons: one is the tectonic movement of the seafloor after the previous campaign observations, and the other is the effect of the sound speed gradient $V_{EB} + V_{EC} > (V_{EA} + V_{ED})$. Thus, we need the lateral sound speed gradient to estimate the crustal movement by GPSA positioning.

Examples of GPSA positioning presumably affected by this problem are shown in Fig. 26. A position on the seafloor is given from every acoustic positioning of GPSA observations near the center of a PXP array. The estimated position varies with errors in the KGPS positioning, the reception of acoustic return signals, the correction for the vessel's motion, and so on. These errors are basically random. On the other hand, lateral variations in the sound speed results in variations in the position with the period of the sound speed variation. The results in Fig. 26 indicate that the sound speed structure in the Nankai Trough area seems to vary with a relatively short period. However, in the Japan Trench area, the period is half a day, induced probably by ocean tides. Therefore, we usually make GPSA measurements for one day at a site to reduce the effect of sound speed variation. Gagnon *et al*. (2005) estimated that the final positions of two arrays changed by less than 1 cm after 80 hours of continuous data collection in the subduction zone off Peru. A key problem, in a practical sense, however, remains to be solved. That is, reducing the observation time required for 1 cm precision to less than a day.

As mentioned above, the JCG and Nagoya groups have coped with this problem by making measurements over a PXP array as uniformly as possible within a relatively short period of 4–6 hours. Then, they average the results over about one day to reduce the effect of horizontal velocity gradients on the seafloor positioning. As of 2011, the JCG group was continuing to make GPSA measurements at 6 sites along the Japan Trench and at 6 sites along the Nankai Trough. They can carry out GPSA observations cruising at several to ten knots by using a vessel equipped with an acoustic transducer on its bottom. Sato (2012) summarized the results

doi:10.5047/meep.2014.00202.0023

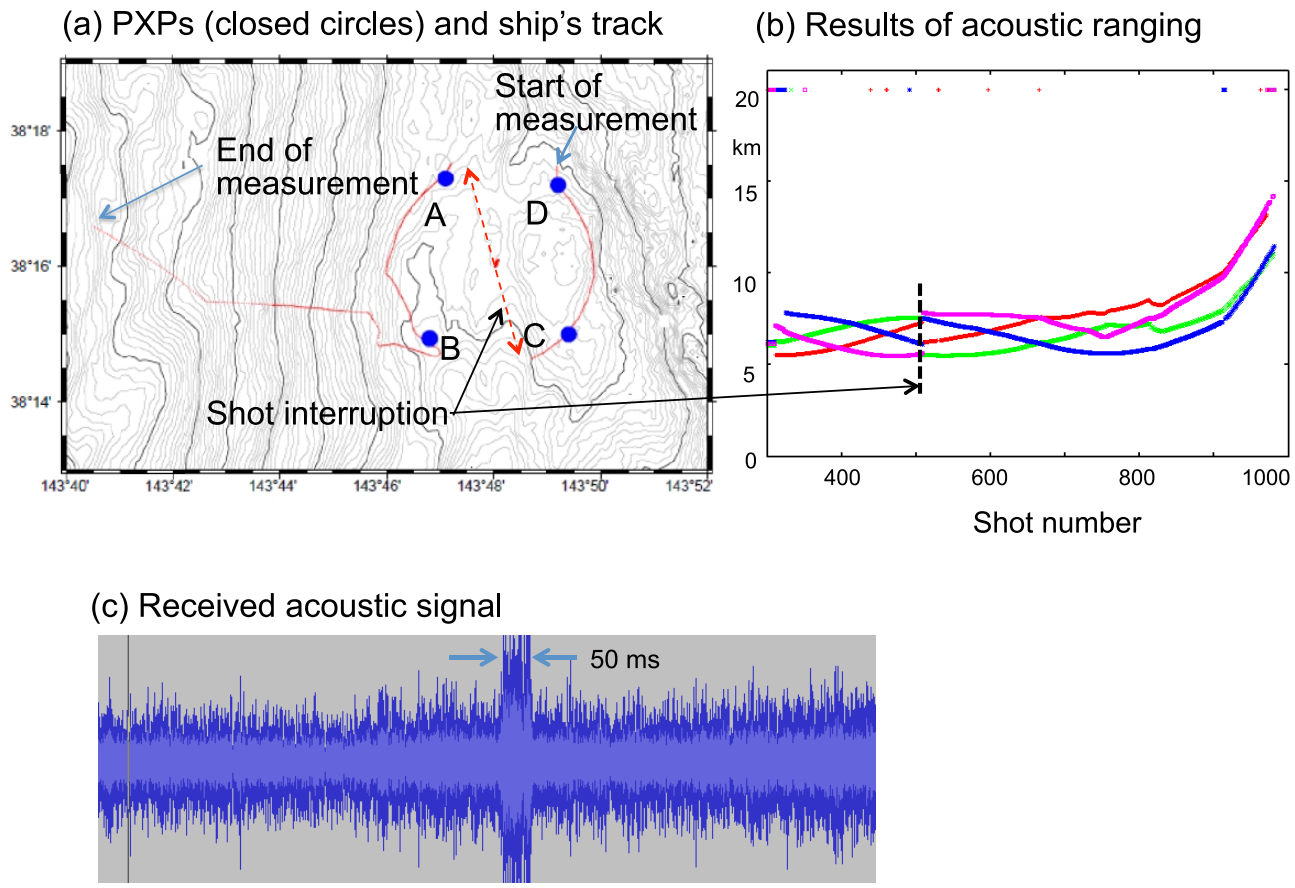

Fig. 23. A result of a trial experiment carried out to evaluate the maximum slant range with the new PXPs (courtesy of Prof. M. Kido). (a) The array of PXPs (closed circles A–D) and the ship's track (red lines). The measurement started near D, was interrupted near C, and restarted near A. (b) Results of acoustic ranging showing reliable ranging up to 13 km. The vertical axis shows the slant range, and the horizontal axis shows the shot number. Slant ranges from the PXPs are shown with different colors; A: green, B: blue, C: pink, D: red. The offsets of the slant ranges at a shot number of about 500 result from the interruption of the measurement between C and A. Some dots at slant ranges of 20 km show unsuccessful observations. (c) An example of a received acoustic wave (a header of 50 ms) showing a sufficient S/N ratio at a slant range of 13 km.

and estimated the repeatability of the seafloor positioning to be about 2 cm in the Nankai Trough area, and about 3 cm in the Japan Trench area. She suggested that the difference resulted from a more complex sound speed structure in the Japan Trench area; the area is one of the major fishing grounds in the world, where cold and warm ocean currents meet. It seems that the method of the JCG and Nagoya groups has been fairly successful in most cases. A problem is that a lateral variation of sound speed is corrected as part of temporal variations, and it causes a positioning error in some cases.

The Tohoku group has used a towed buoy for the GPSA observations and cannot adopt the method mentioned above. Instead, Kido (2007) proposed an approach to estimate the horizontal gradient of sound speed in the ocean simultaneously with the position of a PXP array. The new method requires five seafloor transponders to estimate five parameters: two components of the horizontal position of a PXP array, the average sound speed, and two components of the horizontal gradient of the sound speed. Simplified diagrams in Fig. 27 show one- and two-dimensional cases. Kido (2007) numerically evaluated the geometrical strength of the five transponders' layout and observation point to avoid possible trade-off among the estimated parameters. We carried out an experiment by using five PXPs to examine the proposed method. The result in Fig. 28 shows travel time residuals to five PXPs after reduction of the effect of the temporal variation in the vertically averaged sound speed. The results are compared with the effect of the apparent horizontal displacement of the PXP array center caused by KGPS positioning errors and that of a lateral speed gradient in the ocean. Because errors in KGPS positioning can be detected by inspecting the vertical positions from the sea surface, most of the residual travel times shown in Fig. 28(a) might be caused by the lateral gradient of the sound speed. However, these results suggest that there are fairly local and short period variations in the sound speed common among a few PXPs, and the effect can be only partly removed by this analysis.

Another idea for estimating the lateral sound speed variation was proposed by the Nagoya group (Tadokoro *et al.*, personal communication). They plan to carry out an experiment using a few anchored buoys, instead of adding PXPs, to measure the lateral variation in the sound speed. This method is reasonable because the sound speed varies mostly in the shallow part of the ocean, but it is not efficient due to the time required for the deployment and the recovery of the buoys on the deep-sea floor. The Tohoku group plans

doi:10.5047/meep.2014.00202.0023

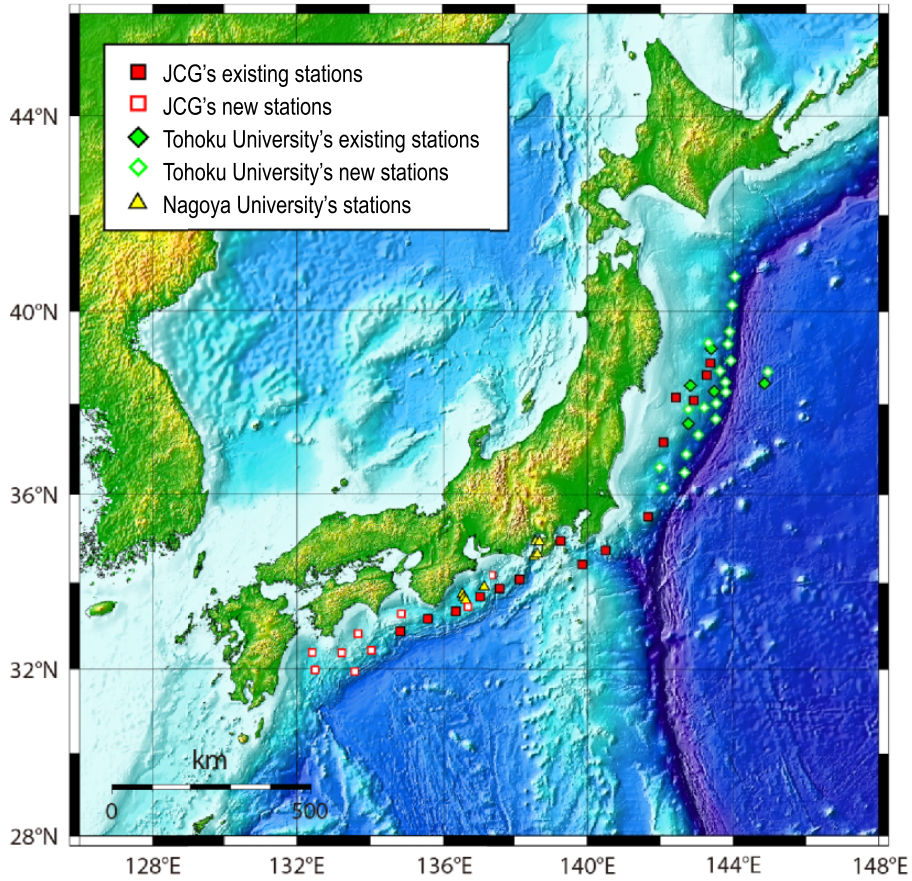

Fig. 24. GPSA observation sites around Japan as of December 2012 (courtesy of Dr. M. Sato). The sites at the northernmost closed green diamonds and two of the easternmost yellow triangles have ceased to work due to exhausted batteries.

to realize the idea by using autonomous surface buoys. We are trying to use a self-navigating vehicle shown in Fig. 29. This can move at a maximum speed of three knots for 2 days with the power of a diesel engine (Burton and Dobbin, 2013). It has been confirmed that acoustic noises under the vehicle are quite low when the engine is turned off, and are moderate when it is on. A Wave Glider^{TM} shown in Fig. 30 is an alternative to the surface buoy, if the ocean currents are not strong. The glider can sail at a maximum speed of 1.5 knots powered by sea waves. We can monitor the ships nearby the glider and can let it avoid a ship that is coming close to it. Solar batteries and an additional regular battery can supply the power required for GPSA observations. The Japan Agency for Marine-Earth Science and Technology (JAMSTEC) has deployed a Wave Glider near the Japan Trench in September 2013 as an experiment into maintaining the glider's position for half a year (Y. Hamano, personal communication). It has survived in the rough seas of a few typhoons, but it seems that maintaining its position in a small area is difficult due to its limited maximum speed.

We plan to carry out GPSA observations using a ship and a buoy, each of which is equipped with a GPSA system as shown in Fig. 31. We assume the case shown in Fig. 25 where the sound speed increases eastward in the upper 1,000 m. One of the two vehicles will remain near the center of a PXP array (E), and the other about 700 m to the west (F) for a precise measurement of the longitude of the PXP array. The sound speeds in the surface layer along the ray paths to the PXPs (V_{EA} to V_{ED} and V_{FA} to V_{FD}) include deviations from the laterally uniform value. We can measure sound speed variations e.g., $V_{EB} - V_{FB} = \delta V_{EB}$, and $V_{EC} - V_{FC} = \delta V_{EC}$, by nearly simultaneous acoustic measurements combined with KGPS positioning at E and F. In this measurement, the effect of a displacement of the seafloor, after the previous GPSA campaign, is negligible. The lateral sound speed gradient that affects the E-W seafloor positioning can be calculated from the difference between $V_{EB} + V_{EC}$ and $V_{EA} + V_{ED}$. Considering the similar location of the ray paths shown by the dotted lines, we can estimate $V_{EA} \sim V_{FB}$, and $V_{ED} \sim V_{FC}$. Then $V_{EB} + V_{EC} - (V_{EA} + V_{ED}) = V_{EB} + V_{EC} - (V_{FB} + V_{FC}) = V_{EB} - V_{FB} + V_{EC} - V_{FC} = \delta V_{EB} + \delta V_{EC}$. Thus, an approximate effect of the sound speed gradient on seafloor positioning can be estimated. By changing the position of F relative to E and making simultaneous measurements at E and F, we can estimate two components of the sound speed gradient. We can reduce the observation time with this approach without averaging the observed results over a one-day period. If two self-navigating buoys, as well as a ship, are available, a precise position can be obtained at each acoustic positioning. We plan to carry out an experiment to validate this method. We hope to realize a precision of about 1 cm within two hours of observations. If we require one hour

doi:10.5047/meep.2014.00202.0023

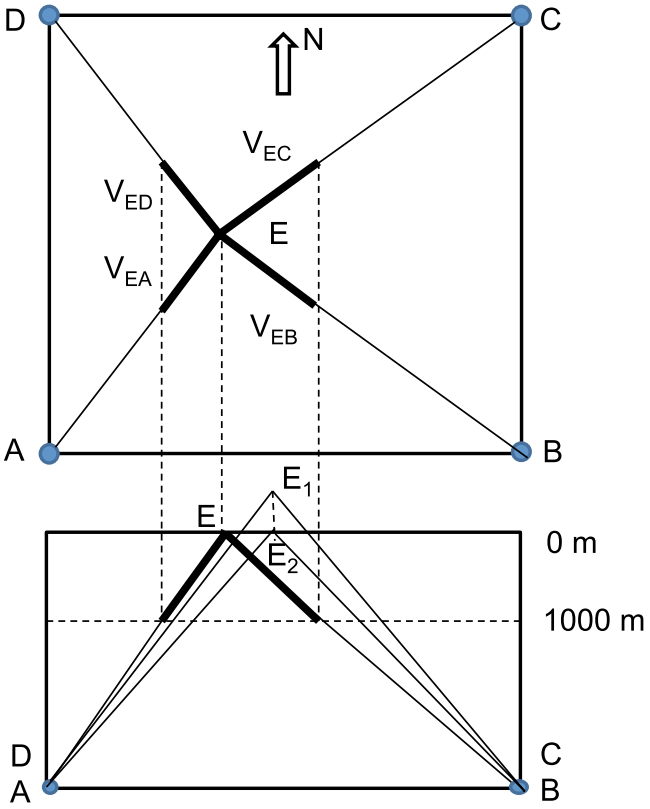

Fig. 25. Simplified explanation of underwater acoustic positioning in the case of GPSA geodetic observations on the seafloor at 3,000 m water depth. The sound speed is assumed to be laterally uniform in the layer deeper than 1,000 m, and increases eastward in the upper layer. The thin dotted lines show the depth of 1,000 m. E: the location of an acoustic transducer of the sea surface unit. The diagram on the bottom shows the E-W positioning in a vertical profile. See the text for more detail.

for the deployment of the two buoys and one hour to recover them, we can complete the GPSA observations at a site in about four hours. Considering four hours to be the average transit time between two GPSA sites shown in Fig. 21, we can carry out observations at three sites in a day.

The Japan Trench area is, however, a major fishery field, and many fishing nets longer than 10 km are used there. Vehicles maintaining their positions might be caught in a fishing net. If there was no such risk, and if a revised surface glider had a maximum speed higher than 2 knots, we would carry out GPSA observations using 3 wave gliders without a survey ship; after observations at a given PXP array, a set of three vehicles would move to the next PXP array by themselves. A pair of two gliders can also remain above a PXP array for long-term observations. We hope to carry out trial experiments with two autonomous surface buoys upon consultation with fishermen.

(3) An approach to real-time continuous observations

Being able to conduct real-time continuous measurements is an even more challenging goal of marine geodetic observations. A realistic target at the moment is to obtain a daily position of the seafloor. There are two major problems with semi-real-time GPSA observations. Firstly, the GPSA observation needs a sea surface vehicle, a moored buoy or a self-navigating buoy, for GPS positioning. The vehicle should survive in rough seas associated with typhoons, or strong winds in the winter season. As discussed above, a single vehicle is not enough for the precise positioning of a PXP array in a short period of time.

The second problem is precise GPS positioning. The KGPS method requires the transmission of the GPS data from the sea to the coast to process the data in combination with those obtained at a land station. Radio bands are strictly controlled in Japan, and wireless communication is available only 10–20 km offshore. The alternative is to use highly expensive satellite communication. With this approach, we would need to reduce the data volume. We tested how the volume of the GPS data could be reduced assuming 2 Hz sampling with 3 GPS receivers (M. Kido, personal communication). The data volume from a receiver at 1 Hz sampling is approximately 3.6 MB/hour = 1 kB/s = 8 kbps. If we use a standard compact format, the volume can be reduced to 1/10. Then the bit rate is 8,000 (bps/Hz/receiver) × 2 (Hz) × 3 (receivers) × 0.1 = 4,800 (bps). Acoustic data are smaller by one order of magnitude; if an acoustic signal of 30 ms from 4 PXPs is sampled at 100 kHz with 4 bits, the data volume is 100,000 × 0.03 × 4 × 4 = 48,000 bits. If acoustic positioning is once per minute, the bit rate is 48,000/60 = 800 (bps). It is true that there are commercial services of satellite communication that support a bit rate higher than 4,800 bps, but the huge cost involved is out of the range of our funding.

A kinematic precise point positioning (KPPP) technique for GPS can be used with a reduced precision of positioning. It requires the information of the clocks and the orbits of the GPS satellites. The volume of data is smaller than the observed GPS data, but it is still too large to be transmitted through satellite communication.

"Real-time KPPP", which receives the clock and orbit information from a commercial satellite, is a possible solution to obtain the daily seafloor position with a precision of a few centimeters. The "StarFire™" global subscription service, based on the real-time GIPSY software (Bertiger *et al.*, 1999), has been developed for commercial purposes. Receiving globally corrected signal via geostationary satellites, the precise real-time KPPP is realized without the need for local ground base stations. Yamamoto *et al.* (2013) assessed the stability of the kinematic solution of a station on land in October 2012. They confirmed that the standard deviation of the time series of the real-time KPPP is less than 1.8 cm, and that the horizontal position is within 2 cm from the daily position deduced from the GIPSY-OASIS II software, which we use for the KGPS positioning.

4. Ocean Bottom Pressure Observation

4.1 Instruments and some results of observations

The ocean bottom pressure (OBP) varies with seawater mass above the seafloor, and its monitoring has been important in both physical oceanography and seafloor geodesy. The pressure due to seawater mass of a unit thickness is given by the density multiplied by gravity. Assuming seawater density of 1,030 kg m^{-3} and gravity 9.80 m s^{-2}, a local seafloor uplift by 1 cm results in a pressure decrease by 1.01 hPa. Such

doi:10.5047/meep.2014.00202.0023

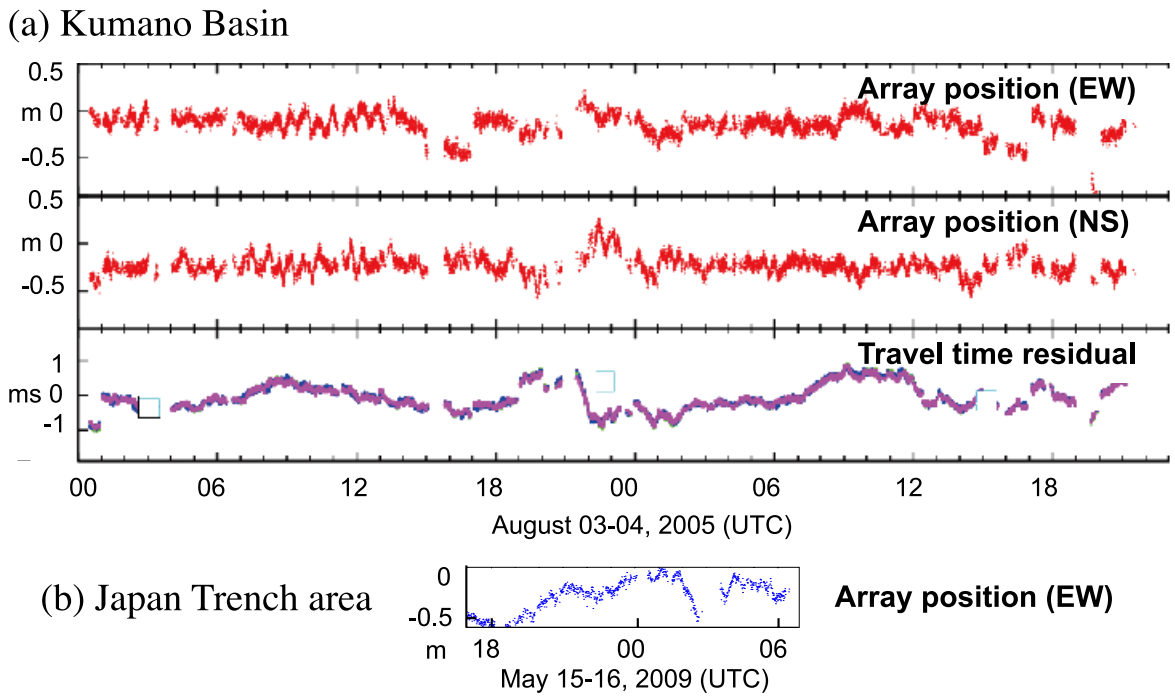

Fig. 26. Examples of GPSA positioning probably affected by the lateral variation in the sound speed structure in the ocean (courtesy of Prof. M. Kido). (a) Temporal variations in the PXP array position and vertically averaged travel time residuals obtained by GPSA observations for two days in Kumano Basin. (b) Temporal variations in the EW position observed off Miyagi in the Japan Trench area are shown at the same scale as (a).

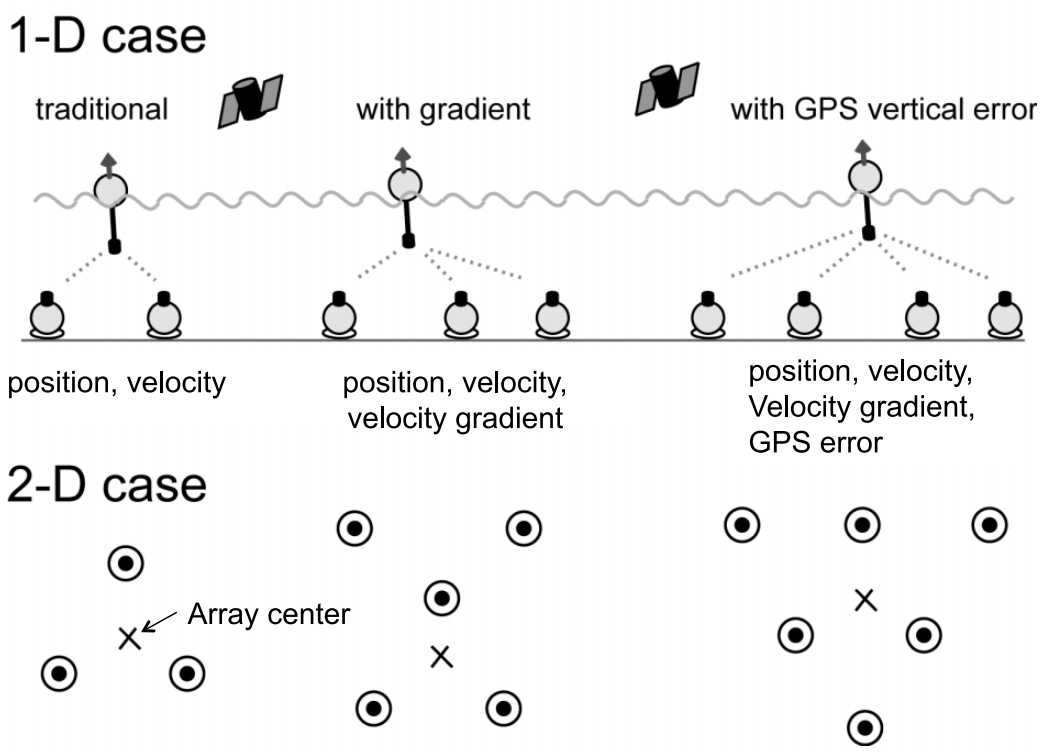

Fig. 27. Simplified diagrams in one- and two-dimensional cases showing the concept to estimate the horizontal gradient of the sound speed in the ocean simultaneously with the position of a PXP array (courtesy of Prof. M. Kido). The number of estimated parameters increases with the number of PXPs. The cross in each array denotes the array center.

doi:10.5047/meep.2014.00202.0023

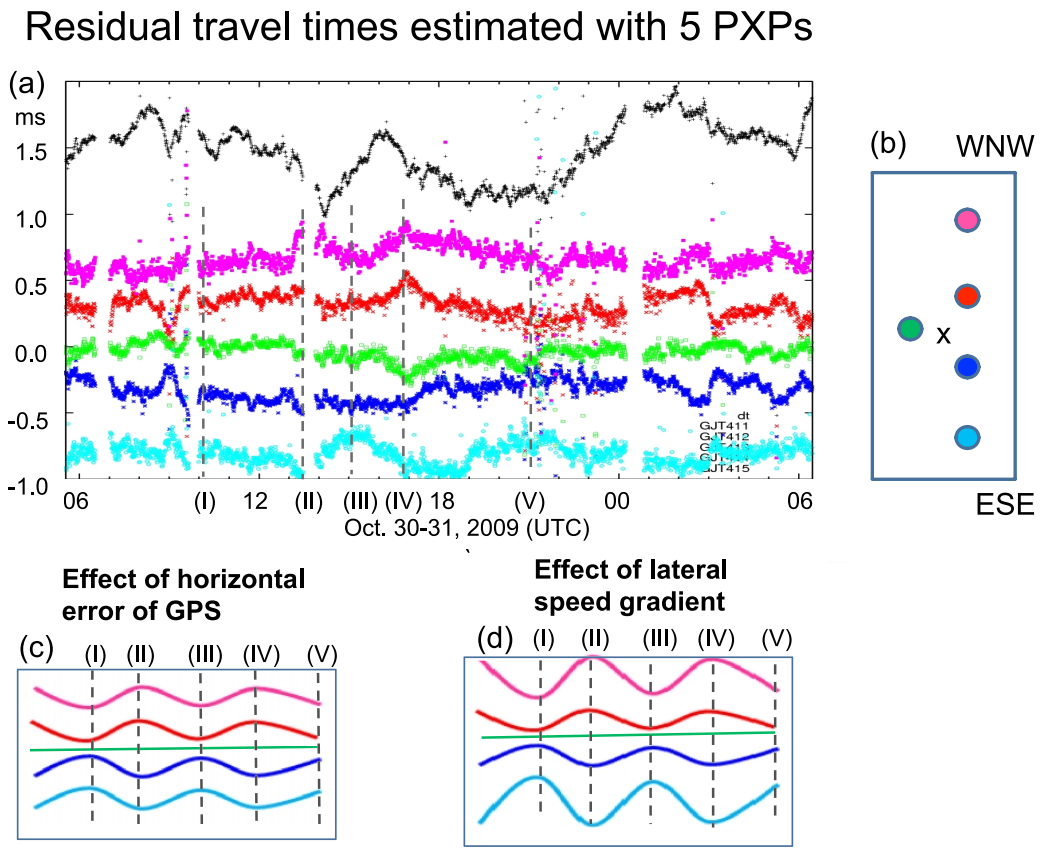

Fig. 28. (a) Temporal variation in the travel time residuals to five PXPs observed in 2009 at GJT4 shown in Fig. 16 (courtesy of Prof. M. Kido). Black dots show the effects of variations in the average sound speed on the residuals derived from the analysis without assuming a lateral variation of sound speed. Residual travel times to five PXPs are corrected for these effects in the process E_1 to E_2 in Fig. 25, and are shown with color dots. Each vertical position is shifted for the convenience of display. The results must be affected by the horizontal translation of the PXP array and the lateral variation of sound speed. (b) A simplified map showing the relative location of the five PXPs deployed in the strike-parallel direction. The color of each PXP corresponds to that of the dots in (a). The cross denotes the PXP array center where the GPSA observations were carried out. (c) The effect of apparent horizontal displacement of the array center caused by a horizontal error of the KGPS positioning on residual travel times to the five PXPs. (d) The effect of the lateral gradient of the sound speed on the residual travel times. The variations at the times of the vertical dotted lines (I to V) show similar features with those in (a) to a certain extent.

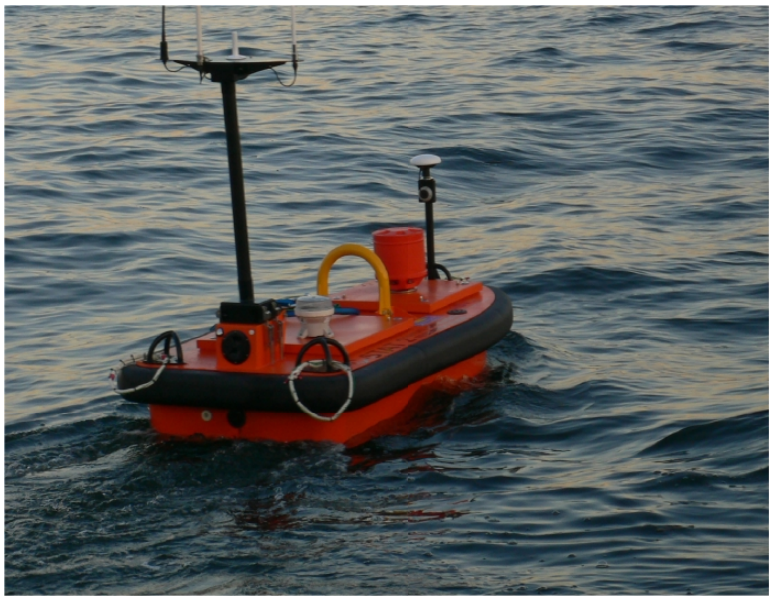

Fig. 29. A photo of a self-navigating vehicle CSTAT-2 taken during the Kaiko III cruise off Tohoku in August 2013. It was manufactured by ASV (Autonomous Surface Vehicles Ltd.), UK. It is powered by a diesel engine, and is equipped with a GPS antenna, a motion sensor, and an acoustic unit.

doi:10.5047/meep.2014.00202.0023

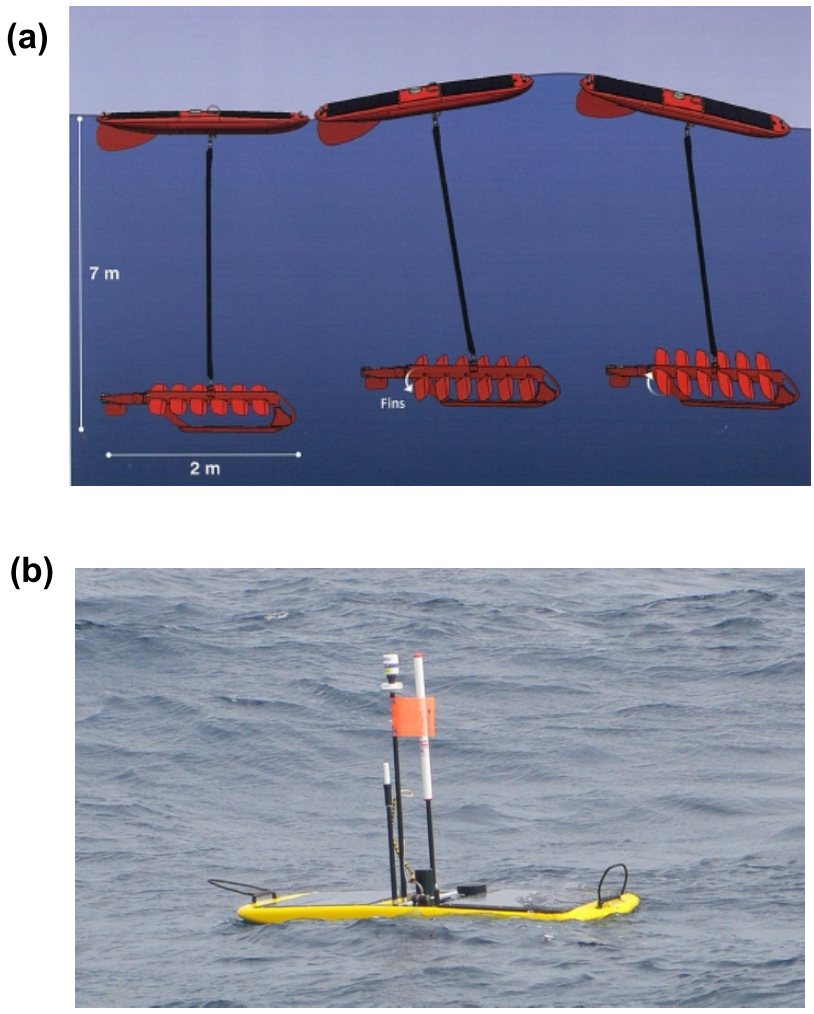

Fig. 30. (a) Concept of a Wave Glider™ that makes use of wave energy as its propulsion source (http://liquidr.com/technology/wave-motion.html). (b) A photo of a wave glider on the sea surface taken during the Yokosuka YK13-7 cruise in September 2013.

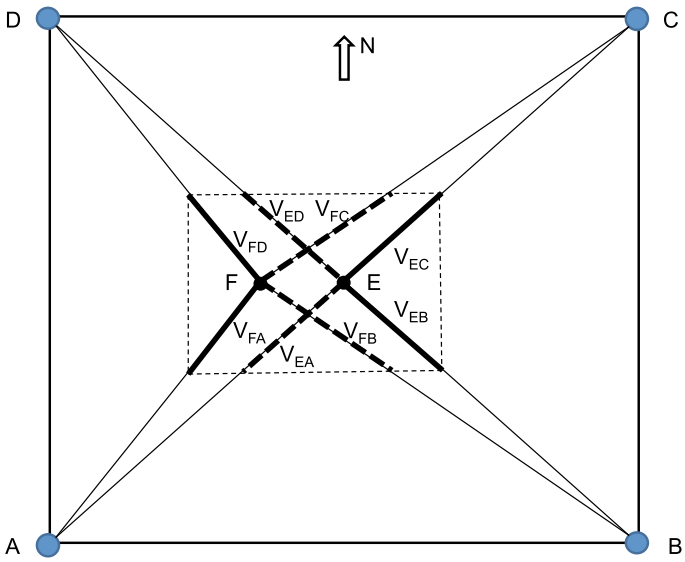

Fig. 31. A simplified map showing the concept of a precise measurement of the longitude of the PXP array, assuming the same sound speed structure as in Fig. 25. Sound speed is assumed to be laterally uniform in the layer deeper than 1,000 m, and to increase eastward in the upper layer. The sound speeds in the surface layer along the ray paths to the PXPs (V_{EA} to V_{ED} and V_{FA} to V_{FD}) include deviations from the laterally uniform value. See the text for more detail.

doi:10.5047/meep.2014.00202.0023

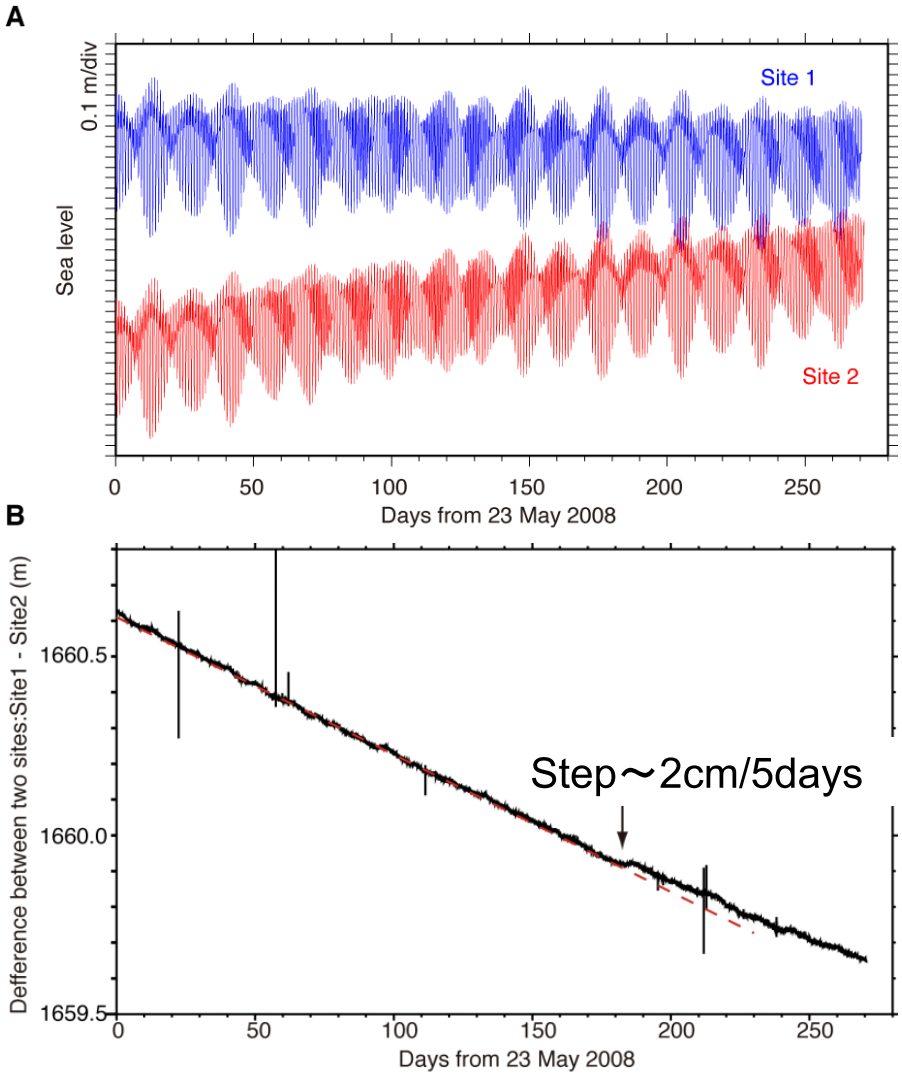

Fig. 32. An example of pressure data showing that a simple difference between the time series observed at two sites can detect a small step suggesting relative vertical crustal movements (courtesy of Dr. Y. Ito). (a) Ocean bottom pressure data expressed in terms of water depth observed at two sites for about 9 months. (b) Relative variation between the two time series.

an observation can be continuous with a simple system of OBPR. While acoustic ranging on the seafloor is useful for the observation of a horizontal crustal movement, an OBPR array can detect relative vertical movement (see Fig. 6).

Quartz-oscillator-based pressure sensors have been used most widely for OBPRs because of their high resolution of less than 0.1 hPa, as well as their long-term stability. Paroscientific Digiquartz pressure sensors are very popular now. They measure pressure with a temperature-insensitive quartz oscillator and simultaneously measure temperature with a temperature-sensitive oscillator (Paros, 1983). The two sensors are closely arranged in order to correct the temperature effect accurately. A bourdon tube transmits the bottom pressure to the quartz oscillator (Paros, 1984), and this mechanism is subject to gravity; the pressure value varies by about 10 hPa if the sensor is installed horizontally and if it is rotated around its axis.

Although ocean tide is the most prominent cause of variation in ocean bottom pressure, its effect can be accurately corrected using an ocean tide model (e.g., NAO.99b, Matsumoto *et al.*, 2000) or harmonic analysis (e.g., BAYTAP-G, Tamura *et al.*, 1991) owing to the precisely determined periods of the tidal components. Atmospheric pressure variation is basically compensated at the sea surface, and its effect on bottom pressure is usually neglected. Although water masses in the ocean are basically in a state of isostatic compensation, ocean dynamics such as ocean currents and mesoscale eddies cause pressure variations of 5–10 hPa.

An important problem is that observed pressure variations show the combined effects of ocean and crustal dynamics. A simple way to solve the problem is to use a small array of OBPRs. The horizontal scale of ocean dynamics is much larger than that of the array. For example, the horizontal scale of a mesoscale eddy is a few hundred kilometers. The scale of a local OBPR array is smaller by one order of magnitude. Then the effects of ocean dynamics on a local OBPR array would be reduced (Fujimoto *et al.*, 2003). Another approach to this problem is discussed in Section 4.2.

doi:10.5047/meep.2014.00202.0023

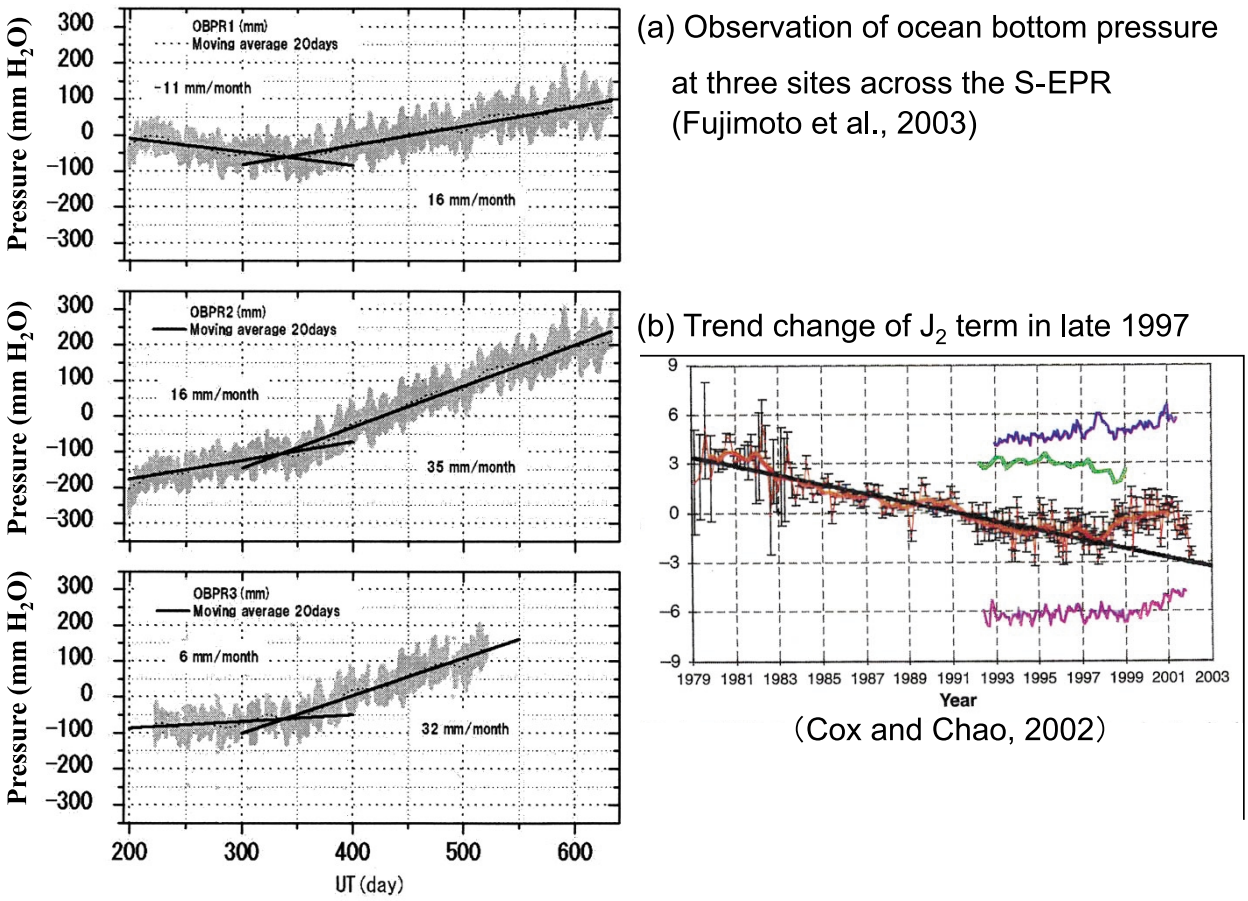

Fig. 33. (a) Ocean bottom pressure observation across the S-EPR at 18 degrees S (July 1997–September 1998). The horizontal axis shows days from Jan. 1, 1997. The trend changed simultaneously at three sites in late 1997: OBPR1 on the eastern bank, OBPR2 in the axial valley, and OBPR3 on the western bank (modified from Fujimoto *et al*., 2003). (b) The change in the trend of the J_2 term in late 1997 (from Cox, C. M., and B. F. Chao (2002), Detection of a large-scale mass redistribution in the terrestrial system since 1998, *Science*, *297*, 831–833, reprinted with permission from AAAS).

If there is an abrupt change in the relative pressure, it would show a relative vertical displacement between two sites. A beautiful example of such a result is shown in Fig. 32. A simple difference between the two time series shows a simple trend and a small step of about 2 cm over the course of several days (Ito *et al*., 2013). The step shows a slow slip event detected in the Japan Trench area for the first time as discussed below.

This type of pressure observation has been pursued to monitor crustal activities in the spreading center of mid-ocean ridges. OBPRs were deployed every year since 1987 at depths around 1,600 m in the summit caldera of Axial Seamount, an active submarine volcano on the Juan de Fuca Ridge in the northeast Pacific Ocean. They observed small deflation events of 10 cm or less in magnitude several times during a five-year period (Fox, 1990, 1993). Then in January 1998, two OBPRs measured large crustal displacements associated with a major dike intrusion and an eruption of Axial Seamount: subsidence of the seafloor by 3.2 m in the center of the caldera and 1.4 m near the center (Fox, 1999; Fox *et al*., 2001). Analyzing the OBP data after the eruption, Chadwick *et al*. (2006) estimated the rate of the inflation of the volcano. The uplift rate in the center of the caldera declined from 20 cm/month in the months immediately following the eruption to a steady rate of 15 cm/year. The total uplift during the 6-year period was about 1.5 m, about half of the subsidence at the eruption.

Based on 14 months of observations with three OBPRs across the spreading center of the East Pacific Rise in the southeastern Pacific, we detected the effects of both ocean and crustal dynamics (Fujimoto *et al*., 2003). One is a simultaneous pressure increase at three sites starting in December 1997 (Fig. 33(a)) at almost the same time as the termination of the 1997–98 El Niño. It is also coincident with a remarkable change in the J_2 term of the Earth's gravity field (Cox and Chao, 2002) shown in Fig. 33(b). These results suggest that the El Niño might have brought about a mass redistribution in the eastern Pacific Ocean, as was suggested by Dickey *et al*. (2002).

We have recently received a comment that the abrupt changes in the observed pressure variations might be mostly due to crustal deformation because, (1) sea surface height (SSH) near the study area was relatively stable in late 1997, (2) Kelvin wave activity at 18 S was weak relative to the equator, and (3) OBP data did not return to "normal" after the upwelling trade winds returned to normal in 1998 (S. McK-

doi:10.5047/meep.2014.00202.0023

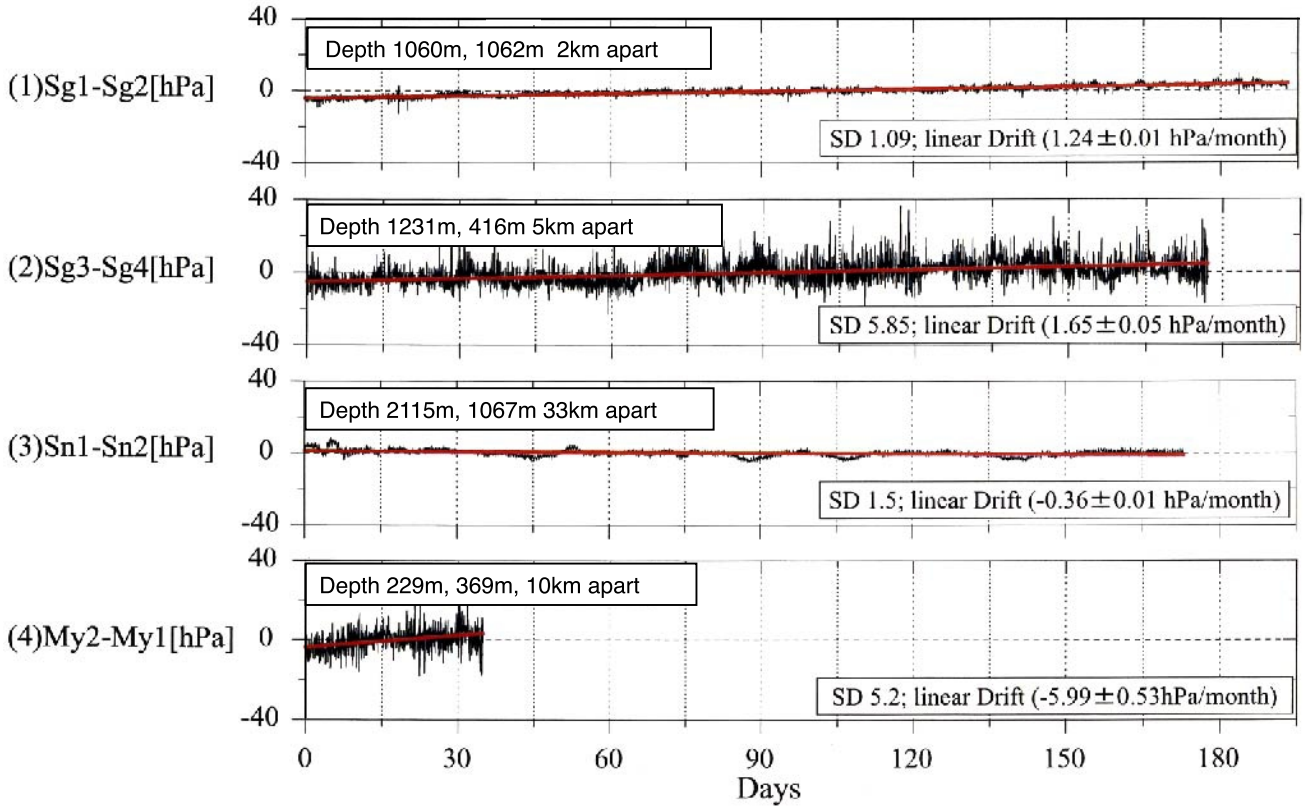

Fig. 34. Examples of differential pressure variations. Three time series for about half a year at distances of 2–33 km indicate a small difference between the drift rates of two Paroscientific pressure sensors. The short record on the bottom suggests a large drift rate in one of the OBPRs. The data are interpreted to indicate a crustal movement on the seafloor associated with volcanic activity of Miyake Island, Izu-Ogasawara ridge, in 2001 (Tamaki *et al*., 2002).

innell, personal communication). The OBP observation was carried out as one of many geophysical and geochemical observations across the S-EPR under the JAMSTEC MODE'97 Project. There was no observed data suggesting any tectonic or volcanic activity. For example, the continuous horizontal acoustic ranging across the spreading center (Nagaya *et al*., 1999), mentioned in Section 2.3, showed quite stable values throughout the observation period. The cause of the abrupt change is yet to be resolved.

The other interesting feature in Fig. 33(a) is the difference in the rate of secular pressure variations among the three sites. The result suggests subsidence in the middle and western part of the spreading center; a deep magma source is estimated beneath the western part of the spreading center from the MELT experiment (Forsyth *et al*., 1998). The apparent subsidence of 2 cm/month can be quantitatively estimated assuming thermal contraction of the crust after the previous spreading event (Fujimoto *et al*., 2003).

The long-term stability of a pressure sensor is a serious problem in the analysis of long-term variations in ocean bottom pressure. A quartz oscillator has a good long-term stability in general, and the frequency of its vibration changes exponentially or approximately linearly with time. We call the linear trend the drift rate of the sensor. Studying the drift of Digiquartz pressure sensors, Wearn and Larson (1982) showed that the drift is smooth, monotonic, reproducible, and reversible. This study suggests that the drift can be accurately estimated (Hino *et al*., 2009). An example of the drift rate is shown in Fig. 34. Three time series of the relative pressure variation for about half a year at distances of 2–33 km show the difference between the drift rates of two OBPRs. Judging from the results of more than 10 pressure sensors, most of the drift rates of pressure sensors are in the range -1 to $+1$ hPa/month (Fujimoto *et al*., 2003).

The calibration of the drift rates of the pressure sensors during an observation has been realized by Chadwick *et al*. (2006). They have carried out campaign-style pressure measurements every year since 2000 at an array of OBPRs with a mobile pressure recorder equipped with three pressure sensors mounted on a remotely operated vehicle. The repeatability of the pressure measurements progressively improved each year from 15 hPa in 2000 to 0.9 hPa in 2004, as errors were eliminated and the technique was refined. Their report shows that it is possible to measure the small vertical crustal movement of an overlying plate in a subduction zone; for example, subsidence at a rate of about 1 cm/yr is estimated landward of the Japan Trench (T. Iinuma, personal communication). If this method is applied to a cabled OBPR array, long-term pressure monitoring can be a new approach to the study of interplate locking on the plate boundary. Continuous observation can also detect gradual crustal movements such as slow slip events. In particular, a cabled OBPR array can

doi:10.5047/meep.2014.00202.0023

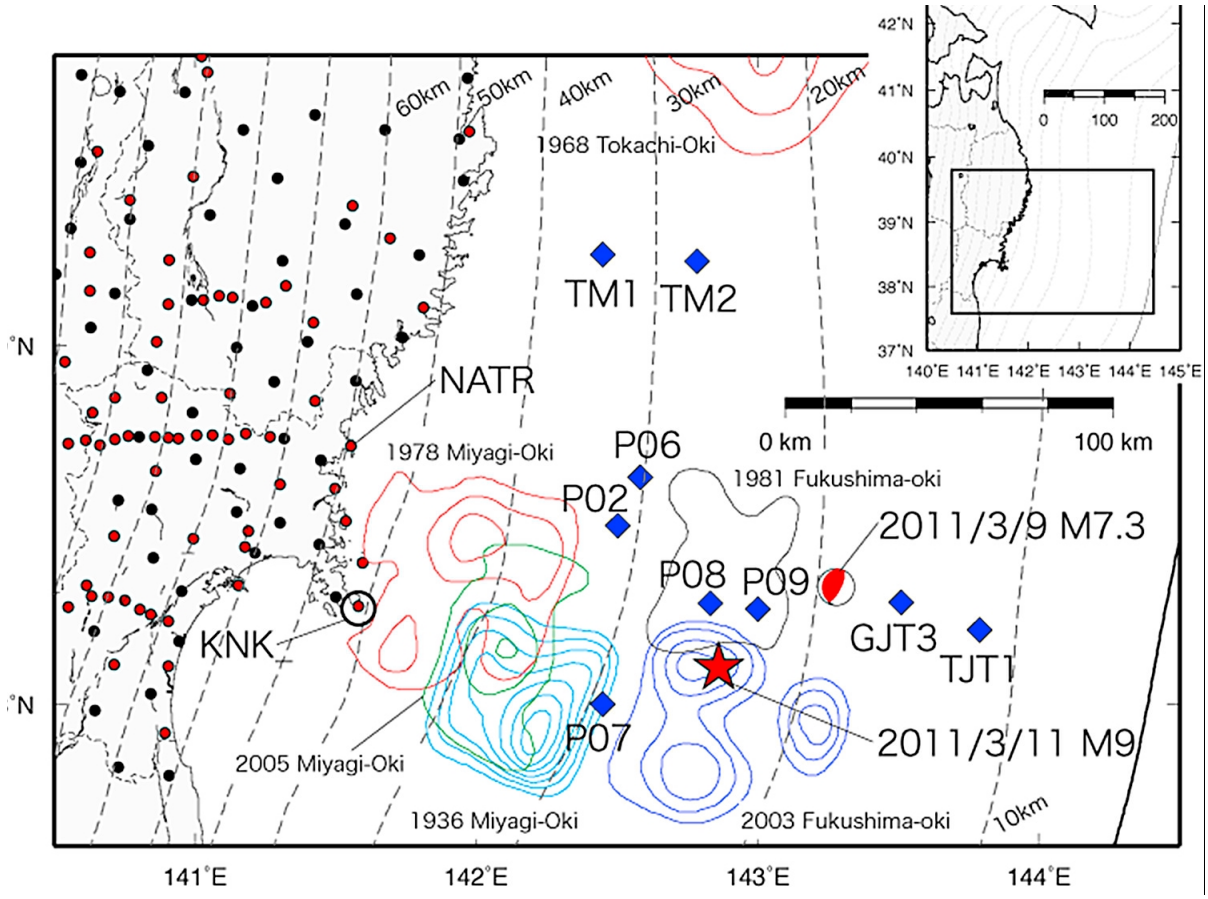

Fig. 35. The location map of GPS (small closed circles), OBPRs (blue diamonds) and a volumetric strainmeter (black open circle at KNK) near the focal zone of the Tohoku-oki earthquake (modified from Ohta *et al*., 2012a). The red star indicates the epicenter of the mainshock determined by the Japan Meteorological Agency. The thin dashed line shows isodepth contours of the subducting Pacific plate interface at 10 km intervals compiled by Kita *et al*. (2010). Colored contours indicate the spatial distribution of past earthquake source regions estimated by Yamanaka and Kikuchi (2004).

be used to monitor the crustal activity in an area between the source regions of two large earthquakes, such as the Tonankai and Nankai earthquakes. When one of them ruptures, it is of primary importance to monitor the crustal movement in the area between the two seismogenic zones, because almost all the past megathrust Tonankai earthquakes were followed by a Nankai earthquake within a few years.

Ocean bottom pressure observations can also be applicable to monitor the stability of the seafloor during the extraction of natural resources, or the storage of CO_2 beneath the seafloor. Zumberge *et al*. (2008) began making time-lapse seafloor gravity and pressure measurements in 1998 as discussed in Chapter 5. They carried out repeated measurements on many stable platforms made of concrete, in oil and gas fields, and on a reference one outside of the area. They estimated the repeatability of pressure observations to be approximately 0.5 hPa owing to elaborate measurements on stable platforms.

Ocean bottom pressure monitoring has played key roles in the study of the 2011 Tohoku-oki earthquake owing to its continuous observation. Firstly, two cabled OBPRs off Kamaishi (Kanazawa and Hasegawa, 1997) operated by the Earthquake Research Institute, University of Tokyo, (hereafter referred to as the ERI) detected the huge tsunami in real-time. The observed tsunami waves showed two-step tsunami waveforms: a gradual increase of sea level (∼2 m) followed by an impulsive tsunami wave (3 to 5 m) (Fujii *et al*., 2011). The gradual increase is interpreted to be caused by the coseismic slip in the broad source region, and the impulsive wave by an exceptionally large slip near the trench. If the observed results had been used in a real-time tsunami warning, the tsunami casualties would have been fewer.

The Tohoku group had deployed OBPRs, as well as the GPSA stations, above the two seismogenic zones off Miyagi indicated in Fig. 2 (Hino *et al*., 2009). That is why we could observe seafloor crustal movements associated with preseismic and postseismic slips, as well as large coseismic slips of the Tohoku-oki earthquake. The location map of the OBPR and GPSA sites is shown in Fig. 35, with nearby seismogenic zones. Some of the OBPR data that detected crustal movements are shown in Fig. 36. An M 7.3 foreshock occurred at the subducting plate interface on March 9, 51 hours before the mainshock. Ohta *et al*. (2012a) estimated a coseismic and postseismic slip model of the foreshock based on the data of 9 OBPRs, as well as land-based GPS and strain observations. The estimated coseismic slip and afterslip areas show complementary spatial distributions; the afterslip distribution is located at the up-dip part of the coseismic slip of the foreshock and northward of the hypocenter of the Tohoku-

doi:10.5047/meep.2014.00202.0023

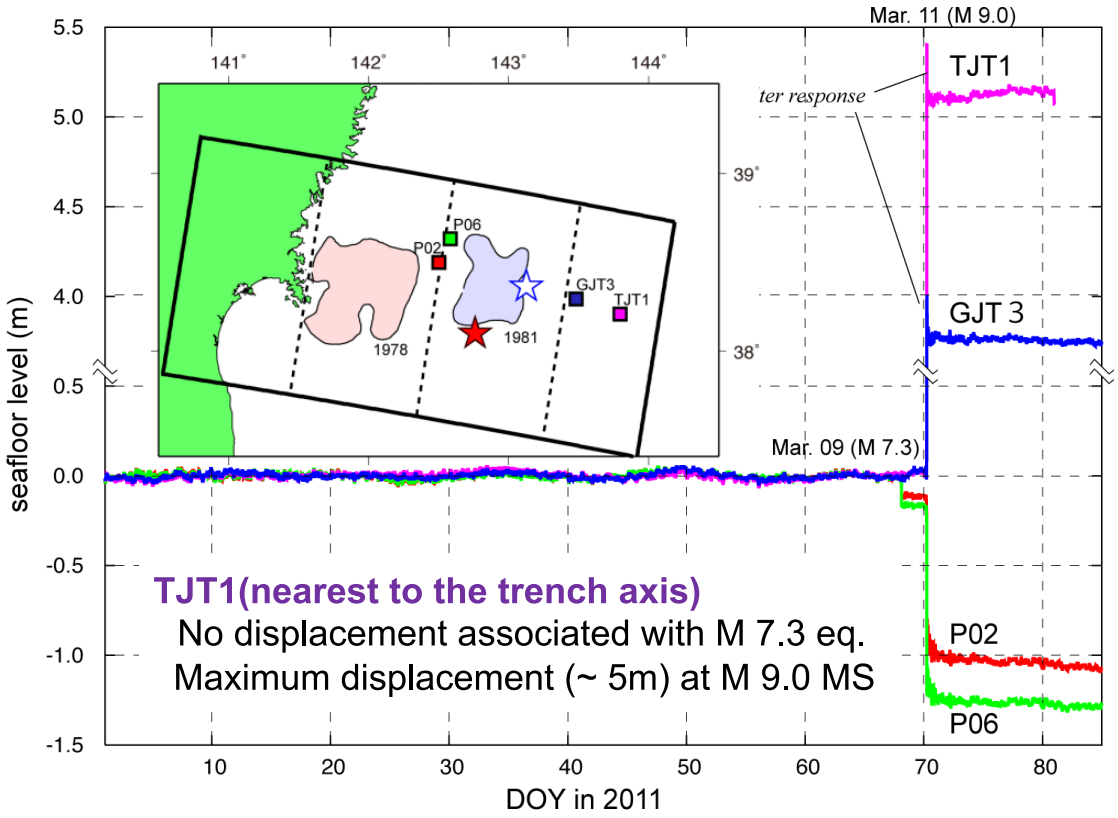

Fig. 36. Some of the OBPR data that detected crustal movements associated with the 2011 Tohoku-oki earthquake (modified from Iinuma *et al*., 2012a) (courtesy of Prof. R. Hino).

oki earthquake. A volumetric strainmeter time series also suggests that this event advanced with a rapid decay time constant compared with other typical large earthquakes.

Two OBPRs were deployed near the trench: TJT1 about 25 km from the trench axis, and GJT3 about 50 km from the axis. A coseismic uplift of 5.1 m was observed at TJT1 and 3.8 m at GJT3 (Fig. 36). Based on the results, Ito *et al*. (2011b) postulated that there should be a slip as large as 80 m on the plate boundary extending to the trench axis. As is mentioned above, Iinuma *et al*. (2012a) estimated the distribution of the huge coseismic slip up to 85 m with the 4 OBPR data shown in Fig. 36 combined with GPS and GPSA data.

Analyzing the available OBP data, Hino *et al*. (2012) showed that the proportion of the coseismic slip between the deep seismogenic zone and the trenchward zone was nearly 1 to 3. They pointed out that the background seismicity was especially low in the most trenchward zone where the coseismic slip was the largest. In contrast, the $M \sim 7.5$ earthquakes offshore of Tohoku since the 1930's, with a dislocation of ~2 m (e.g. Yamanaka and Kikuchi, 2004), have repeatedly occurred in the deeper portion of the plate boundary. The amount of this slip accounts for ~2/3 of the slip deficit that accumulated within the recurrence interval (~40 years) at a convergence rate of ~0.08 m/year (Apel *et al*., 2006). The amount of coseismic slip is reasonably explained if the near-trench aseismic zone had been fully coupled and if the Tohoku-Oki earthquake released the strain accumulated since the previous M 9.0 earthquake (Hino *et al*., 2012).

As discussed in Section 3.4, the observed OBP data indicated that the distribution of postseismic displacements is heterogeneous; substantial slip occurred at the down-dip side of the plate boundary, whereas minor slip occurred around the hypocenters and along the trench axis. The overall feature suggests that the effect of visco-elastic relaxation in the mantle is important, as well as the postseismic slip on the plate boundary (R. Hino and T. Iinuma, personal communication).

Through the studies of the Tohoku-oki earthquake, we realized the importance of two transient slow slip events that occurred before the earthquake (Ito *et al*., 2013). The first transient crustal deformation, which occurred over a period of a week in November 2008, was recorded simultaneously using two OBPRs at TJT1, as shown in Fig. 32, and the volumetric strainmeter in Kinka-san Island; this deformation has been interpreted to be an M 6.8 episodic slow slip event. The second had a duration exceeding 1 month and was observed in February 2011, just before the 2011 Tohoku-oki earthquake. This event reached M 7.0. The two events preceded interplate earthquakes of magnitudes M 6.1 (December 2008) and M 9.0 (March 2011), respectively. The results indicate that these slow slip events caused an increase in shear stress, which, in turn, triggered the interplate earthquakes. The source area of the second slow slip event is shown in Fig. 37. Its location within the down-dip portion of the huge coseismic-slip area of the Tohoku-oki earthquake indicates that episodic slow slip and seismic behavior occurred on the

doi:10.5047/meep.2014.00202.0023

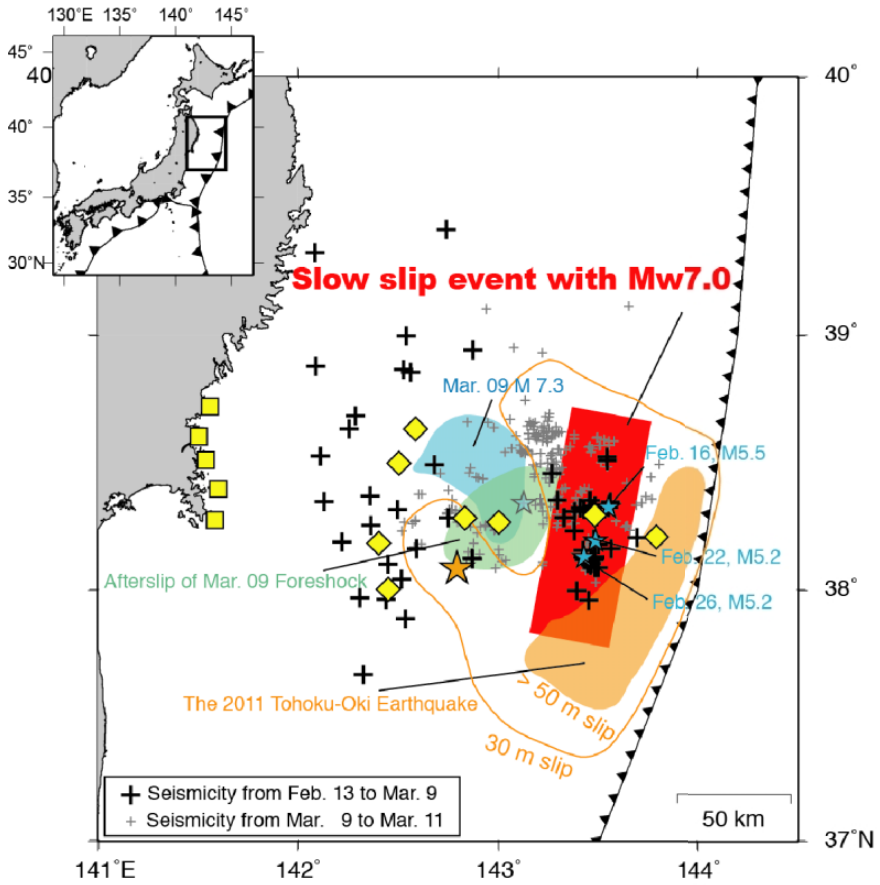

Fig. 37. A map showing the source area of the slow slip event that occurred one month before the Tohoku-oki earthquake (from *Tectonophysics*, Ito, Y., R. Hino, M. Kido, H. Fujimoto, Y. Osada, D. Inazu, Y. Ohta, T. Iinuma, M. Ohzono, S. Miura, M. Mishina, K. Suzuki, T. Tsuji, and J. Ashi, Episodic slow slip events in the Japan subduction zone before the 2011 Tohoku-Oki earthquake, Copyright 2013, in press, with permission from Elsevier). The red rectangle shows the source area of the *M* 7.0 slow slip event in February 2011. The epicenter (orange star), area of coseismic slip exceeding 50 m (orange shade), and coseismic slip region of 30 m (orange contour) of the 2011 Tohoku-oki earthquake (Iinuma *et al*., 2012a) are also shown. Light blue and green shaded areas show the coseismic and afterslip areas of the foreshock on March 9 (Ohta *et al*., 2012a). Seismicity activated after the 2011 slow slip event are marked by crosses. OBP and on-shore observation sites used to estimate fault parameters are shown by yellow diamonds and squares, respectively.

same portions of the megathrust fault (Ito *et al*., 2013).

4.2 Ongoing research activities

In the case of a large subduction thrust earthquake, the real-time early warning of strong ground motion and a tsunami is of primary importance to hazard mitigation. Cabled ocean bottom seismometers and pressure recorders are important infrastructures for the warning system. Recognizing the high occurrence probability of a giant earthquake in the Nankai Trough, JAMSTEC deployed the Dense Oceanfloor Network System for Earthquakes and Tsunamis (DONET, http://www.jamstec.go.jp/donet/e/) with 20 observation stations above the seismogenic zone of the Tonankai earthquake off the Kii Peninsula, southwest Japan, in 2009 with a fund from the MEXT Japan. Each station comprises high precision seismometers and a quartz pressure sensor. Another cabled seafloor observatory, DONET-2, is in progress above the seismogenic zone of the Nankai earthquake off Shikoku.

The Pacific coast of Northeast Japan was damaged by the 2011 Tohoku-oki earthquake, and had been repeatedly visited by large tsunamis. The National Research Institute for Earth Science and Disaster Prevention (NIED) is now deploying a big cabled ocean floor observatory with about 150 stations along the Japan Trench (Fig. 38) with a fund from the MEXT, Japan (Uehira *et al*., 2012).

The Tohoku-oki earthquake demonstrated that the tsunami warning system in Japan had a serious problem. The Japan Meteorological Agency is now revising the tsunami forecasting system, utilizing recent research works. Tsushima *et al*. (2009) proposed a method for real-time near-field tsunami forecasting from data acquired by cabled offshore OBPRs. The first step is inverting tsunami waveforms recorded at OBPRs to estimate the spatial distribution of the initial sea-surface displacements in the tsunami source region without making any assumptions about the fault geometry and the earthquake magnitude. The next step is to synthesize the coastal tsunami waveforms from the estimated sea-surface displacement distribution using pre-computed tsunami Green's functions. They tested the method by simulating the 1896 Sanriku tsunami earthquake, which caused a devastating tsunami with a maximum run-up height of 38 m along the Pacific coast of Northeast Japan. The simulation demonstrated that the method provided accurate estimations

doi:10.5047/meep.2014.00202.0023

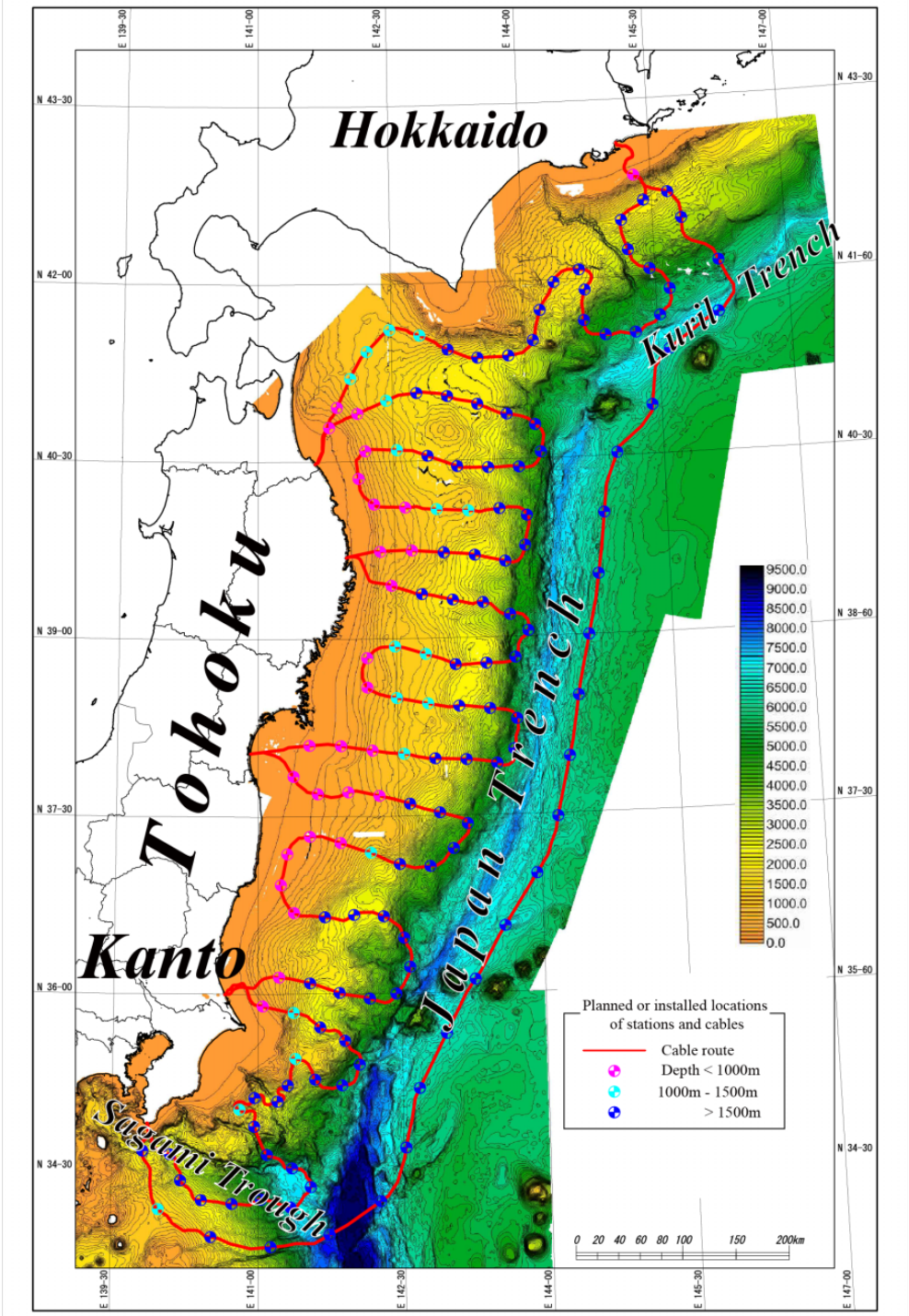

Fig. 38. A plan of the cabled ocean floor observatory along the Japan Trench (courtesy of Dr. K. Uehira). The average interval of the stations will be 30 km offshore Northeast Japan and 40 km on the outer rise near the trench. Three-component seismometers and two pressure sensors will be installed at each station.

of the coastal arrival times and the amplitudes of the first peak of the tsunami, more than 20 minutes before the maximum amplitude wave reached the coastal site nearest to the source.

The source region of an earthquake which causes a large tsunami is generally broad, and OBPRs in the source region record the effects of both the tsunami and the vertical displacement of the seafloor. Tsushima *et al*. (2012) proposed a method of tsunami waveform inversion to accurately estimate a tsunami source by incorporating the effect of permanent seafloor displacements observed by OBPRs within the source region.

These methods need a longer time for a larger earthquake due to the longer period of the tsunami generated by a broader source region. Ohta *et al*. (2012b) developed an algorithm to estimate static ground displacements due to earthquake faulting from real-time kinematic GPS (RTK-GPS) time series.

doi:10.5047/meep.2014.00202.0023

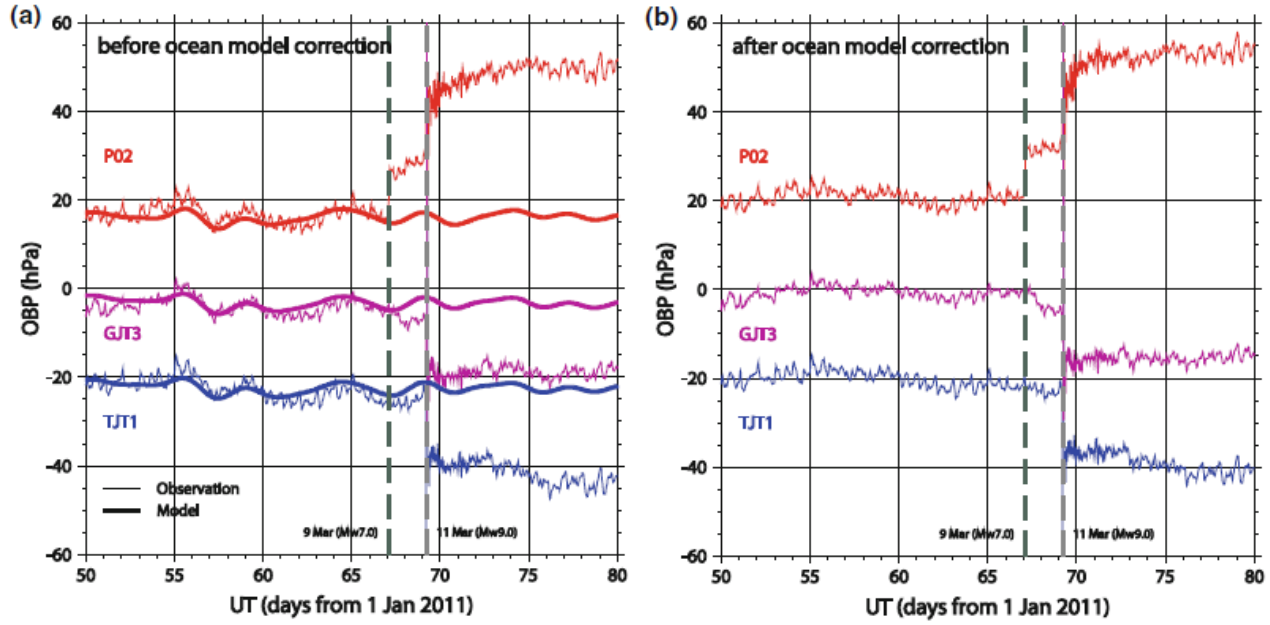

Fig. 39. Time series of OBPR data in the source region of the Tohoku-oki earthquake before and after the correction with a global barotropic ocean model (with kind permission from Springer Science+Business Media: *Mar. Geophys. Res.*, A global barotropic ocean model driven by synoptic atmospheric disturbances for detecting seafloor vertical displacements from in situ ocean bottom pressure measurements, *33*, 2012, 127–148, Inazu, D., R. Hino, and H. Fujimoto, figure 11).

They applied the algorithm to data obtained from the 2011 Tohoku-oki earthquake to detect coseismic displacement and to estimate a fault model. The inversion estimated a fault model with M 8.7 within five minutes from the origin time. Once the fault model is estimated, tsunami waveforms can be synthesized within one more minute by using the method of Tsushima *et al.* (2009). The relatively small moment magnitude estimated by the algorithm is not a serious problem for the early warning. The arrival time and the height of the first big wave estimated at coastal sites were much the same as the observed results.

One problem remains to be studied further: the problem that ocean bottom pressure observations include the effect of ocean dynamics as well as that of crustal dynamics. Relative pressure monitoring among a local OBPR array is one way to cancel the effects of the ocean, but an array extending over a wide area needs another approach. Inazu *et al.* (2012) developed a global barotropic ocean model forced by atmospheric disturbances to estimate the effect on the ocean bottom pressure. The model accuracy is validated by deep-sea OBPR data at more than 100 sites distributed in the global ocean. The correction of the OBPR data for the effect of ocean dynamics using this model can reduce the rms residuals of the observed non-tidal pressure component by 18% on average. The time series of OBPR data in the Japan Trench area before and after the correction are shown in Fig. 39. The results show that the correction is important to estimate the pre- and postseismic displacements, but further studies are needed.

5. Submarine Gravimetry

Submarine gravity measurements have been carried out basically for two purposes: geophysical mapping and monitoring subseafloor mass change. A tectonic fault is associated with some changes in the subterranean structure and often coincides with a belt of large horizontal gravity gradients. Hydrothermal ore deposits may result in a small gravity anomaly, less than 0.5 mGal (1 mGal $= 10^{-5}$ m s^{-2}), due to their higher density than the average (Fujimoto *et al.*, 2011b). Ocean bottom gravimetry with a precision of some 0.05 mGal has been carried out for these studies. Although a surface ship gravimeter can carry out continuous gravity measurement, its precision is about 1 mGal, and measurements at the sea surface, thousands of meters above the seafloor, result in a poor spatial resolution.

ERI developed an ocean bottom gravimeter (OBG) in 1996 for stand-alone measurements, and for use with an underwater vehicle (Fujimoto *et al.*, 1998a, b). The gimbal suspension with an oil damper roughly maintains a sensor package of Scintrex CG-3M/SB vertically, as shown in Fig. 40, and the effect of the remaining tilt is numerically corrected by using the tiltmeters of the gravimeter. The gimbals and the sensor are in a pressure-tight spherical housing made of titanium alloy rated to a water depth of 6000 m.

Precise mapping of gravity anomalies in local areas near the coast was carried out by using the OBG. For example, seafloor gravimetry with a precision of 0.05 mGal was carried out with the OBG in the shallow water off Aomori Prefecture, northern Japan. Detailed and seamless gravimetry on land and on the seafloor confirmed the horizontal extension of an underground intrusive rock (Fujimoto *et al.*, 2009).

Considerable time is required to make a gravity map from seafloor gravimetry with an OBG. Therefore, ERI is now developing a hybrid gravity survey system using a gravimeter and a gravity gradiometer to survey the sub-seafloor density

doi:10.5047/meep.2014.00202.0023

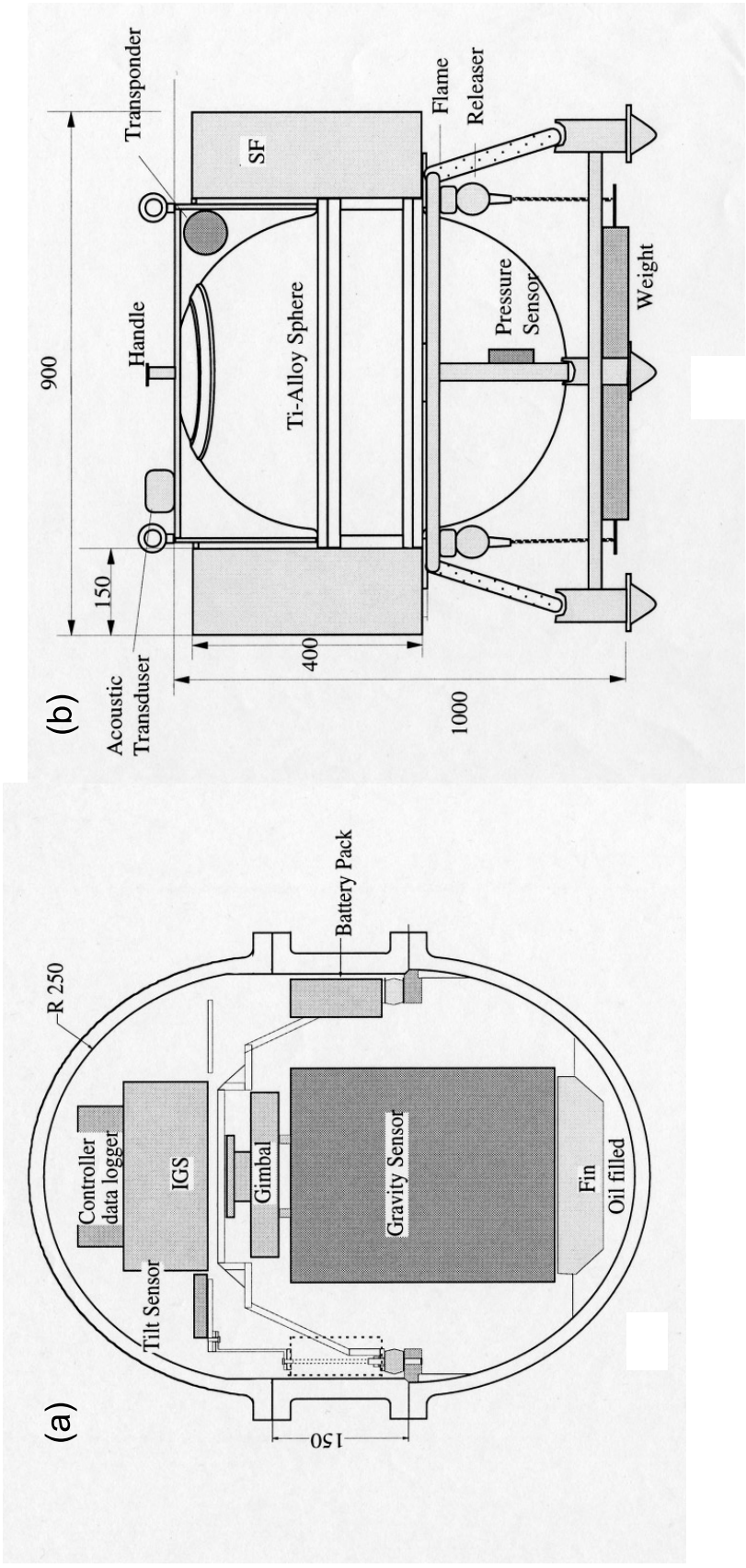

Fig. 40. (a) An ocean bottom gravimeter with a self-surfacing system. (b) A diagram inside the pressure housing (from Fujimoto *et al.*, 2009).

doi:10.5047/meep.2014.00202.0023

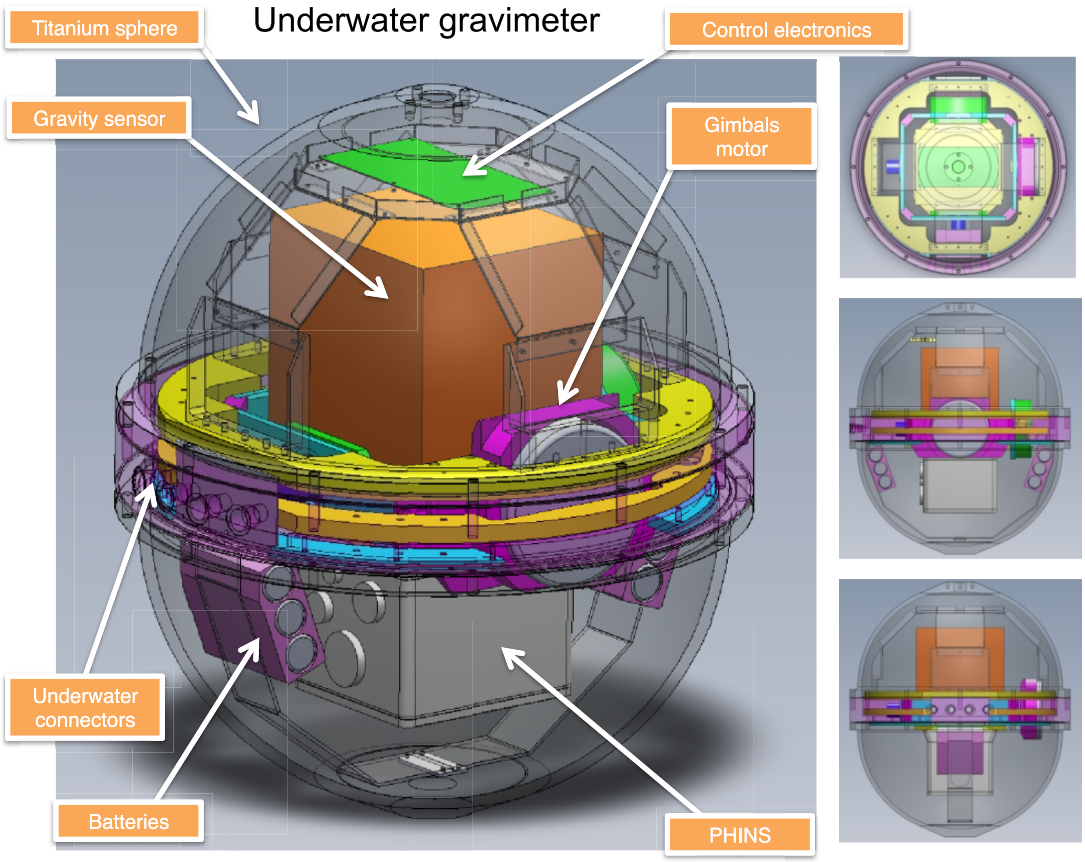

Fig. 41. A gravimeter developed for underwater gravimetry developed by ERI, University of Tokyo (from Shinohara *et al.*, 2013).

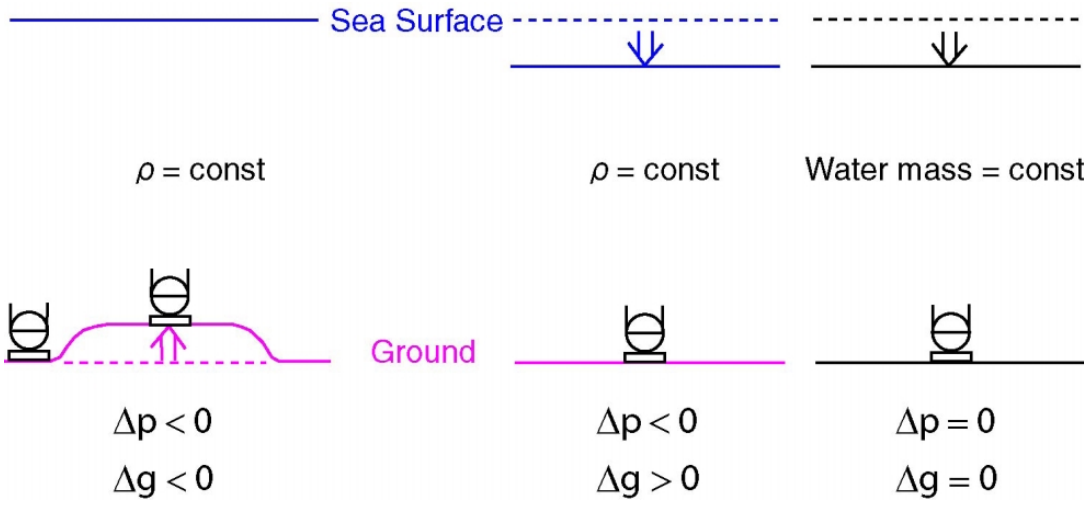

Fig. 42. Schematic illustration showing the effects of variations in the ocean and the crust on bottom pressure and gravity.

structure (Fujimoto *et al.*, 2011b; Shinohara *et al.*, 2013). Micro-g LaCoste S-174 was adopted as the gravity sensor. The sensor is mounted on forced gimbals with a fiber gyroscope as shown in Fig. 41. The maximum depth rating is 4,200 m with a titanium-sphere pressure housing. In September 2012, the first sea trial was carried out in Sagami Bay, Central Japan, by using JAMSTEC's autonomous underwater vehicle (AUV) Urashima. Both the gravimeter and the gravity gradiometer were mounted on the AUV. The whole system was controlled and monitored on the support vessel Yokosuka via an acoustic link to the AUV. According to preliminary analyses, the resolution of the observed gravity values is estimated to be about 0.1 mGal (Shinohara *et al.*, 2013).

The ratio of a gravity change to a vertical crustal movement is basic information for the study of crustal activities on

doi:10.5047/meep.2014.00202.0023

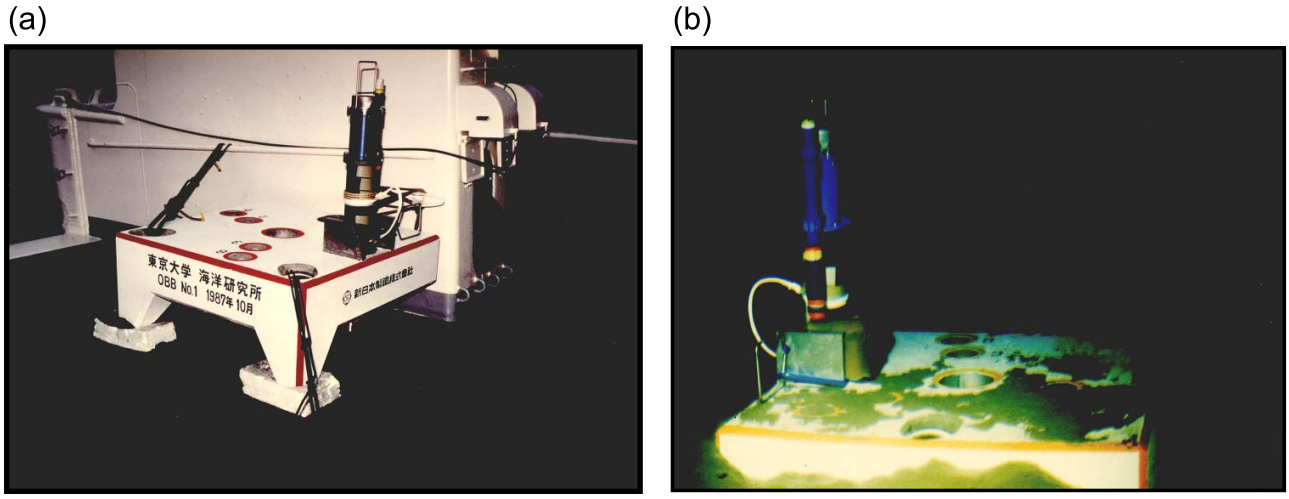

Fig. 43. A concrete platform before the deployment (a), and after deployment on the seafloor (b).

land. Theoretically speaking, seafloor gravimetry and ocean bottom pressure monitoring are a good combination to distinguish between ocean and crustal dynamics as shown in Fig. 42. However, the resolution of a vertical crustal movement detected from a pressure change is higher than that from a gravity change by about one order of magnitude, and the pressure data are mainly used to monitor water depth variations during seafloor gravity measurements.

Most gravity sensors are in temperature-regulated housings in order to reduce the effect of temperature variation. Consequently, an OBG requires a certain amount of electric power and is not an appropriate instrument for continuous observation on the seafloor. Then, gravity change on the seafloor should be detected from repeated measurements at exactly the same places on the seafloor. We installed a concrete platform for seafloor geodetic observations on the seafloor in Sagami Bay, Central Japan, in 1987, as shown in Fig. 43 (Fujimoto *et al*., 1990). We tried seafloor gravimetry on the benchmark with the ERI's OBG in vain; a JAMSTEC manned submersible "Shinkai 2000" equipped with only one hand at that time could not precisely handle the OBG.

Similar observations have been carried out by a group from Scripps Institution of Oceanography, UCSD. Zumberge *et al*. (2008) began making time-lapse seafloor gravity and pressure measurements in 1998 in oil and gas fields offshore Norway. Three relative gravity sensors mounted in a single frame were carried by an ROV to concrete platforms permanently placed on the seafloor. Reference platform sites outside the reservoir boundaries assumed to provide stable fiducial points. Typical surveys lasted from a few days to a few weeks and covered from 8 to 80 platforms, with multiple observations of each. They estimated that the intra-survey repeatability was approximately 3 microgals in gravity and approximately 5 mm in benchmark depth from the pressure monitoring. They attributed the improved precision to several operational factors, including the use of multiple gravity sensors, frequent benchmark reoccupation, precise relocation and orientation of the sensors, repeated calibrations on land, and minimization of vibrational and thermal perturbations to the sensors. They estimated that changes with gravity over time can track changes in the height of a gas-water contact in a flooded reservoir, with a precision of a few meters.

6. Summary

I have tried to summarize seafloor geodetic observations, mostly carried out by my colleagues, with a focus on the observation systems. It has been said for a long time that the observations of crustal movements on the seafloor is important. It has taken time because geodetic observation on the seafloor requires high precision measurements at many sites over a long time, continuously or repeatedly. The seafloor geodesy group of Scripps Institution of Oceanography, led by Fred Spiess, did pioneering work. It is the continued effort of the Headquarters for Earthquake Research Promotion of Japan that has extended the GPSA observation array along the Japan Trench and the Nankai Trough, and the Japan Coast Guard has been doing good work by using the GPSA array.

The 2011 Tohoku-oki earthquake was an historical event from the viewpoint of seafloor geodesy. It has demonstrated that seafloor geodetic observations are crucial to cope with a giant earthquake. It was also realized that seafloor geodetic networks were quite limited and the real-time tsunami warning system should be revised. The Japanese government has doubled the number of GPSA observation sites and is installing large cabled ocean floor observatories along the Japan Trench and the Nankai Trough. The Japan Meteorological Agency is now improving the tsunami warning system.

Although I did not mention due to my little contribution, high-resolution geodetic observations using seafloor boreholes is important for monitoring crustal activities near a plate boundary. A group of JAMSTEC and ERI did pioneering work in two boreholes near the Japan Trench. JAMSTEC is now developing real-time borehole observatories in the Nankai Trough area.

Acknowledgments. This paper owes much to the geodetic research works of colleagues and coworkers, including M. Kido, R. Hino, T. Iinuma, Y. Ito, Y. Ohta, Y. Osada, S. Miura, T. Sato, I.

doi:10.5047/meep.2014.00202.0023

Wada, F. Tomita, H. Tsushima, D. Inazu, M. Funakoshi, T. Tamaki from Tohoku University, and T. Kanazawa, M. Shinohara, A. Araya, T. Yamada, T. Furuta, J. Segawa, Y. Tomoda from the University of Tokyo, K. Tadokoro from Nagoya University, F. Spiess, D. Chadwell, J. Hildebrand, R. Zimmerman from SIO, UCSD, and H. Murakami, T. Kawakami from Kaiyo Denshi, Inc. The author is very grateful for helpful discussions with many researchers, including A. Asada, M. Mochizuki, M. Fujita, M. Sato, Y. Matsumoto, T. Ishikawa, and K. Wang. Assistance in revising the early version of the manuscript was kindly provided by I. Wada. The editor S. Okubo and two anonymous reviewers provided insightful reviews that much improved this work. This work has been partially supported by programs for improvement of GPSA observation systems from the MEXT, Japan. This work was partially supported by Grants-in-aid for Scientific Research (Kiban-A20244070) from the Japan Society for the Promotion of Science. Marine geodetic observations were supported with many cruises of the R/V Tansei-maru and Hakuho-maru operated by JAMSTEC and the Atmosphere and Ocean Research Institute, University of Tokyo.

References

Apel, E. V., R. Burgmann, G. Steblov, N. Vasilenko, R. King, and A. Prytkov (2006), Independent active microplate tectonics of northeast Asia from GPS velocities and block modeling, *Geophys. Res. Lett.*, *33*, doi:10.1029/2006GL026077.

Bertiger, W. I., Y. E. Bar-Sever, B. J. Haines, B. A. Iijima, S. M. Lichten, U. J. Lindqwister, A. J. Mannucci, R. J. Muellerschoen, T. N. Munson, A. W. Moore, L. J. Romans, B. D. Wilson, S. C. Wu, T. P. Yunck, G. Piesinger, and M. Whitehead (1999), "A Real-Time Wide Area Differential GPS System", Invited Contribution to Institute of Navigation "Red Books," Global Positioning System: Papers Published in Navigation, Vol. IV.

Burton, J., and V. Dobbin (2013), Station-keeping autonomous surface vehicle, *Sea Tech.*, *54*(3), 10–12.

Chadwell, C. D., and F. N. Spiess (2008), Plate motion at the ridge-transform boundary of the south Cleft segment of the Juan de Fuca Ridge from GPS-Acoustic data, *J. Geophys. Res.*, *113*, B04415, doi:10.1029/2007JB004936.

Chadwell, C. D., J. A. Hildebrand, F. N. Spiess, J. L. Morton, W. R. Normark, and C. A. Reiss (1999), No spreading across the southern Juan de Fuca ridge axial cleft during 1994–1996, *Geophys. Res. Lett.*, *26*, 2525–2538.

Chadwick, W. W., and M. Stapp (2002), A deep-sea observatory experiment using acoustic extensometers: Precise horizontal distance measurements across a Mid-Ocean Ridge, *IEEE Ocean Eng.*, *27*, 193–201.

Chadwick Jr., W. W., H. B. Milburn, and R. W. Embley (1995), Acoustic extensometer: measuring mid-ocean spreading, *Sea Tech.*, *36*, 33–38.

Chadwick, W. W., S. L. Nooner, M. A. Zumberge, R. W. Embley, and C. G. Fox (2006), Vertical deformation monitoring at Axial Seamount since its 1998 eruption using deep-sea pressure sensors, *J. Volcanol. Geotherm. Res.*, *150*, 313–327.

Chen, C.-T., and F. J. Millero (1977), Speed of sound in seawater at high pressures, *J. Acoust. Soc. Am.*, *62*, 1129–1135.

Colombo, O. L., A. G. Evans, M. I. Vigo-Aguiar, J. M. Ferrandiz, and J. J. Benjamin (2000), Long-baseline (>1000km), sub-decimeter kinematic positioning of buoys at sea, with potential application to deep sea studies, *Proc. ION GPS 2000*, Salt Lake City, U.S.A.

Cox, C. M., and B. F. Chao (2002), Detection of a large-scale mass redistribution in the terrestrial system since 1998, *Science*, *297*, 831–833.

DeMets, C., R. G. Gordon, D. F. Argus, and S. Stein (1994), Effect of recent revisions to the geomagnetic reversal time scale on estimates of current plate motions, *Geophys. Res. Lett.*, *21*, 2191–2194.

Dickey, J. O., S. L. Marcus, O. de Viron, and I. Fukumori (2002), Recent Earth oblateness variations: Unraveling climate and postglacial rebound effects, *Science*, *298*, 1975–1977.

Forsyth, D. W., D. S. Scheirer, S. C. Webb *et al.* (1998), Imaging the deep seismic structure beneath a mid-ocean ridge: The MELT experiment, *Science*, *280*, 1215–1218.

Fox, C. G. (1990), Evidence of active ground deformation on the mid-ocean ridge: Axial Seamount, Juan de Fuca Ridge, April–June, 1988, *J. Geophys. Res.*, *95*, 12813–12822.

Fox, C. G. (1993), Five years of ground deformation monitoring on Axial Seamount using a bottom pressure recorder, *Geophys. Res. Lett.*, *20*, 1859–1862.

Fox, C. G. (1999), In situ ground deformation measurements from the summit of Axial Volcano during the 1998 volcanic episode, *Geophys. Res. Lett.*, *26*, 3437–3440.

Fox, C. G., W. W. Chadwick Jr., and R. W. Embley (2001), Direct observation of a submarine volcanic eruption from a sea-floor instrument caught in a lava flow, *Nature*, *412*, 727–729.

Francois, R. E., and G. R. Garrison (1982a), Sound absorption based on ocean measurements. Part 1: pure water and magnesium sulfate contributions, *J. Acoust. Soc. Am.*, *72*, 896–907.

Francois, R. E., and G. R. Garrison (1982b), Sound absorption based on ocean measurements. Part 2: boric acid contribution and equation for total absorption, *J. Acoust. Soc. Am.*, *72*, 1879–1890.

Fujii, Y., K. Satake, S. Sakai, M. Shinohara, and T. Kanazawa (2011), Tsunami source of the 2011 off the Pacific coast of Tohoku Earthquake, *Earth Planets Space*, *63*, 815–820.

Fujimoto, H., J. Segawa, T. Furuta, and H. Murakami (1990), Installation of ocean bottom bases for observation of seafloor crustal movement, *Mar. Geod.*, *14*, 177–184.

Fujimoto, H., K. Koizumi, Y. Osada, and T. Kanazawa (1998a), Development of instruments for seafloor geodesy, *Earth Planets Space*, *50*, 905–911.

Fujimoto, H., A. Oshida, T. Furuta, and T. Kanazawa (1998b), Development of an ocean bottom gravimeter, *J. Jpn. Soc. Mar. Surv. Tech.*, *10*, 25–38 (in Japanese with English Abstract).

Fujimoto, H., M. Mochizuki, K. Mitsuzawa, T. Tamaki, and T. Sato (2003), Ocean bottom pressure variations in the southeastern Pacific following the 1997–98 El Nino event, *Geophys. Res. Lett.*, *30*, 1456, doi:10.1029/2002GL016677.

Fujimoto, H., K. Nozaki, Y. Kawano, N. Demboya, A. Oshida, K. Koizumi, S. Mitsuishi, K. Iwamoto, and T. Kanazawa (2009), Remodeling of an ocean bottom gravimeter and littoral seafloor gravimetry—toward the seamless gravimetry on land and seafloor—, *J. Geod. Soc. Jpn.*, *55*(3), 325–339.

Fujimoto, H., M. Kido, Y. Osada, K. Tadokoro, T. Okuda, Y. Matsumoto, and K. Kurihara (2011a), Long-term stability of acoustic benchmarks deployed on thick sediment for GPS/Acoustic seafloor positioning, in *Modern Approaches in Solid Earth Sciences*, Vol. 8, 263–272, doi: 10.1007/978-90-481-8885-7, Springer.

Fujimoto, H., T. Kanazawa, M. Shinohara, A. Araya *et al.* (2011b) Development of a hybrid gravimeter system onboard an underwater vehicle, UT2011, Hawaii.

Fujita, M., T. Ishikawa, M. Mochizuki, M. Sato, S. Toyama, M. Katayama, K. Kawai, Y. Matsumoto, T. Yabuki, A. Asada, and O. L. Colombo (2006), GPS/Acoustic seafloor geodetic observation: method of data analysis and its application, *Earth Planets Space*, *58*, 265–275.

Fujiwara, T., S. Kodaira, T. No, Y. Kaiho, N. Takahashi, and Y. Kaneda (2011), The 2011Tohoku-Oki earthquake: displacement reaching the trench axis, *Science*, *334*, 1240.

Gagnon, K., C. D. Chadwell, and E. Norabuena (2005), Measuring the onset of locking in the Peru-Chile trench with GPS and acoustic measuring, *Nature*, *434*, 205–208.

Geographical Survey Institute (GSI) (2004), The earthquake SE off Kii peninsula on September 5, in the summary of the 159 meeting of the Coord. Com. Earthq. Pred., http://cais.gsi.go.jp/YOCHIREN/JIS/159/index159.html.

Gold, R. (1967), Optimal binary sequences for spread spectrum multiplexing, *IEEE Trans. Inf. Theory*, pp. 612–621.

Golumb, S. W. (1967), *Shift Register Sequences*, Holden-Day, San Francisco, Ca.

Hashimoto, C., A. Noda, T. Sagiya, and M. Matsu'ura (2009), Interplate seismogenic zones along the Kuril–Japan trench inferred from GPS data inversion, *Nat. Geosci.*, *2*, 141–144, doi:10.1038/NGE0421.

Hatanaka, Y., T. Iizuka, M. Sawada, A. Yamagiwa, Y. Kikuta, J. M. Johnson, and C. Rocken (2003), Improvement of the analysis strategy of GEONET, *Bull. Geogr. Surv. Inst.*, *49*, 11–37.

Headquarters for Earthquake Research Promotion of Japan (2003), Long-term evaluation of the Miyagi-Oki earthquakes, http://www.jishin.go.jp/main/index.html (in Japanese).

Hino, R., S. Ii, T. Iinuma, and H. Fujimoto (2009), Continuous long-term seafloor pressure observation for detecting slow-slip events in Miyagi-oki on the landward Japan trench slope, *J. Disaster Res.*, *4*, 72–82.

doi:10.5047/meep.2014.00202.0023

Hino, R., Y. Ohta, Y. Ito, Y. Osada, M. Kido, D. Inazu, and H. Fujimoto (2012), Coseismic and postseismic seafloor deformation by the 2011 Tohoku-Oki earthquake detected by ocean-bottom pressure monitoring, The 8th APRU Research Symposium, Sendai.

Hori, T., and S. Miyazaki (2011), A possible mechanism of *M* 9 earthquake generation cycles in the area of repeating *M* 7∼8 earthquakes surrounded by aseismic sliding, *Earth Planets Space*, *63*(7), 773–777.

Ide, S., A. Baltay, and G. C. Beroza (2011), Shallow dynamic overshoot and energetic deep rupture in the 2011 Mw 9.0 Tohoku-Oki earthquake, *Science*, *332*(6036), 1426–1429, doi:10.1126/science.1207020.

Igarashi, T., T. Matsuzawa, and A. Hasegawa (2003), Repeating earthquakes and interpolate aseismic slip in the northeastern Japan subduction zone, *J. Geophys. Res.*, *108*, doi:10.1029/2002JB001920.

Iinuma, T., M. Ohzono, Y. Ohta, and S. Miura (2011), Coseismic slip distribution of the 2011 off the Pacific coast of Tohoku Earthquake (*M* 9.0) estimated based on GPS data—Was the asperity in Miyagi-oki ruptured?, *Earth Planets Space*, *63*(7), 643–648, doi:10.5047/eps.2011.06.013.

Iinuma, T., R. Hino, M. Kido, D. Inazu, Y. Osada, Y. Ito, M. Ohzono, H. Tsushima, S. Suzuki, H. Fujimoto, and S. Miura (2012a), Coseismic slip distribution of the 2011 off the Pacific Coast of Tohoku Earthquake (M9.0) refined by means of seafloor geodetic data, *J. Geophys. Res.*, *117*, B07409, doi:10.1029/2012JB009186.

Iinuma, T., R. Hino, M. Kido, D. Inazu, Y. Osada, M. Sato, Y. Ohta, H. Fujimoto, Y. Ito, and S. Suzuki (2012b), Postseismic slip distribution associated with the 2011 Tohoku Earthquake (M9.0) based on terrestrial and seafloor geodetic data, T13F-2694, AGU 2012 Fall Meeting, San Francisco.

Inazu, D., R. Hino, and H. Fujimoto (2012), A global barotropic ocean model driven by synoptic atmospheric disturbances for detecting seafloor vertical displacements from in situ ocean bottom pressure measurements, *Mar. Geophys. Res.*, *33*, 127–148, doi:10.1007/s11001-012-9151-7.

Ito, Y., and E. Obara (2006), Very low earthquakes with accretionary prisms are very low stress-drop earthquakes, *Geophys. Res. Lett.*, *33*, L09302, doi:10.1029/2006GL025883.

Ito, T., K. Ozawa, T. Watanabe, and T. Sagiya (2011a), Slip distribution of the 2011 off the Pacific coast of Tohoku Earthquake inferred from geodetic data, *Earth Planets Space*, *63*(7), 627–630, doi:10.5047/eps.2011.06.023.

Ito, Y., T. Tsuji, Y. Osada, M. Kido, D. Inazu, Y. Hayashi, H. Tsushimai, R. Hino, and H. Fujimoto (2011b), Frontal wedge deformation near the source region of the 2011 Tohoku-Oki earthquake, *Geophys. Res. Lett.*, *38*, L00G05, doi:10.1029/2011GL048355.

Ito, Y., R. Hino, M. Kido, H. Fujimoto, Y. Osada, D. Inazu, Y. Ohta, T. Iinuma, M. Ohzono, S. Miura, M. Mishina, K. Suzuki, T. Tsuji, and J. Ashi (2013), Episodic slow slip events in the Japan subduction zone before the 2011 Tohoku-Oki earthquake, *Tectonophysics*, in press.

Japan Coast Guard (2012), Seafloor movements obtained by seafloor geodetic observations after the 2011 off the Pacific Coast of Tohoku Earthquake, *Rep. Coord. Comm. Earthq. Predict. Jpn.*, *88*, 150–154, http://cais.gsi.go.jp/YOCHIREN/report/kaihou88/03_06.pdf.

Kanazawa, T., and A. Hasegawa (1997), Ocean-bottom observatory for earthquakes and tsunami off Sanriku, north-east Japan using submarine cable, in *Proc. Internl. Workshop on Scientific Use of Submarine Cables*, edited by H. Utada *et al.*, pp. 208–209, Comm. Sci. Use of Submarine Cables, Okinawa, Japan.

Kanazawa, T., M. Shinohara, and H. Shiobara (2009), Recent progress in seafloor earthquake observations and instruments in Japan, *Zisin 2*, *61*, S55–S68 (in Japanese with English Abstract).

Kido, M. (2007), Detecting horizontal gradient of sound speed in ocean, *Earth Planets Space*, *59*, e33–e36.

Kido, M., H. Fujimoto, S. Miura, Y. Osada, K. Tsuka, and T. Tabei (2006), Seafloor displacement at Kumano-nada caused by the 2004 off Kii Peninsula earthquake, detected through repeated GPS/Acoustic surveys, *Earth Planet Space*, *58*, 911–915.

Kido, M., Y. Osada, and H. Fujimoto (2008), Temporal variation of sound speed in ocean: a comparison between GPS/acoustic and in situ measurements, *Earth Planets Space*, *60*, 229–234.

Kido, M., Y. Osada, H. Fujimoto, R. Hino, and Y. Ito (2011), Trench normal variation in observed seafloor displacements associated with the 2011 Tohoku-Oki earthquake, *Geophys. Res. Lett.*, *38*, L24303, doi:10.1029/2011GL050057.

Kita, S., T. Okada, A. Hasegawa, J. Nakajima, and T. Matsuzawa (2010), Existence of interplane earthquakes and neutral stress boundary between the upper and lower planes of the double seismic zone beneath Tohoku and Hokkaido, northeastern Japan, *Tectonophysics*, *496*, 68–82, doi:10.1016/j.tecto.2010.10.010.

Koketsu, K. *et al.* (2011), A unified source model for the 2011 Tohoku earthquake, *Earth Planet. Sci. Lett.*, *310*, 480–487, doi:10.1016/j.epsl.2011.09.009.

Lichten, S. M., and J. S. Border (1987), Strategies for high precision global positioning system orbit determination, *J. Geophys. Res.*, *92*, 12751–12762.

Matsumoto, K., T. Takanezawa, and M. Ooe (2000), Ocean tide models developed by assimilating TOPEX/POSEIDON altimeter data into hydrodynamical model: A global model and a regional model around Japan, *J. Oceanogr.*, *56*, 567–581.

Matsumoto, Y., M. Fujita, T. Ishikawa, M. Mochizuki, T. Yabuki, and A. Asada (2006), Undersea co-seismic crustal movements associated with the 2005 Off Miyagi prefecture earthquake detected by GPS/Acoustic seafloor geodetic observation, *Earth Planets Space*, *58*, 1573–1576.

Matsumoto, Y., T. Ishikawa, M. Fujita, M. Sato, H. Saito, M. Mochizuki, T. Yabuki, and A. Asada (2008), Weak interplate coupling beneath the subduction zone off Fukushima, NE Japan, inferred from GPS/acoustic seafloor geodetic observation, *Earth Planets Space*, *60*, e9–e12.

Matsu'ura, M., D. D. Jackson, and A. Cheng (1986), Dislocation model for aseismic crustal deformation at Hollister, California, *J. Geophys. Res.*, *91*, 12661–12674.

Medwin, H. (2005), *Sounds in the Sea*, 643 p., Cambridge University Press, New York.

Mitsui, Y., and Y. Iio (2011), How did the 2011 off the Pacific coast of Tohoku Earthquake start and grow? The role of a conditionally stable area, *Earth Planets Space*, *63*(7), 755–759.

Miura, S., A. Sweeney, H. Fujimoto, H. Osaki, E. Kawai, R. Ichikawa, T. Kondo, Y. Osada, and D. Chadwell (2002), Evaluation of accuracy in kinematic GPS analyses using a precision roving antenna platform, *Eos Trans. AGU*, *83*, F352.

Morton, J. L., W. R. Normark, C. A. Reiss, and S. P. Tucker (1994), Seafloor horizontal deformation measurements using dual-frequency intelligent transponders, in *Proc. Int. Symp. On Marine Positioning*, pp. 81–86, Univ. of Hannover, Hannover, Germany.

Nagaya, Y., T. Urabe, and T. Yabuki (1999), Crustal deformation observation at the crest of the EPR 18.5S with the seafloor acoustic ranging method, *Eos Trans. AGU*, *80*(46), Fall Meeting Suppl., F1076.

Nishimura, T., S. Miura, K. Tachibana, K. Hashimoto, T. Sato, S. Hori, E. Murakami, T. Kono, K. Nida, M. Mishina, T. Hirasawa, and S. Miyazaki (2000), Distribution of seismic coupling on the subducting plate boundary in northeastern Japan inferred from GPS observations, *Tectonophysics*, *323*, 217–238.

Nishimura, T., T. Hirasawa, S. Miyazaki, T. Sagiya, T. Tada, S. Miura, and K. Tanaka (2004), Temporal change of interplace coupling in northeastern Japan during 1995-2002 estimated from continuous GPS observations, *Geophys. J. Int.*, *157*, 901–916, doi:10.1111/j.1365-246X.2004.02159.x.

Ohta, Y., R. Hino, D. Inazu, M. Ohzono, Y. Ito, M. Mishina, T. Iinuma, J. Nakajima, Y. Osada, K. Suzuki, H. Fujimoto, K. Tachibana, T. Demachi, and S. Miura (2012a), Geodetic constraints on afterslip characteristics following the March 9, 2011, Sanriku-oki earthquake, Japan, *Geophys. Res. Lett.*, *39*, L16304, doi:10.1029/2012GL052430.

Ohta, Y., T. Kobayashi, H. Tsushima, S. Miura, R. Hino, T. Takasu, H. Fujimoto, T. Iinuma, K. Tachibana, T. Demachi, T. Sato, M. Ohzono, and N. Umino (2012b), Quasi real-time fault model estimation for near-field tsunami forecasting based on RTK-GPS analysis: Application to the 2011 Tohoku-Oki Earthquake (M_w 9.0), *J. Geophys. Res.*, *117*, B02311, doi:10.1029/2011JB008750.

Ohzono, M., Y. Yabe, T. Iinuma, Y. Ohta *et al.* (2012), Strain anomalies induced by the 2011 Tohoku Earthquake (M_w 9.0) as observed by a dense GPS network in northeastern Japan, *Earth Planets Space*, *64*, 1231–1238.

Osada, Y., H. Fujimoto, S. Miura, A. Sweeney, T. Kanazawa, S. Nakao, S. Sakai, J. A. Hildebrand, and C. D. Chadwell (2003), Estimation and correction for the effect of sound velocity variation on GPS/Acoustic seafloor positioning: An experiment off Hawaii Island, *Earth Planets Space*, *55*, e17–e20.

Osada, Y., M. Kido, H. Fujimoto, and Y. Kaneda (2008a), Development of a seafloor acoustic ranging system toward the seafloor cable network system, *Ocean Eng.*, *35*, 1401–1405.

Osada, Y., T. Mizukami, M. Kido, Y. Ohta, H. Tsushima, S. Miura, and H.

doi:10.5047/meep.2014.00202.0023

Fujimoto (2008b), Introduction of 10 Hz GPS receiver for the improved observation of seafloor crustal movement, *J. Geod. Soc. Jpn.*, *54*(3), 141–151.

Osada, Y., M. Kido, and H. Fujimoto (2012a), A long-term seafloor experiment using an acoustic ranging system: precise horizontal distance measurements for detection of seafloor crustal deformation, *Ocean Eng.*, *51*, doi:10.1016/j.oceaneng.2012.05.006.

Osada, Y., M. Kido, Y. Ito, Y. Ohta, R. Hino, and H. Fujimoto (2012b), Seafloor crustal movement observed off Miyagi after the 2011 Tohoku Earthquake using GPS-Acoustic observation system, T13F-2693, AGU 2012 Fall Meeting, San Francisco.

Ozawa, S., T. Nishimura, H. Suito, T. Kobayashi, M. Tobita, and T. Imakiire (2011), Coseismic and postseismic slip of the 2011 magnitude-9 Tohoku-Oki earthquake, *Nature*, *475*, 373–376, doi:10.1038/nature10227.

Park, P. O., T. Tsuru, S. Kodaira, P. R. Cummins, and Y. Kaneda (2002), Splay fault branching along the Nankai subduction zone, *Science*, *297*, 1157–1160.

Paros, J. M. (1983), Isolating and temperature compensating system for resonators, U.S. Patent 4,406,966.

Paros, J. M. (1984), Digital pressure transducer, U.S. Patent 4,455,874.

Satake, K., Y. Fujii, T. Harada, and Y. Namegaya (2013) Time and space distribution of coseismic slip of the 2011 Tohoku earthquake as inferred from tsunami waveform data, *Bull. Seismol. Soc. Am.*, *103*, 1473–1492, doi:10.1785/0120120122, 2013.

Sato, M. (2012), Elucidation of seafloor crustal movements off northeastern Japan by GPS/acoustic technique with evaluation of sailing observation data from hull-mounted system, 93p., Doctor Thesis, Tohoku University.

Sato, M., H. Saito, T. Ishikawa, Y. Matsumoto, M. Fujita, M. Mochizuki, and A. Asada (2011a), Restoration of interplate locking after the 2005 off-Miyagi prefecture earthquake, detected by GPS/Acoustic seafloor geodetic observation, *Geophys. Res. Lett.*, *38*, L01312, doi:10.1029/2010GL045689.

Sato, M., T. Ishikawa, N. Ujihara, S. Yoshida, M. Fujita, M. Mochizuki, and A. Asada (2011b), Displacement above the hypocenter of the 2011 Tohoku-Oki earthquake, *Science*, *332*, 1395, doi:10.1126/science.1207401.

Shinohara, M., T. Yamada, T. Kanazawa, K. Uehira *et al.* (2013), Development of an underwater gravimeter and the first observation by using autonomous underwater vehicle, UT2013, Tokyo.

Spiess, F. N. (1985), Suboceanic geodetic measurements, *IEEE Trans. Geosci. Remote Sens.*, *GE 23*, 502–510.

Spiess, F. N., D. E. Boegeman, C. D. Lowenstein, and F. V. Pavlicek (1980), Precision transponder and method for communicating therewith, U.S. Patent, 4,214,314.

Spiess, F. N., C. D. Chadwell, J. A. Hildebrand, L. E. Young, G. H. Purcell Jr., and H. Dragert (1998), Precise GPS/Acoustic positioning of seafloor reference points for tectonic studies, *Phys. Earth Planet. Inter.*, *108*, 101–112.

Suito, H. (2010), Estimation of interseismic slip deficit in Japan based on GEONET, *114th Meet. Geod. Soc. Jpn. Progr. Abstr.*, 75–76 (in Japanese).

Suito, H., T. Nishimura, M. Tobita, T. Imakiire, and S. Ozawa (2011), Interplate fault slip along the Japan Trench before the occurrence of the 2011 off the Pacific coast of Tohoku Earthquake as inferred from GPS data, *Earth Planets Space*, *63*, 615–619.

Suwa, Y., S. Miura, A. Hasegawa, T. Sato, and K. Tachibana (2006), Interplate coupling beneath NE Japan inferred from three-dimensional displacement field, *J. Geophys. Res.*, *111*, B04402, doi:10.1029/2004JB003203.

Tadokoro, K., M. Ando, R. Ikuta, T. Okuda, G. M. Besana, S. Sugimoto, and M. Kuno (2006), Observation of coseismic seafloor crustal deformation due to M7 class offshore earthquakes, *Geophys. Res. Lett.*, *33*, L23306, doi:10.1029/2006GL026742.

Tadokoro, K., R. Ikuta, T. Watanabe, M. Ando, T. Okuda, S. Nagai, K. Yasuda, and T. Sakata (2012), Interseismic seafloor crustal deformation immediately above the source region of anticipated megathrust earthquake along the Nankai Trough, Japan, *Geophys. Res. Lett.*, *39*, L10306, doi:10.1029/2012GL051696.

Tamaki, T., H. Hino, H. Fujimoto, T. Yamada, T. Kanazawa, and H. Murakami (2002), Vertical crustal movement on the seafloor detected with differential pressure monitoring, Abstract UT2002, IEEE-OES, Tokyo.

Tamura, Y., T. Sato, M. Ooe, and M. Ishiguro (1991), A procedure for tidal analysis with a Bayesian information criterion, *Geophys. J. Int.*, *104*, 507–516.

Tsushima, H., R. Hino, H. Fujimoto, Y. Tanioka, and F. Imamura (2009), Near-field tsunami forecasting from cabled ocean bottom pressure data, *J. Geophys. Res.*, *114*, B06309, doi:10.1029/2008JB005988.

Tsushima, H., R. Hino, Y. Tanioka, F. Imamura, and H. Fujimoto (2012), Tsunami waveform inversion incorporating permanent seafloor deformation and its application to tsunami forecasting, *J. Geophys. Res.*, *117*, B03311, doi:10.1029/2011JB008877.

Uchida, N., and T. Matsuzawa (2011), Coupling coefficient, hierarchical structure, and earthquake cycle for the source area of the 2011 off the Pacific coast of Tohoku earthquake inferred from small repeating earthquake data, *Earth Planets Space*, *63*, 675–679, doi:10.5047/eps.2011.07.006.

Uchida, N., T. Matsuzawa, A. Hasegawa, and T. Igarashi (2003), Interplate quasistatic slip off Sanriku, NE Japan, estimated from repeating earthquakes, *Geophys. Res. Lett.*, *30*(15), doi:10.1029/2003GL017452.

Uehira, K., T. Kanazawa, S. Noguchi, S. Aoi, T. Kunugi, T. Matsumoto, Y. Okada, S. Sekiguchi, K. Shiomi, M. Shinohara, and T. Yamada (2012), Ocean bottom seismic and tsunami network along the Japan Trench, 2012 AGU Fall Meeting Abstract OS41C-1736, San Francisco, California, December 2012.

Urick, R. J. (1983), *Principles of Underwater Sound*, 3rd edn. Los Altos, CA, Peninsula Publishing.

Wang, K., Y. Hu, and J. He (2012), Deformation cycles of subduction earthquakes in a viscoelastic Earth, *Nature*, *484*, 327–332, doi:10.1038/nature11032.

Watanabe, T., K. Tadokoro, R. Ikuta, S. Sugimoto, T. Okuda, S. Nagai, S. Eto, and M. Kuno (2012), Accuracy evaluation of kinematic GPS analysis based on the difference of GPS satellite ephemerides, *J. Geod. Soc. Jpn.*, *58*, 61–76 (in Japanese with English abstract).

Wearn, R. B., and N. G. Larson (1982), Measurements of the sensitivities and drift of Digiquartz pressure sensors, *Deep-sea Res.*, *29*, 111–134.

Yaginuma, T., T. Okada, Y. Yagi, T. Matsuzawa, N. Umino, and A. Hasegawa (2006), Coseismic slip distribution of the 2005 off Miyagi earth-quake (M7.2) estimated by inversion of teleseismic and regional seismograms, *Earth Planets Space*, *58*, 1549–1554.

Yamamoto, J., Y. Osada, Y. Ohta, S. Hirahara, T. Demachi, T. Nakayama, K. Tachibana, T. Sato, M. Kido, H. Fujimoto, R. Hino, S. Miura, and M. Uchida (2013), Real time GPS processing utilizing satellite communications—Toward more reliable real-time crustal deformation monitoring under a situation of ground communication failure—, *J. Geod. Soc. Jpn.*, in press (in Japanese with English abstract).

Yamanaka, Y., and M. Kikuchi (2003), Source process of the recurrent Tokachi-oki earthquake on September 26, 2003, inferred from teleseismic body waves, *Earth Planets Space*, *55*, e21–e24.

Yamanaka, Y., and M. Kikuchi (2004), Asperity map along the subduction zone in northeastern Japan inferred from regional seismic data, *J. Geophys. Res.*, *109*, B07307, doi:10.1029/2003JB002683.

Zumberge, J. F., M. B. Heflin, D. C. Fefferson, M. W. Watkins, and F. H. Webb (1997), Precise point positioning for the efficient and robust analysis of GPS data from large networks, *J. Geophys. Res.*, *102*, 5005–5017.

Zumberge, M., H. Alnes, O. Eiken, G. Sasagawa, and T. Stenvold (2008), Precision of seafloor gravity and pressure measurements for reservoir monitoring, *Geophysics*, *73*, WA133–WA141, doi:10.1190/1.2976777.

doi:10.5047/meep.2014.00202.0023